GA–A24147

INERTIAL CONFINEMENT FUSION

ANNUAL REPORT

October 1, 2001
Through
September 30, 2002

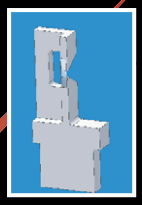

1994

Single Foil Mounted Polymer Targets

1995

Additional Layers

1996

Increased Quality

1997

1998

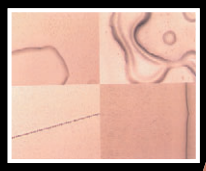

Metallic Coatings

Doped Polymer Targets

INCREASING COMPLEXITY

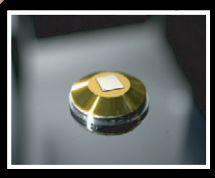

1999

Aluminum EOS Targets

2000

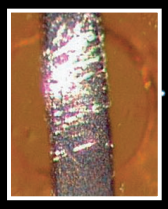

Foam Targets

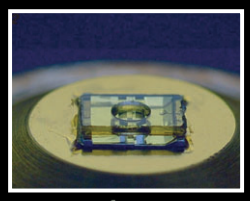

2001

Multiple Material EOS Targets

2002

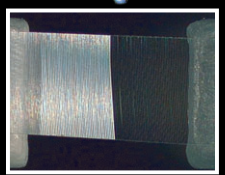

Targets with Variable Parameters

INCREASING PRECISION

Schafer

GENERAL ATOMICS

The complexity of the ICF targets we provide for DOE has increased greatly over the years. The timeline on the cover shows representative ICF planar targets starting with simple polymer targets in 1994 and progressing to complex targets with several materials and varying parameters in 2002. While the earlier, less complex targets are now relatively straightforward to make, at the time they were challenging and required months of development just as the more complex targets do today. Planar targets represent only a portion of the ICF targets that GA/Schafer produces for DOE, but the increase in complexity is common to every aspect of ICF target fabrication. (Contributed by Tom Walsh)

GA–A24147

INERTIAL CONFINEMENT FUSION TARGET COMPONENT FABRICATION AND TECHNOLOGY DEVELOPMENT SUPPORT

ANNUAL REPORT TO THE U.S. DEPARTMENT OF ENERGY

OCTOBER 1, 2001 THROUGH SEPTEMBER 30, 2002

by
PROJECT STAFF

W.J. Miller, Technical Editor
D.K. Forster, Copy Editor

Work prepared under
Department of Energy
Contract No. DE-AC03-01SF22260

GENERAL ATOMICS PROJECT 30095
DATE PUBLISHED: MARCH 2003

DISCLAIMER

This report was prepared as an account of work sponsored by an agency of the United States Government. Neither the United States Government nor any agency thereof, nor any of their employees, makes any warranty, express or implied, or assumes any legal liability or responsibility for the accuracy, completeness, or usefulness of any information, apparatus, product, or process disclosed, or represents that its use would not infringe privately owned rights. Reference herein to any specific commercial product, process, or service by trade name, trademark, manufacturer, or otherwise, does not necessarily constitute or imply its endorsement, recommendation, or favoring by the United States Government or any agency thereof. The views and opinions of authors expressed herein do not necessarily state or reflect those of the United States Government or any agency thereof.

ACRONYMS

AFM	atomic force microscope
CDR	Conceptual Design Report
CPL	cryogenic pressure loader
CTM	cryogenic target mount
CW	continuous wave
D_2TS	deuterium test system
D-GDP	deuterated polymer
DT	deuterium-tritium
DTRA	Defense Threat Reduction Agency
DVB	divinylbenzene
EDAX	energy dispersive x-ray analysis
EOS	equation of state
FI	fast ignition
GA	General Atomics
GDP	glow discharge polymer
HD	hydrogen deuteride
HEDP	high energy density plasma
ICF	Inertial Confinement Fusion
IDL™	Interactive Data Language
IFE	Inertial Fusion Energy
IFT	Inertial Fusion Technology
ILE	Institute of Laser Engineering, Japan
IPA	isopropanol
IR	infrared
LANL	Los Alamos National Laboratory
LEH	laser entrance hole
LLNL	Lawrence Livermore National Laboratory

NCTS	NIF Cryogenic Target System
NIF	National Ignition Facility
NNSA	National Nuclear Security Administration
NRL	Naval Research Laboratory
PAMS	poly(α-methylstyrene)
PCHMS	polycyclohexyl-methylsilylene $C_7H_{14}Si$
PVA	polyvinyl alcohol
RF	radio frequency
RT	Rayleigh-Taylor
SEM	scanning electron microscopy
Si-GDP	silicon-doped glow discharge polymer
SM	spheremapper
SM/WM	spheremapper/wallmapper
SNL	Sandia National Laboratory
TARPOS	TARget POSitioner
TGA	thermogravimetric analysis
TIC	target insertion cryostat
TPX	commercial designation of the polymer produced by the polymerization of 4-methylpentene-1
UR/LLE	University of Rochester/Laboratory for Laser Energetics
UV	ultraviolet
WBS	work breakdown structure
WETF	Weapons Engineering Tritium Facility
WM	wallmapper
XRF	x-ray fluorescence

TABLE OF CONTENTS

LIST OF FIGURES

LIST OF TABLES

1. ABSTRACT

This report documents fiscal year 2002 activity on the U.S. Department of Energy (DOE) National Nuclear Security Administration (NNSA) task order contract for Inertial Confinement Fusion (ICF) Target Component Fabrication and Technology Development Support with General Atomics (GA) and partner/subcontractor Schafer Corporation. Work performed spans development, production, and engineering of planar and spherical targets, target components, and cryogenic systems for the NNSA ICF Laboratories: Lawrence Livermore National Laboratory; Los Alamos National Laboratory; Sandia National Laboratory; the University of Rochester Laboratory for Laser Energetics; and the Naval Research Laboratory in Washington, D.C.

For more than ten years, the GA/Schafer Inertial Confinement Technology team has partnered with the NNSA ICF Laboratories developing and providing targets and related technologies for ongoing and future driver target interaction laboratory experiments. The team expertise is broad with interests and capabilities in all of the relevant areas of polymer and metal component fabrication, gas filling (including tritium), machining, characterization, and handling as diagrammed in Fig. 1–1.

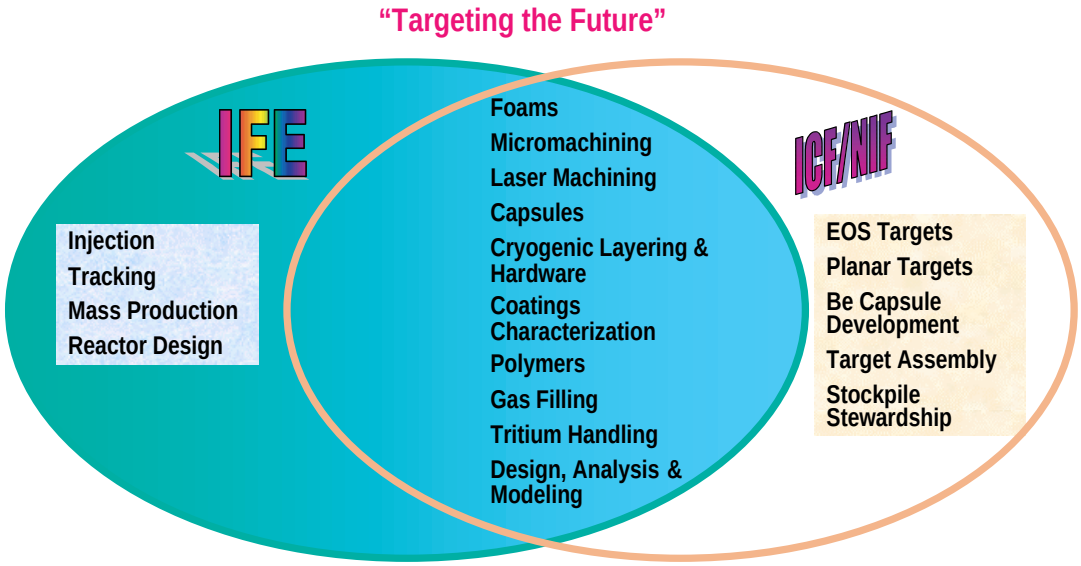

Fig. 1–1. The GA/Schafer Inertial Confinement Technology team expertise supports the NNSA national security missions as well as derivative missions such as Inertial Fusion Energy.

Highlights of the GA/Schafer ICF technology work performed under DOE Contract No. DE-AC03-01SF22260 in FY02 comprise the subject of this report. Comments and requests for further information may be directed to the GA Inertial Fusion Technology Program Manager, Jill Dahlburg [Jill.Dahlburg@gat.com, (858) 455–3571)].

2. INTRODUCTION

Inertial Confinement Fusion (ICF) is a research and development activity supported under the auspices of the U.S. Department of Energy (DOE) National Nuclear Security Administration (NNSA). The goal of ICF research is controlled laboratory implosion of fusionable material to a condition of ignition and propagating burn.

ICF relies on inertia to confine fusionable material, usually a mixture of deuterium and tritium (DT), for the time required to create a fusion reaction. Matter, which reaches this inertially confined state by means of compression from lasers or x-rays, can be considered to be a high energy density plasma (HEDP) for essentially all phases of the process from earliest compression through energy production through replete, extinguishing burn.

The canonical implosion scenario is that of central hot spot ignition in which a hollow, impermeable DT sphere is symmetrically imploded to a density (ρ), radius (R) product of 0.3 g/cc and a temperature (T) of order 10 keV. In the limit of radial symmetry, success (propagating burn) is predicted for a wide range of driver-capsule configurations.

The two most commonly envisioned central hot spot systems are direct and indirect drive ICF. In direct drive, the driving beams, usually high intensity lasers (a few $\times 10^{14}$ W/cm^2) of short wavelength light (0.33 to 0.25 μm) directly irradiate a spherical capsule surface. As the surface is heated, matter boils off and the capsule implodes. For shaped pulse driving beams, in which the intensity is controlled so as to drive well-timed shocks in the shell and accelerate the compressed hollow sphere walls inward to high final velocities (3×10^7 cm/s), a design space has been found where fusion conditions are predicted to occur. For indirect drive, the process is similar, with laser light replaced by a spatially uniform bath of x-rays (wavelength ~0.1 μm). The x-rays are produced and contained in a spherical or cylindrical can, a hohlraum, that is fabricated of metals of high atomic number. NNSA drivers used to generate the hohlraum x-rays include lasers and z-pinches.

It is generally agreed that five criteria determine a successful ICF implosion, each with outstanding issues and active research. First, a sufficient amount of driver energy must be transferred to the shell. Plasma instabilities in the shell corona can inhibit successful coupling of driver energy into the target. This continues to be an area of ongoing research with regimes identified that minimize plasma instabilities and allow for up to 80% driver energy absorption. Second, the capsule must be imploded on a sufficiently low adiabat for fusion conditions to be achievable with laboratory-scale drivers. Adverse preheat mechanisms include shock mistimings (5% or greater), radiation effects, and mixing from very short wavelength instabilities. Considerable research in equation of state and opacity results from this criterion. Third, the implosion must be sufficiently symmetric at length scales long relative to the shell thicknesses for the generation of a well-formed hot spot. This criterion, which sets a shell uniformity requirement of a few percent and also limits time

independent drive asymmetry at long perturbation wavelengths ($l < 32$) to a few percent, is achievable with existing technologies. Fourth, the shell must be sufficiently stable to the short wavelength Rayleigh-Taylor (RT) instability to confine the core gas to full implosion in order for ignition conditions to be achieved. This instability, which is seeded by all of the small-scale imperfections of real-world driving beams and shell surface and mass, is the subject of intense ongoing research. Because the RT instability is vortical in nature, mitigation is sought primarily in a tailoring of the ICF pellet gradients to reduce the vorticity source term (a function of the cross product of gradients of ρ and T) at both the outer and inner shell surfaces and to increasing the ablation velocity at the shell surfaces in order to pull away as much as possible the vorticity generated. Fifth, the pellet must reach a condition of sufficient ρR and T for alpha-particle-driven ignition and propagating burn to occur.

As with many systems with well-defined postulates, the relaxation of one criterion can sometimes lead to the most interesting alternate systems. A classic example is the birth of complex variable theory which came about when parallel lines were allowed to meet at infinity in an otherwise Euclidean space. In the case of ICF, relaxing completely the fourth criterion has led to the idea of fast ignition (FI). In FI, the ρR for ignition is first achieved with standard drivers and capsules that range from spherical shells to hemispheres of webbed foams. The ignition beam is then envisioned to be generated from high intensity, collimated electrons or ions that result from petawatt laser matter interaction. While compression is relatively easy and has, to some level, already been demonstrated in the laboratory, coupling the ignitor "match" to the compressed fuel is far from determined. The introduction of this concept in the early 1990s, along with the development of very high intensity (order 10^{18} W/cm^2 or higher) laser drivers, has resulted in significant active research in very high intensity laser matter and laser plasma interactions.

The GA/Schafer team fabricates components and complete target assemblies for the NNSA ICF laboratories (Lawrence Livermore National Laboratory, Los Alamos National Laboratory, Sandia National Laboratory, the University of Rochester Laboratory for Laser Energetics, and the Naval Research Laboratory) to address a wide range of experimental criteria that are relevant to ICF and HEDP physics. These components include: gasbags for plasma instability studies, doped planar and shaped targets for radiation preheat and shock timing investigations, well-characterized spheres with a variety of gas fills for low-mode asymmetry studies under a range of conditions, targets that enable investigation of the Richtmyer-Meshkov and RT instabilities, and we are assisting in the development of National Ignition Facility ignition targets and cryogenic systems.

The work of target and target component fabrication is fundamentally cross-disciplinary in nature. Most new target types and developments are research results from proactive teams of chemists, material scientists, physicists, and characterization and fabrication engineers, who, together, produce new target systems and capabilities. An example result from the GA/Schafer target fabrication team, a complex assembled target that enabled the investigation of a high intensity laser interacting with a preformed plasma, is shown in Fig. 2–1.

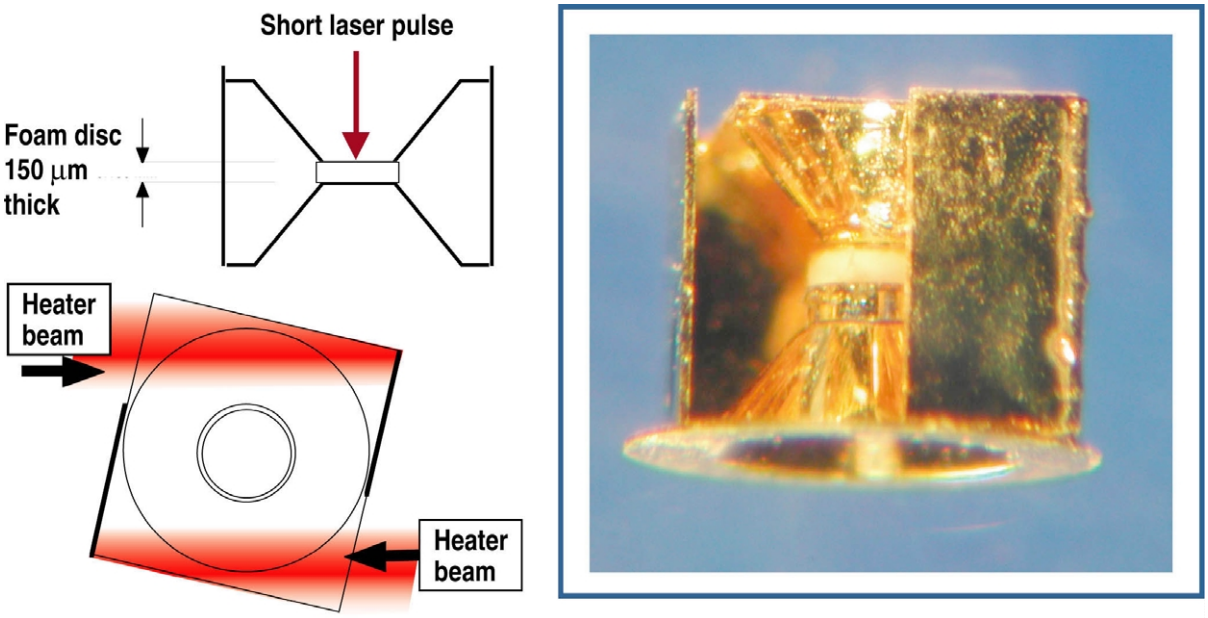

Fig. 2–1. Miniature hohlraum used to make a hot plasma.

3. PROGRAM ACCOMPLISHMENTS

3.1. PROGRAM OVERVIEW

Under the U.S. Department of Energy (DOE) National Nuclear Security Administration (NNSA) Inertial Confinement Fusion (ICF) Target Component Fabrication and Technology Development Support contract, General Atomics (GA) and its partner/subcontractor Schafer Corporation are responsible for NNSA target and target component fabrication and production as well as design, development, and fielding of associated technologies that range from large-scale cryogenic systems to precision hohlraum assembly stations. GA/Schafer supplies components to the five ICF laboratories: Lawrence Livermore National Laboratory (LLNL), Los Alamos National Laboratory (LANL), Sandia National Laboratory (SNL), the University of Rochester Laboratory for Laser Energetics (UR/LLE), and the Naval Research Laboratory (NRL). In order to continue to meet the needs of the developing NNSA ICF program, the GA/Schafer team is structured as a capabilities-based organization under the direction of the GA/Schafer team Program Manager, Jill Dahlburg, with Keith Shillito, Associate Program Manager for Schafer Activities and Gottfried Besenbruch, Associate Program Manager for GA Activities. This organization is comprised of ten centers with contract task responsibilities divided among the centers as appropriate: the Center for Advanced Cryogenic Layering, headed by Donald Bittner; the Center for Foam Target Development and Production, headed by Diana Schroen; the Center for Advanced Planar Targets, headed by Tom Walsh; the Operations Office, headed by Wayne Miller; the GA/Schafer Characterization Innovation and Development Office, headed by Richard Stephens; the GA/Schafer Supercenter for High Energy Density Plasma (HEDP) Targets, headed by Dan Goodin; the Center for Advanced Cryogenic Technology, headed by Gottfried Besenbruch; the Center for Target Component Fabrication and Fabrication Development, headed by James Kaae; the Center for Polymer and Coatings and Foam Capsule Development, headed by Abbas Nikroo; and the Center for Capsule Production, headed by David Steinman. The organizational chart in Fig. 3–1 provides contact information.

Highlights of some of this year's GA/Schafer Inertial Fusion Technology (IFT) accomplishments include: fabrication of foam shells for use on experiments on OMEGA, confinement of noble diagnostic gasses inside glass shells, fabrication of large diameter thin-walled aluminum hohlraums, deposition of tungsten metal on glass shells for novel HEDP targets, updating of the design concept of the target insertion cryostat for the National Ignition Facility (NIF) cryogenic target system for a rear loading cryogenic target positioner, and a vibration analysis of the clamshell shroud opening of Mark-I NIF cryostat. These and other IFT program accomplishments reported in the sections following are detailed as task activities from the perspectives of the GA/Schafer team capabilities structure.

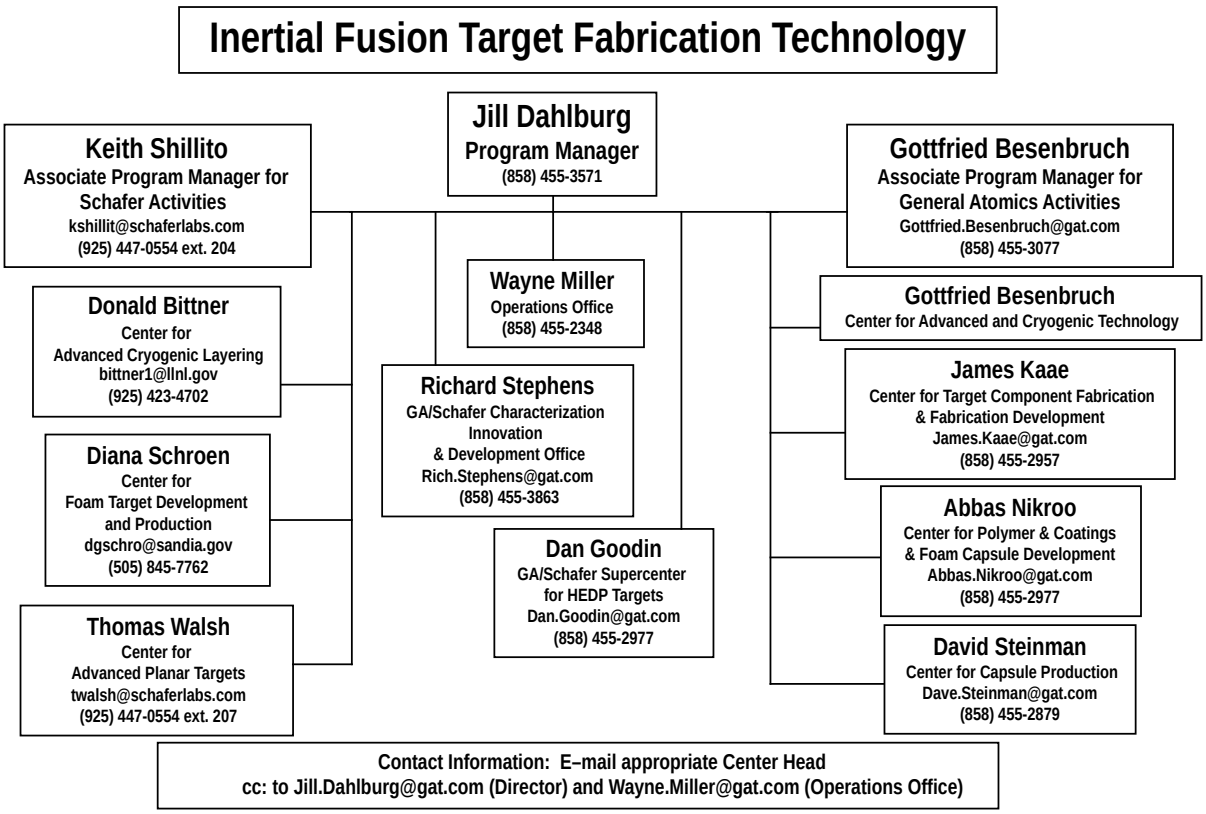

Fig. 3–1. GA/Schafer organizational chart.

3.2. CENTER FOR ADVANCED AND CRYOGENIC TECHNOLOGY

Center head: Gottfried Besenbruch

Scientists: Neil Alexander, Rémy Gallix, Chuck Gibson (GA), and John Sheliak (part of the year, GA)

Designers: Tom Drake (GA); Jerry Stewart, and Bud Fraze (Schafer)

Technician: Bob Stemke (GA)

Overview

The Center for Advanced and Cryogenic Technology focuses on the design, assembly, and testing of cryogenic target systems for ICF, Inertial Fusion Energy (IFE), and Z-Pinch devices. We are an integral part of the design team for the NIF Cryogenic Target System (NCTS). The NCTS is the system that fills ignition targets with deuterium-tritium (DT) or other fuels, cools the targets to cryogenic temperatures, layers the fuel in the targets, inserts the targets into the NIF target chamber, and exposes the target just before it is shot by the NIF lasers. The NCTS is being designed to deliver indirect drive ignition targets using capsules made from polymers or beryllium alloys. A direct drive option is also being investigated. In addition, the NCTS includes a system for delivery of nonignition cryogenic targets, the Mark-I. The work breakdown structure (WBS) of the NCTS is shown in Fig. 3–2, where the GA/Schafer areas of participation are indicated.

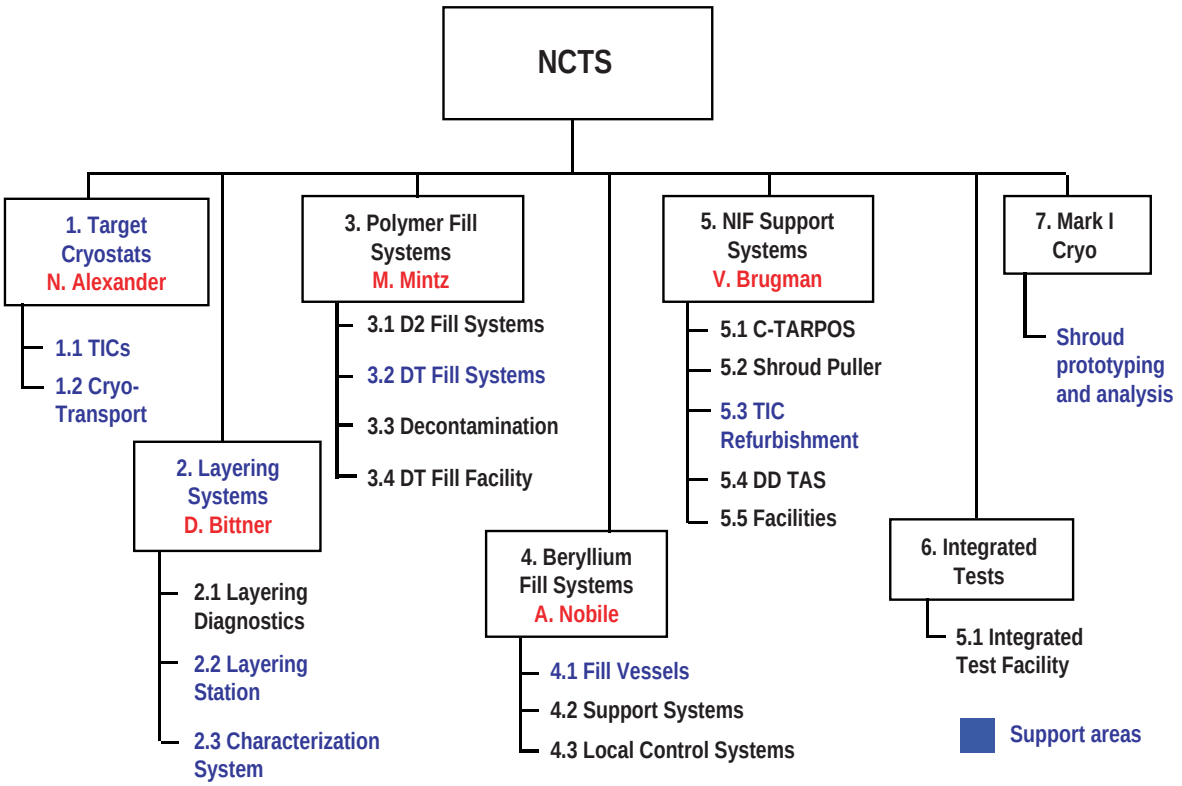

Fig. 3–2. GA/Schafer support the NCTS in several areas.

The GA/Schafer team has been assigned the lead for the design and development of the Target Cryostats subsystem and the Layering subsystem. In addition, we provided design and analysis support for the Mark-I Cryogenic Target System and the Beryllium Fill System.

This year, our early activities focused on investigating design concepts for the NCTS and estimating cost and schedule in preparation for the conceptual design of the system. While the earlier efforts were aimed at the Target Insertion Cryostat (TIC) and the polymer fill cryostat, the emphasis was shifted towards the Mark-I design and the Beryllium Fill System after the beginning of the calendar year. Our efforts on (1) the TIC, (2) the Mark-I Cryogenic Target System, and (3) the Beryllium (Be) Fill System are described in detail in the following sections.

3.2.1. The Target Insertion Cryostat (TIC) (Neil Alexander, GA)

The TIC houses the target and maintains it at cryogenic temperatures as it is moved between the filling station, the layering and characterization station, and the NIF chamber until the target is shot. The TIC is held in a vacuum and support box — the TIC transporter. Some of the major components of the TIC are a liquid helium tank, a Cold Head, a target gripper, a shroud to protect the target from thermal radiation and gas condensation, neutron shielding, and a hexapod fine-positioning stage which provides for positioning the target with 6 deg of freedom.

Last year's conceptual model of the TIC was updated in several areas (see Fig. 3–3): an initial concept of the Cold Head was modeled and incorporated into the TIC model, the target gripper model was incorporated into the TIC model, and the shroud latching mechanisms were repositioned to accommodate a new shroud design. This new shroud design allows the shroud to clear the NIF laser beams after a shorter stroke and prevents knocking off backlighter diagnostics during retraction of the shroud at shot time. A vent port was added to the back of the liquid helium tank to aid in filling the tank with liquid helium.

We started to examine the effect of the blast of the target on the TIC. A blast shield is included in the design of the TIC to reduce the pressure pulse transmitted to the TIC from the x-rays emitted from an imploded target, which ablate nearby surfaces onto which they impinge. The TIC is protected in the shadow of the blast shield. An aluminum foam layer in the blast shield attenuates the pressure pulse to the TIC. The residual pressure pulse at the backside of the foam has been estimated to be 2.4 MPa. When the size of the shield plus an estimate of the dynamic load factor were considered, it was estimated that the TIC would experience a force of 8000 N (1800 lbf) from a 20 MJ ignition shot. In the previous model of the TIC, the blast shield was supported off of the target gripper, so all of this force would be transmitted into the Cold Head. When the support tubes of the Cold Head were sized to withstand this force, the heat conducted down the support tubes lead to an unacceptably high usage rate for the liquid helium coolant. A thermal heat balance model was constructed in Excel to examine this and other thermal issues. The thermal model considers the conduction heat leaks of the supports of the Cold Head and the liquid helium tank; thermal radiation on the target, the Cold Head, and the liquid helium tanks; and externally applied heat to the

target [e.g., for infrared (IR) layering or thermal shimming of the hohlraum]. To solve the heat load problem caused by the stout support tubes, the support of the blast shield "donut" was moved from the gripper to trusses that are mounted directly to the nosecone (Fig. 3–4). This eliminated the load path through the Cold Head and allowed thinner, lower heat leak support tubes. It also reduced the thermal radiation heat load on the Cold Head by removing the area of the blast shield from the target gripper.

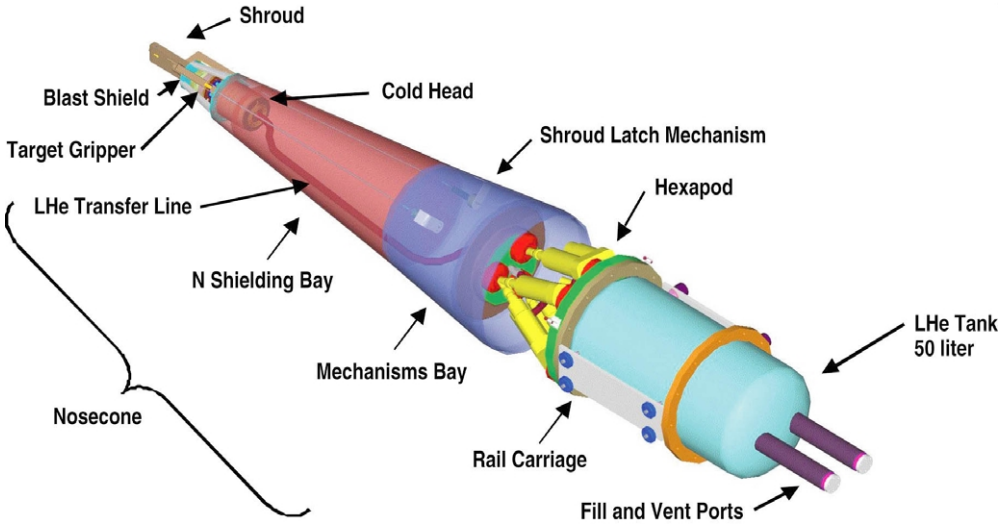

Fig. 3–3. The Cold Head and target gripper were incorporated into the TIC conceptual model. The nosecone shown is for indirect drive targets.

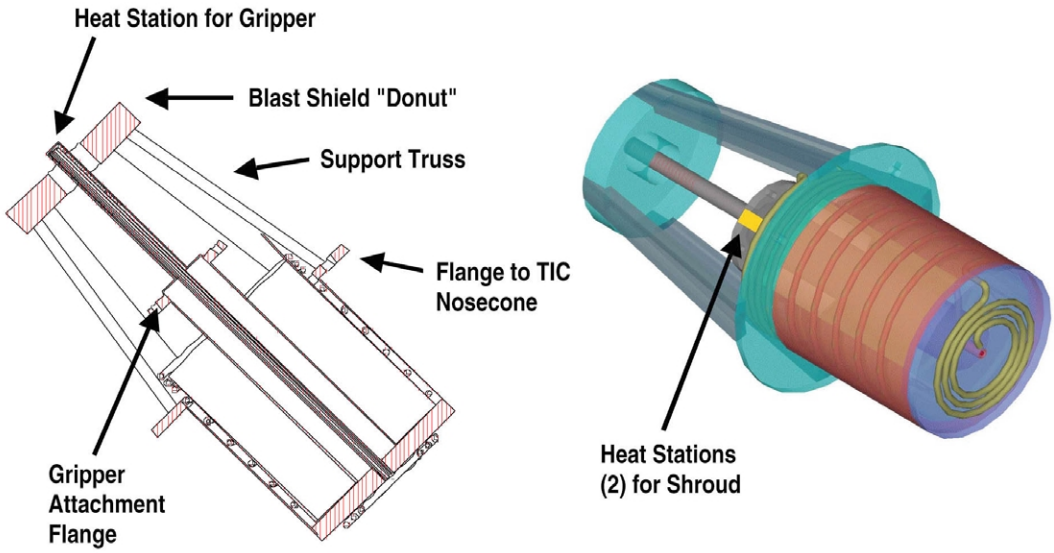

Fig. 3–4. This is the updated conceptual model of the Cold Head with the blast shield shown attached. The blast shield supports were moved from the target gripper to the flange that bolts the Cold Head to the TIC nosecone. This eliminated the blast load path going through the Cold Head, allowing for thinner support tubes in the Cold Head.

The heat balance thermal model indicates that the TIC can operate for 24 h on 48.5 liters of liquid helium. This is for one-phase flow into the Cold Head with the Cold Head at 8 K and a 1.44 W heat load being applied. One-phase flow will allow for higher temperature stability. The model also indicated that the shroud heat station would be at 46 K and that the vapor-cooled thermal shield of the liquid helium tank would be at 52 K. The heat loads in the liquid helium transfer line have not yet been considered so the actual liquid helium consumption will be higher.

3.2.2. The Mark-I Cryogenic Target System (Neil Alexander and Rémy Gallix, GA; Jerry Stewart, Bud Fraze, Schafer)

From the first NIF shots, the Mark-I Cryosystem will allow the fielding for nonignition shots of a wide range of targets on the NIF, including hohlraums, gas bags, planar targets, and equation of state (EOS) targets. It will be capable of controlling the Cold Head temperature between 5 K and 300 K and filling targets with up to three different gasses. It will also be capable of filling and fielding DT targets. The Mark-I Cryosystem is designed to minimize both turnaround time and operational complexity. It will attach to the Target Positioner (TARPOS) mounted on the NIF target chamber.

3.2.2.1. Preliminary Design Study of an Electrically Actuated Clamshell Shroud. GA performed a comprehensive comparison of electrical actuator designs to open and close the clamshell shroud. Linear motors combined with rack and pinion mechanisms, linkages, or cables, as well as rotary motors combined with worm gears or rotor nuts driven rack and pinion mechanisms, were considered. The selection criteria were: operability in vacuum, available space envelope, motion control, balanced dynamic forces, induced vibration, absolute positioning, position holding when de-energized, reliability, simplicity, and material activation. Three-dimensional CAD layouts of the entire Mark-I front end were prepared for each actuator design. A linear motor directly coupled to a rack and pinion mechanism, as shown in Fig. 3–5, was found to be the best solution.

3.2.2.2. Thermal Analysis of the Mark-I Clamshell Shroud. A thermal model was constructed for the shroud of the Mark-I cryostat and the shroud's support-arms and cooling links. These were modeled as a set of equations for a series of connected radiator fins. They describe conduction heat flow through and thermal radiation falling on the fins. The set of fins was arranged in a "Y" pattern. One arm of the Y represented the shroud. Another arm of the Y represented the low thermal conductivity support-arm of the shroud. The third leg represented the cooling link for the shroud. Two cases were considered. In one case, the cooling link was modeling a flexible copper braid (cable). In the other, the cooling link was modeling a spring wiper contact made using MC-Multilam at the end of a copper rod. The endpoints of the arms and shroud tip were constrained to be at fixed distances from each other.

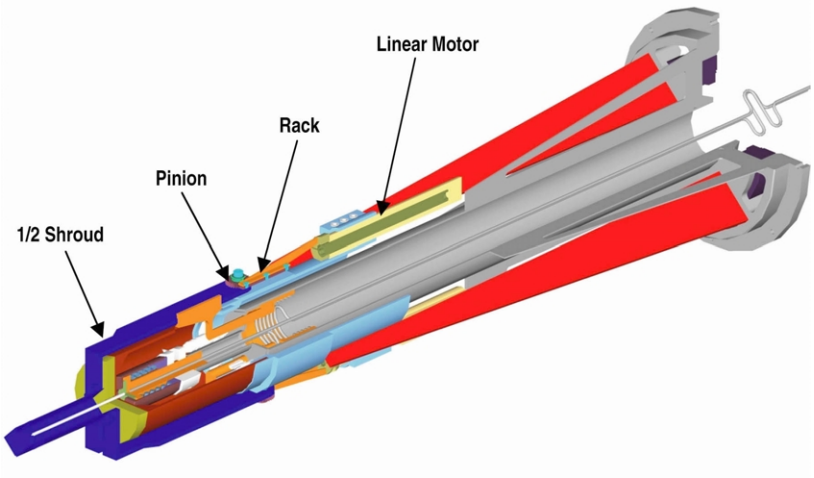

Fig. 3–5. Mark-I front end including shroud actuator with electric linear motor and rack and pinion mechanism.

The model was made to determine an optimum length for the low thermal conductivity support-arm for the shroud. In these models, the low thermal conductivity arm was given the properties of G10 fiberglass. Figure 3–6(a) shows that the temperature of the tip of the shroud is minimized with a G10 length of ~30 mm. This is true for both the braid and MC-Multilam.

The heat load to the Mark-I cryostat at its secondary heat station was also calculated, with this heat station assumed to be at a fixed temperature of 30 K, attached to the cooling link. Figure 3–6(b) shows that the heat for a G10 support length of 30 mm is only slightly higher than the asymptotic minimum heat leak possible. Thus, for the particular Mark-I shroud geometry and material properties considered, the optimum length for the G10 support-arm is ~30 mm.

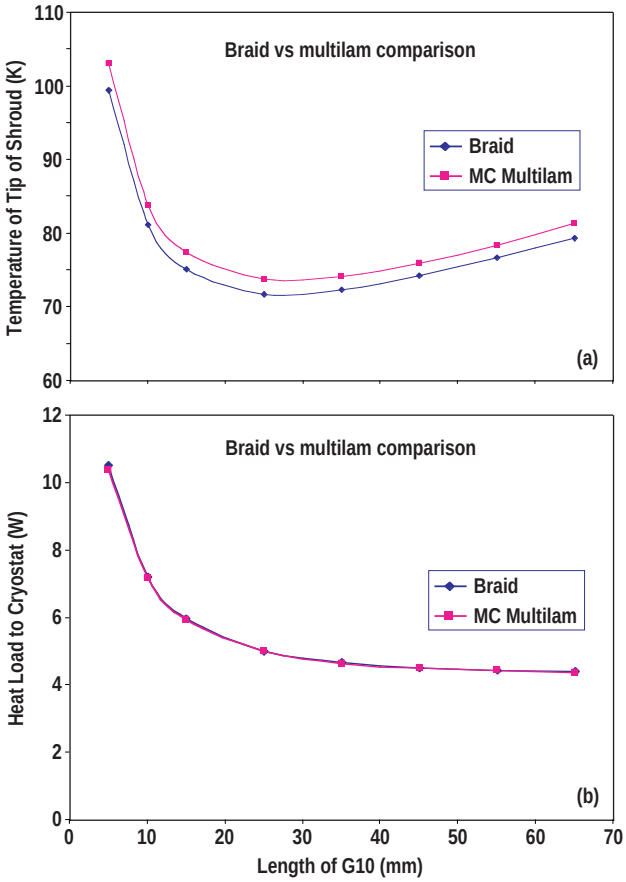

Fig. 3–6. (a) The Mark-I shroud tip temperature is minimized for a ~30 mm support-arm length of G10 fiberglass. (b) At 30 mm (the optimum for minimization of the Mark-I shroud tip temperature), the support-arm length of G10 has only a slightly increased heat leak over the asymptotic heat leak.

3.2.2.3. Dynamic Analyses of the Mark-I Cryosystem. A number of preliminary scoping analyses were performed to determine the order of magnitude of

the target vibration that may be induced by the sudden opening of the clamshell shroud. The complete Mark-I system, holding a typical target, was assumed mounted at the end of the TARPOS boom cantilevered off a vibration-free support. A detailed, three-dimensional finite-element model representing the entire structure, including the detailed Mark-I front-end design shown in Fig. 3–5, was constructed and subjected to modal analysis with the COSMOS program. Figure 3–7 shows the fundamental vibration mode of the model, similar to the deflected shape of the cantilevered system under its own deadweight. The clamshell shroud and its actuator(s) were replaced with time-dependent dynamic forces acting on their attachment points to the Mark-I system. These forces were calculated to model the shroud opening to a stop in 0.5 s. The transient, undampened response of the model, during the 0.5 s shroud opening and beyond, was calculated with COSMOS by the modal time-history method. The analysis confirmed that no perceptible target vibration would be produced if shroud halves and actuators were perfectly balanced. The largest calculated target vibration after shroud opening amounted to ~±0.6 μm. It was obtained with the following assumptions: the inertial forces acting on one-half of the clamshell shroud were 10% larger than those acting on the other half, a single actuator was used to open both shroud halves, and the actuator applied stepwise accelerations and decelerations. With linearly varying accelerations and decelerations, the vibration was reduced by one-third.

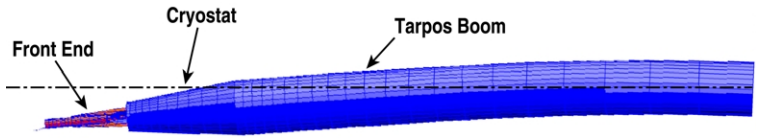

Fig. 3–7. Fundamental vibration mode (19 Hz) of the Mark-I system model.

3.2.2.4. Dynamic Testing of the Clamshell Shroud. The conceptual and preliminary designs of a setup to realistically model the Mark-I cryosystem and test it for target vibration induced by the rapid opening of the shroud were developed. The test setup, shown in Fig. 3–8, included the mechanically functional model of the Mark-I front-end design shown in Fig. 3–5, an adjustable boom, and a rigid support to avoid amplification of ground vibration. The cantilevered length of the boom and its mass can be adjusted to help reproduce the dynamic characteristics of the Mark-I system and the TARPOS boom, i.e., their natural vibration modes and frequencies and their response to shroud opening. A detailed finite-element model of the entire test setup, shown in Fig. 3–9, was constructed and analyzed with the COSMOS program to verify design adequacy, predict target vibration, and guide vibration sensor specification.

3.2.2.5. Design of the Mark-I Cryosystem. During this year, working at LLNL, Schafer personnel continued the design and CAD modeling of the Mark-I cryosystem, with support from GA. This included the design of the front end, with its target gripper and shroud, and the rear end, or cryostat section, which contains the liquid helium tank and mounts on the TARPOS boom. A clamshell shroud design using pneumatic actuators was developed and

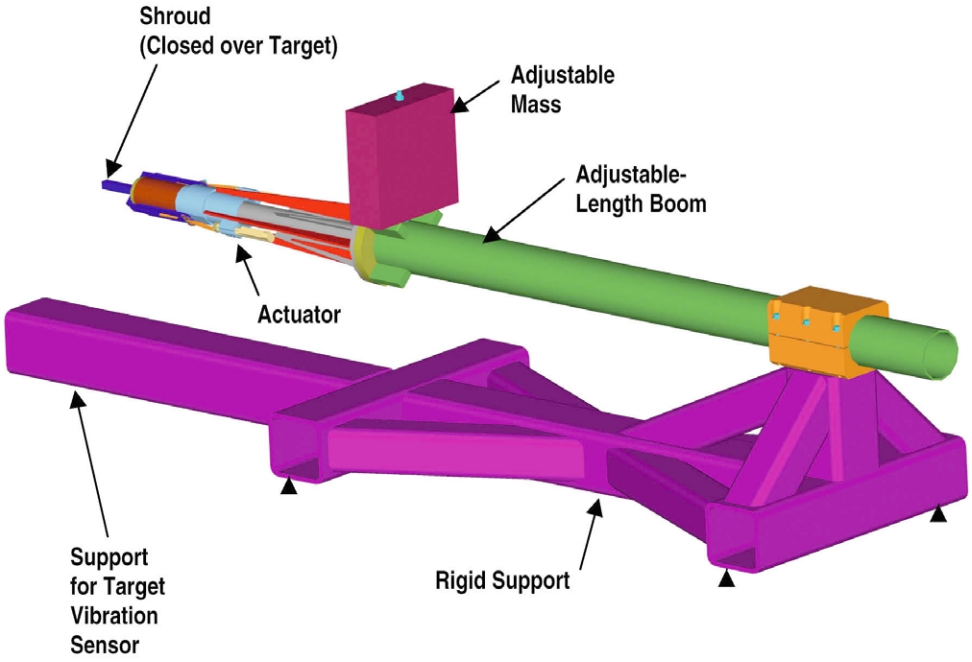

Fig. 3–8. Mark-I shroud/target vibration test setup.

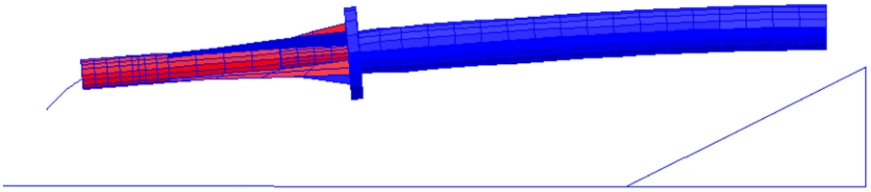

Fig. 3–9. Fundamental vibration mode (19 Hz) of the Mark-I vibration test setup.

the entire front end was modified to fit in a narrower conical envelope. Additionally, the original Mark-I Conceptual Design Report (CDR) 20 liter dewar design was replaced with a dewar 30 liters in size. The support structure, shields, vacuum vessel and dewar suspension system progressed as well. See the illustrations below in Figs. 3–10 and 3–11.

Testing of the specially prepared pneumatic shroud actuation cylinder and control system was performed at LLNL and resulted in the selection of a control system that meets current design and operational parameters. A bench prototype shroud opening mechanism was created and successfully cycled within the 0.5 s period using the subject actuation cylinder. A secondary set of cylinder seals was incorporated into the cylinder mounting design wherein the interstitial space is vacuum pumped. The cylinder with this seal arrangement was tested in a vacuum vessel and successfully passed NIF leak rate criteria. Computer control of the actuation cylinder to obtain desired acceleration, deceleration and position is in process and being advanced.

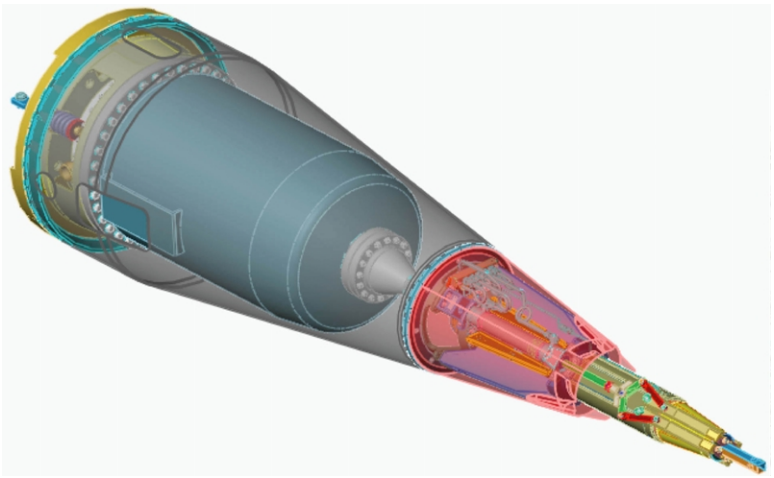

Fig. 3–10. CAD model of the Mark-I system.

Fig. 3–11. Rendered CAD model of the Mark-I system. (Some forward ablation shields removed.)

An LLNL CAD design layout was completed for a thermal test of a semi-custom commercial flow cryostat incorporated into a partial Mark-I thermal mockup of the target-base gripper/shroud end. This design includes heat loads applied via heaters that are placed at or very near the actual source locations per the Mark-I design layout. The purpose of this test is to evaluate the Mark-I thermal design in terms of the cryostat cold end/head and the secondary cooling by the He exhaust. Fabrication drawings for this test hardware are in process.

3.2.3. The Beryllium Fill Systems (Neil Alexander and Rémy Gallix, GA)

To facilitate ignition target fielding, a hollow, spherical, beryllium-alloy capsule is desired that is strong enough to contain high-pressure DT gas at ambient conditions. The

capsule needs to be cooled to cryogenic temperature only when it is time to condense the DT gas and turn it into a smooth layer of DT ice prior to an experimental shot.

Two principal approaches are being investigated to produce such capsules. In the first approach, a small hole is drilled through the wall of a spherical capsule, the capsule is filled with DT through the hole, and the hole is sealed, trapping the DT. In the second approach, two Be-alloy cylinders, each with a hemispherical cavity, are placed in a vessel and then filled with pressurized DT-gas; they are pressed and bonded together at elevated temperature to form a single cylinder containing a spherical cavity filled with high-pressure DT gas. After removal from the vessel, the outer surface of the cylinder is machined into the desired spherical shape.

During this fiscal year, GA has contributed to the development of both approaches.

3.2.3.1. Drilled and Sealed Capsules

Conceptual Study. Using a pulsed femtosecond laser in vacuum, LLNL has developed a method for drilling a hole with a maximum diameter of 3 μm through the ~135 μm thick sheet of Be and is continuing to develop the process. This fiscal year, GA investigated various concepts for filling and sealing the capsule.

The hole need not be completely filled, only sealed so that the capsule can contain the high-pressure DT gas inside without leaking or failing structurally. Due to the very small size of the hole, sealing it with a bonded plug does not appear practical. However, the method used to drill the hole with a laser may be adapted to melting the opening shut by shining a laser beam on the area surrounding the hole. A thermal analysis, reported below, was performed to determine the characteristics of the heat pulse required for laser sealing the hole. The analysis indicated that the operation appears feasible and should be investigated further.

The simplest approach for filling drilled capsules would be to place them in a vessel, evacuate the vessel and the capsules, backfill them with pressurized DT gas at room temperature, and seal weld the opening of the holes by shining a laser at them through a window. However, in the past, porous laser welds have been observed in beryllium in presence of significant hydrogen. Also, focusing the laser beam through high-pressure DT gas may be a problem. Review of previous test data followed by new experiments will be required to determine whether or not satisfactory laser welds can be achieved to seal the opening of representative long and narrow holes in Be alloy shells in high-pressure DT gas.

If it is found that the holes can only be laser sealed in a vacuum, the desired quantity of DT must first be introduced into the capsules, then cryogenically cooled to such a low temperature and vapor pressure that the solid DT remains trapped inside the capsules when the chamber is evacuated prior to laser welding. This can be done either by pressurizing the capsule in a high-pressure DT cell, then cooling the entire cell until all the DT gas in the cell and the capsules condenses (this is the “fill, cool, seal” concept, shown in Figs. 3–12 and 3–13). Or it can be done by placing the inside of the capsule in communication with a source

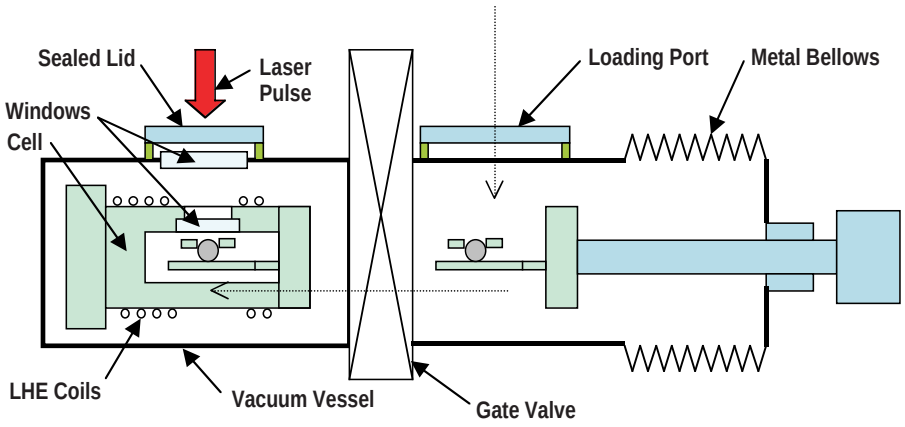

Fig. 3–12. Fill, cool, seal concept 1 — seal in cell.

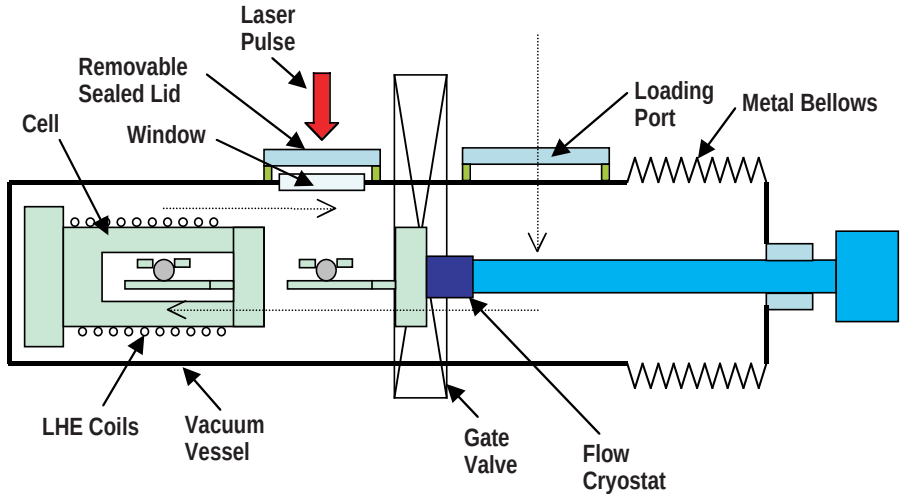

Fig. 3–13. Fill, cool, seal concept 2 — seal in vacuum chamber.

of DT gas and cryocondensing the gas at the bottom of the capsule, without the need for a high-pressure cell (this is the “cryocondense” concept, shown in Figs. 3–14 and 3–15).

In Fig. 3–12, the capsule is sealed inside the high-pressure DT cell after they are cooled and evacuated, so that the cell remains the primary DT containment during sealing and only one cryogenic element is required. However, a second window, fitted in the wall of the high-pressure cell to let in the laser beam, is part of the DT primary containment; it must be designed to resist high internal pressure and may become coated with DT ice, affecting beam transmission. Alternately, in Fig. 3–13 the capsule is transferred back out of the high-pressure DT cell into the vacuum vessel after the cell and the capsule are cooled. There is no window in the high-pressure cell wall and the window in the vacuum vessel wall will remain clear of DT ice. This requires two cryogenic elements and the vacuum vessel, not the cell, is the primary DT containment during sealing, and there is a lot of DT ice inside the open cell and on the capsule holder. This ice may impede the opening of the cell. It may also drop to

the bottom of the room-temperature vacuum vessel, in which case the vacuum vessel itself may have to be a cryostat so that dropping ice cannot vaporize and break the vacuum needed for laser welding.

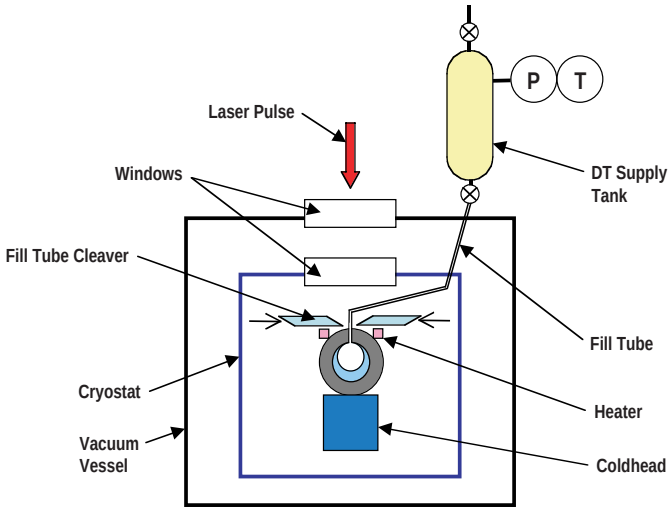

Fig. 3–14. Cryocondense, seal concept 1 — fill tube supply.

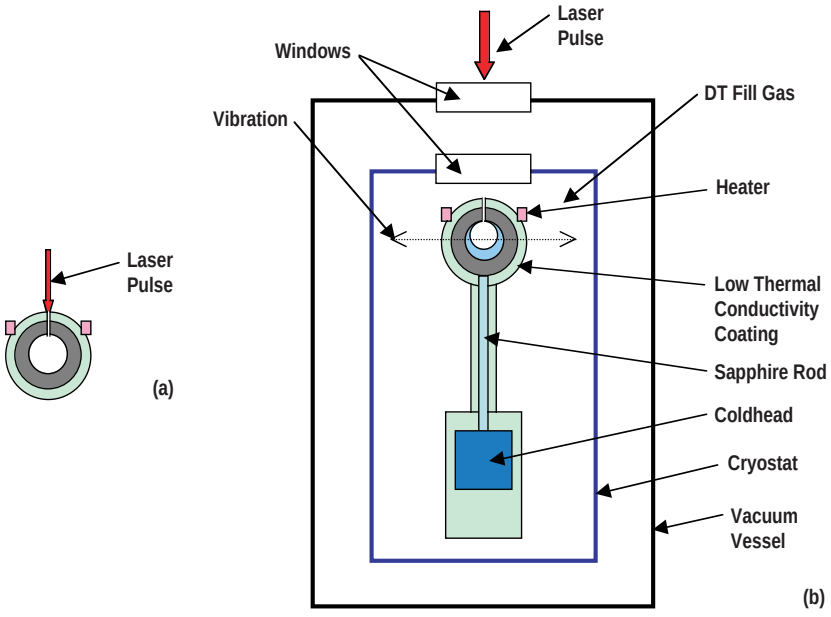

Fig. 3–15. Cryocondense, seal concept 2 — container supply. (a) Pre-drill coating and capsule. (b) Fill and seal capsule.

In the setup shown in Fig. 3–14, the capsule is filled through a tube channeling DT gas directly from an external tank to the hole at the top of the capsule. A thermal gradient is imposed between the top and the bottom of the capsule to condense the gas at the bottom of the capsule and keep the fill hole clear of condensate. An analysis, reported below, was

performed to determine the required thermal parameters. Determination of the DT fill from ΔPVT measurements of the fill tank is relatively straightforward. However, sealing the fill tube to the capsule without plugging the hole may be difficult. Because the fill tube obscures the hole from the sealing laser beam, it would be necessary either to cleave off the tube just before sealing, or to burn through the fill tube with the laser then seal weld the hole. Either way, fill tube residuals may need to be removed after sealing.

Alternately, in Fig. 3–15 the cryostat and the capsule are filled with DT gas near atmospheric pressure and the capsule is cryogenically cooled to condense the desired mass of DT at the bottom of it. As in Fig. 3–14, a thermal gradient is imposed on the capsule to keep the condensed DT out of the fill hole and at the bottom of the capsule. The problems with the fill tube are eliminated but DT is not channeled directly to the capsule fill hole. Significant care is also needed to keep the inner surface of the capsule cold and all other exposed surfaces warmer so that DT does not condense in other parts of the system. Sufficient DT pressure must be maintained in the cryostat to keep the fill time reasonably short. All of this indicates that determination of the DT fill would be difficult (e.g., by measuring capsule vibration).

Thermal Analysis of a Capsule During the Laser Sealing Process. Pulsed lasers, which produce very short and intense pulses of energy at very short intervals, are used to remove material (e.g., drill narrow holes) by repeated thermal ablation of small quantities of material. By contrast, continuous wave (CW) lasers, which continuously deposit heat at moderate rates, can be used for fusion welding. A parametric analysis was performed to determine the feasibility of using such a laser to seal weld the fill hole of a typical Be-alloy capsule, without significantly heating and vaporizing the DT condensed at the bottom of the capsule. The top half of a 0.135 μm-thick, 2.170 μm-o.d. spherical shell with a 3 μm-diameter vertical through-hole at the top was modeled with 800 quadrilateral axisymmetric finite-elements. Beryllium properties taken from literature were used as an approximation of most capsule properties, but test data for Be-6%Cu alloy was used for the temperature-dependent thermal conductivity.

It was determined that seal welding the opening of the 3 μm-diameter hole with a 6 μm-long plug of Be-alloy would be sufficient to resist, in shear, an internal pressure of more than ten times the anticipated DT gas pressure of 400 atm at room temperature. The transient, nonlinear, thermal analysis performed with the COSMOS program calculated the time-dependent temperature distribution throughout the capsule's spherical shell, originally set at 36 K, over the time needed to melt enough metal to seal the hole. It was found that depositing ~1.2 mJ of heat at a rate of 5.7 W for ~0.2 ms on a ~22 μm-o.d. annular area surrounding the hole opening (see Fig. 3–16) would melt more than three times the desired amount of metal, without ablation. At the end of this laser pulse, the maximum temperature on the inner surface of the shell is ~62 K near the hole while the temperature rise over more than 99% of the inner surface is 4 K or less. Typically, a shell's bottom will be cooled to less than 16 K, rather than 36 K (see next section), so that DT should still remain condensed by the end of the laser pulse.

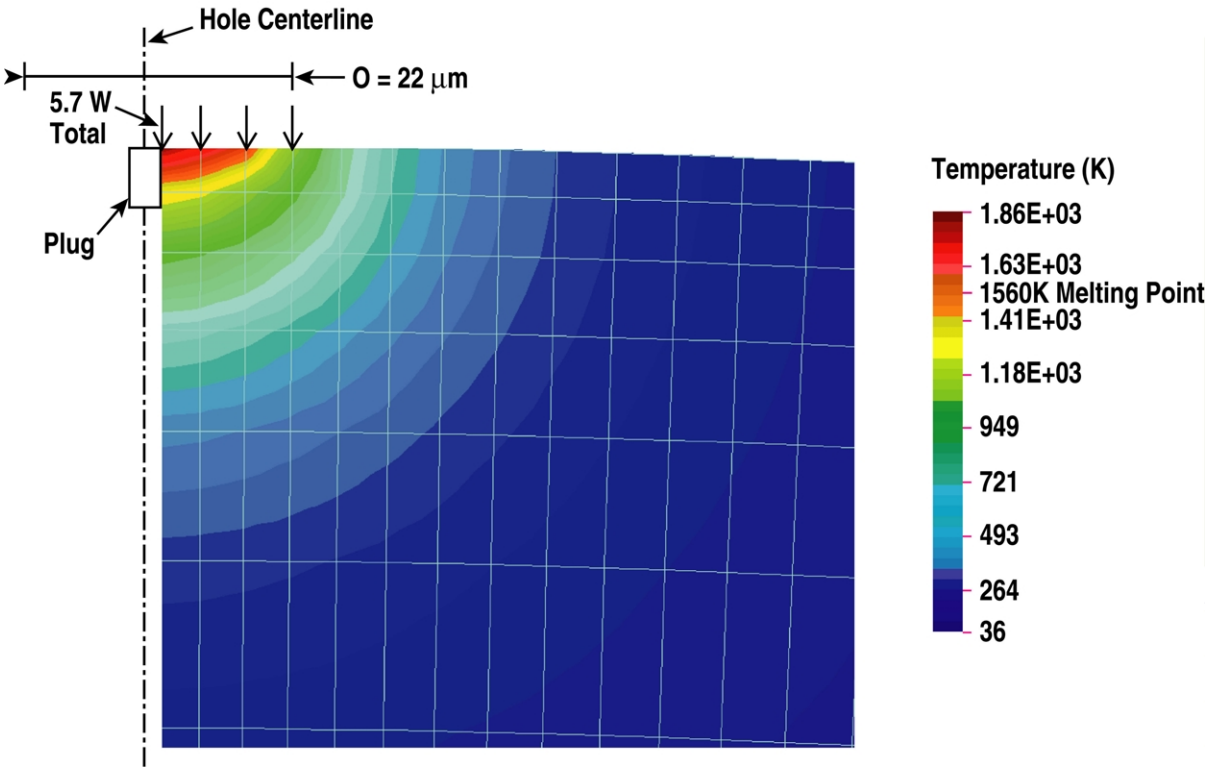

Fig. 3–16. Temperature distribution near the hole opening at 0.2 ms.

If the heat deposition rate is ten times higher, heating is too fast to control melting, the molten metal overheats and starts to vaporize. If the deposition rate is ten times lower, the heat diffuses into the bulk of the shell and, by the time the metal around the hole opening reaches its melting point, the temperature throughout the entire shell exceeds 1350 K.

Commercially available CW Nd:YAG laser systems capable of producing up to 50 W at wavelengths from 532 to 1064 nm could be used to verify the feasibility of this laser sealing approach and develop the sealing process parameters.

Thermal Analysis of a Capsule During the Cryocondensing Process. A parametric analysis was performed to determine the thermal parameters needed to fill a Be-alloy capsule by cryocondensation, as described in Figs. 3–14 and 3–15. An entire spherical shell, with the same characteristic as above, was coarsely modeled with 48 quadrilateral axisymmetric finite-elements. It was assumed that the bottom of the shell was coated with a 10 μm-thick layer of thermally conductive Apiezon N-grease (modeled as a temperature-dependent heat transfer coefficient) and that it was placed on top of a conforming spherical "cup" acting as a cold source at 16 K. A constant heat flux was applied uniformly to a spherical "cap" area at the top of the shell. The steady-state, nonlinear, thermal analysis performed with the COSMOS program calculated the temperature distribution throughout the spherical shell.

It was found that the temperature at the top of the capsule can be kept between 34 K and 36 K, as desired to keep the fill hole clear of DT condensate, with the temperature of the bottom half of the capsule ranging from 18 K to 26 K as required to condense the ambient

DT gas (Fig. 3–17). This required that a heat flux of ~68 mW be applied over a top cap area with a 45 deg full cone angle, and that the cold cap area at the bottom extend over a 75 deg full cone angle.

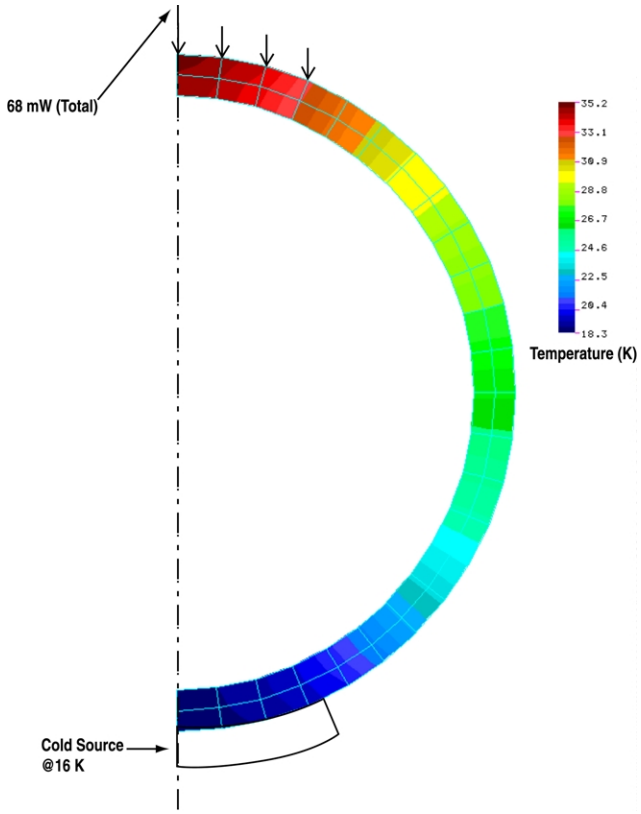

Fig. 3–17. Temperature distribution during cryocondensing.

3.2.3.2. Bonded Capsules

Conceptual Study. The conceptual design of the DT compression system and the Be capsule fill station presented in the CDR, LA-UR-01-6456, was reviewed with LANL. It was decided to determine if the design could be simplified by removing the separate internal DT-containment vessel from the pressurized bonding cell and eliminating the pressure-equalizing helium circuit, including the diaphragm compressor and the syringe pump. The pressure required of the DT compressor would also be reduced and coordination of multiple syringe and compressor strokes would not be required.

A stack of matched pairs of Be-alloy cylinders with hemispherical cavities would be heated for bonding at elevated temperature by a resistance- or induction-heating coil. The inner surface of the bonding cell would be protected from overheating by solid, rather than porous, insulation as shown in Fig. 3–18. The cell would be filled with compressed DT at room temperature, valved off, heated to bonding temperature, returned to room temperature, then valved open to the DT supply system to recover the excess DT. In this manner, the final

mass of DT-fill in the bonded capsules is solely determined by the cell's initial pressure and temperature and the bonding temperature, which are relatively easy to control and measure with accuracy. However the DT temperature, and thus its density, are not uniform during bonding. Therefore, the correlation between the measured parameters and the mass of DT sealed inside the capsules during bonding will have to be determined by experiment.

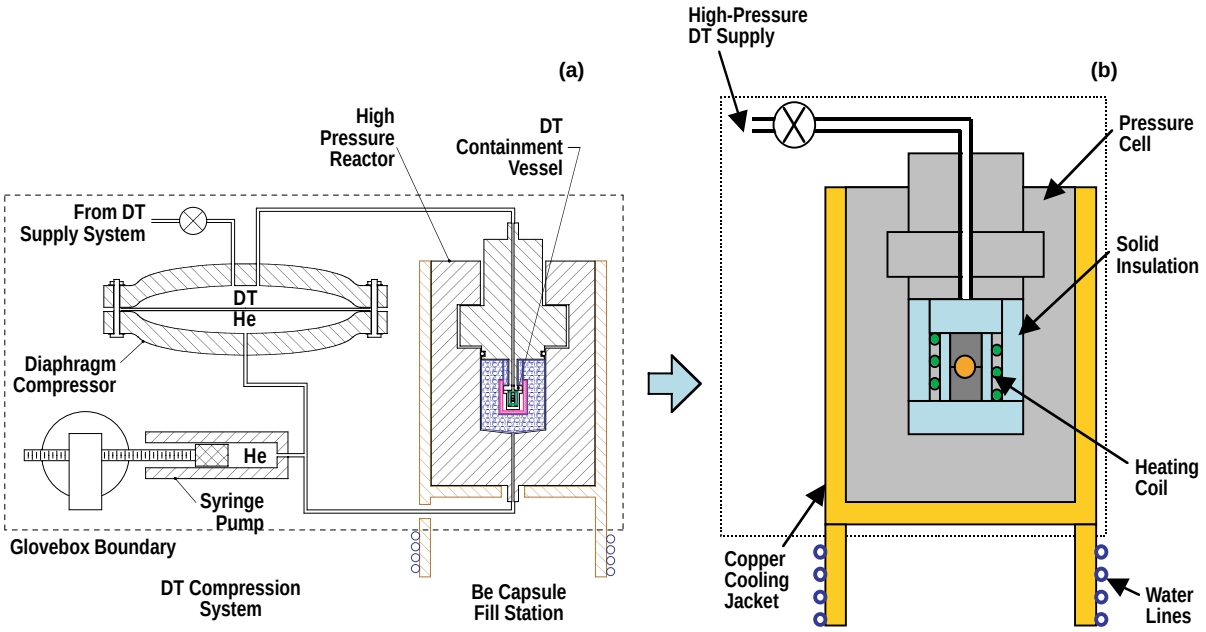

Fig. 3–18. Bonded capsules fill system. (a) CDR design. (b) Proposed concept.

Thermal Analysis of the Bonding Cell. A parametric, one-dimensional spherical thermal model of the bonding cell was analyzed with MathCAD to assess the practicality of the proposed simplified design concept. The parameters included: type, qualitative tritium compatibility, and thickness of the solid insulation material; stainless-steel cell wall thickness; and copper cooling-jacket thickness. Heating power and cell wall inner temperature were plotted versus cooling jacket temperature and insulation thickness for several candidate insulation materials. With fused silica insulation, it would take ~60 W of heating power to achieve a 700°C bonding temperature in a 5 mm-diameter Be-alloy cylinder, with respectively 5, 25, and 5 mm thickness for insulation, cell wall, and cooling jacket. This indicates that the proposed concept is feasible and can be pursued.

3.2.4. Cryogenic Pressure Loader Development and Research at LANL [John Sheliak, GA, Onsite Support at Los Alamos National Laboratory (part time)]

The Cryogenic Pressure Loader (CPL) is a highly integrated and complex system that includes a closed helium cycle cryostat with integrated permeation cell, layering sphere, and target insertion mechanism. This subsystem is contained within a sealed glove box environment and integrated into the Weapons Engineering Tritium Facility (WETF) gas handling system, which provides the necessary high-pressure DT for the capsule fill

operations. The plastic spherical targets that will be used in the CPL tests must be pressurized slowly to prevent collapsing the shells. Since the survival of the target depends on the pressurization rate, it is important to monitor carefully the pressurization process and to determine the pressurization rates. We completed the development and implementation of a new LabView software program that permits us to measure pressure data, filter any high frequency noise present from the sampling, and perform a derivative of the pressure data to provide us with a pressure rate measurement.

3.3. CENTER FOR ADVANCED CRYOGENIC LAYERING

Center head: Don Bittner (Schafer)
Technician: John Burmann (Schafer)
Designers: Raymond Fraze and Jerry Stewart (Schafer)

Overview

The NIF will require the development and fielding of complex cryogenic hohlraum target assemblies. The hohlraum target contains a spherical polymer capsule filled with frozen DT. The DT must be conformal to the interior of the capsule and be extremely smooth. The current baseline design calls for uniform DT layers approximately 100 μm thick on the interior of a 2 mm diameter capsule. The interior DT surface must be smoother than 0.5 μm rms. The development of suitable cryogenic targets is crucial to the success of NIF.

This year, we made substantial progress in using IR to layer hydrogen deuteride (HD) and D_2 and in enhancing β layering in DT. Most of the development has examined the layering of a capsule inside of a spherical container. We are now actively developing techniques to layer a capsule inside the cylindrical geometry of a hohlraum. Related to that, we report on the status of the deuterium test system (D_2TS) which will provide a test bed for engineering technologies that will be incorporated into the NCTS and to provide experimental data on D_2 layers formed in capsules without fill tubes.

3.3.1. Layering Fundamentals

There are three basic layering techniques that have been investigated or are currently under development at LLNL. The first technique, referred to as β layering, relies on the heat produced by the β decay of tritium to redistribute solid DT. The second two techniques are called enhanced layering methods since the β-layering effect is present in all targets containing tritium and these techniques serve to "enhance" the β layer. IR layering augments the β decay volumetric heating of solid DT using absorbed IR laser power. Joule heating uses an electric field typically produced by a microwave cavity to excite electrons in the gas at target center. These electrons are created by the β decay electrons and the excited electrons produce an enhanced heat flux at the gas-solid surface. Joule heating will not be discussed further in this report.

When liquid DT is quickly frozen in an isothermal shell, it forms a rough mass on the bottom of the container. Because the DT solid self heats at a volumetric rate of $q_s = 5.06 \times 10^{-2}$ W/cm^3, there are variations in the temperature of the surface of the ice as the film thickness varies. The thicker areas of the film are warmer and, consequently, have higher vapor pressures, so material tends to sublime away from these regions and recondense at the cooler

areas. If the container is isothermal, the ice surface at equilibrium conforms to the surface of the container. For pure DT, the rate at which the material migrates can be shown to be[1]

$$R_{DT} = \frac{q_s}{s\rho_s} \quad ,$$

where s is the heat of sublimation (1550 J/mol) and $\rho_s = (5.18 \times 10^{-2}\,\text{mol/cm}^3)$ is the density of the solid, so that $1/R_{DT} = 27$ min.

The temperature profile within the solid layer calculated in one dimension is

$$T(x) = \frac{-q_s x^2}{2k_s} + \frac{q_s h x}{k_s} + T_0 \quad ,$$

where k_s is the thermal conductivity of the solid, x is the distance from the inner edge of the container, h is the thickness of the ice, and T_0 is the temperature of the container. For wavelengths that are large compared to the surface thickness, the derivative of the temperature of the solid-gas interface with respect to the solid thickness becomes

$$\frac{dT(h)}{dh} = \frac{q_s}{k_s} \quad .$$

For 100 μm of DT ice, this is 0.15 K/cm. The increase in surface temperature with increasing surface thickness drives the smoothing process. An increase in dT(h)/dh will result in a smoother surface. This is the foundation of the enhancement techniques.

The quick freeze protocol just described for β layering is conceptually simple but does not produce smooth layers. Multiple crystallites nucleate during the rapid cool. Grain boundaries between these crystallites are of sufficient surface energy to remain after the β layering process comes to equilibrium and cause substantial surface defects in the final layer.[2] Quickly frozen β layers are too rough to measure by shadowgraphy. The grain boundaries disrupt the surface finish sufficiently to cause breaks in the bright band. This bright band is caused by reflection of light off of the gas-solid interface. An example from a very smooth layer is shown in Fig. 3–19. The break up of the bright band renders our analysis techniques ineffective. Quick-frozen β layers are not suitable for ignition targets.

Slowly forming a single nucleation site at a temperature just below the triple point and slowly cooling the layer approximately 80 mK at a rate of 0.25 mK/min until the layer is completely formed can produce smoother β layers. Layers formed in this manner have been made as smooth as 0.4 μm rms. However, this number is somewhat stochastic and recent data indicate that it is dependent on the specific crystal orientation of the nucleation seed

[1]Martin, A.J., et al., J. Vac. Sci. Technol. A **6**(3), 1885 (1988); J.K. Hoffer, L.R. Foreman, Phys. Rev. Lett. **60**, 1310 (1988); T.P. Bernat, et al., ICF Quarterly **1**, 57 (1991).
[2]Sater, J., et al., Fusion Technol. **35**, 229 (1999).

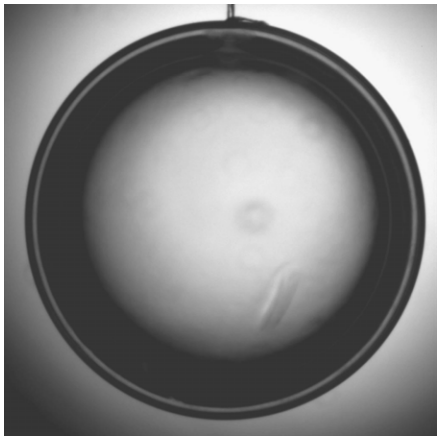

Fig. 3–19. Shadowgraph of a 125 µm layer inside of a 2 mm diameter 40 µm thick polymer capsule with a fill tube. The ice layer is the narrow white band just inside of the capsule edge. The layer roughness is 1.1 µm rms over modes 1 to 50. It is expected that removal of the fill tube and better centering of the shell will reduce the rms substantially by removing a source of low mode defects. The defect in the lower right part of the capsule is left over from where the slowly grown surface met during initial formation. The small circular defects are out of focus dust particles on the polymer capsule surface.

crystal. It is desirable to reduce this roughness to increase the robustness of the target with respect to ignition.

After formation, a DT layer can be cooled to approximately 19.3 K without degrading the surface. Cooling further causes the formation of cracks due to thermal contraction of DT. Most NIF target designs currently specify a DT layer temperature of 18.3 K. If this requirement is to be met, enhancement techniques must be applied to the layer.

3.3.2. IR Layering

To generate bulk heat for mass redistribution (with or without tritium radiation), the collisionally induced IR vibration-rotation band is excited with a laser. The solid volumetric heating rate, Q_{IR}, and thus the redistribution rate, R_{IR}, and surface roughness are adjusted by controlling the incident IR intensity. The maximum Q_{IR} for hydrogen isotopes is limited by the vibrational relaxation time to $Q_{IR} \sim 1000\, Q_{DT}$. As mentioned previously, Q_{DT} is defined as the volumetric heating rate of DT (50 mW/cm^3). These large Q_{IR} values enable control of the hydrogen layer shape as well as enhance the redistribution process in laser-heated hydrogen solids. Proof-of-principle experiments to test the viability of the IR heating process were performed using a square sapphire cell filled with either HD or D_2.[3]

Initial IR layering experiments using shells were attempted with the goal of forming a single component HD layer from a solid lump using a quick freeze protocol. As was the case with DT, the layers formed this way were all found to be extremely rough. In order to improve the quality of the inner solid surface, a technique was developed that is conceptually identical to the slow freeze technique used for the multicomponent DT layers. Here a solid HD sample is first uniformly illuminated with IR radiation and then slowly warmed until the solid melts. As soon as the solid melts, the temperature is lowered until solid starts forming in the shell. At that point, the sample temperature is held constant until the solidification process is complete. This process was developed using volumetric heating rates on the order of 8 Q_{DT} on HD layers 150 µm or greater in thickness. 100 µm layers produced in this fashion have been made as smooth as 0.8 µm rms.[4]

[3]Collins, G.W., et al., J. Vac. Sci. Technol. A **14**, 2897 (1996).
[4]Bittner, D.N., et al., Fusion Technol. **35**, 244 (1999).

In the case of both the tritiated as well as nontritiated hydrogen samples, smooth layers are formed near their respective triple points. This is, however, not the NIF design point temperature. The layers generally tend to remain smooth to approximately 0.5 K below the triple point before starting to degrade. Attempts to slowly cool smooth β layers to 18.3 K (1.5 K below the triple point), have not been successful. At high IR laser powers, on the order of 30 Q_{DT}, we have successfully produced uniform layers 1.5 K below the HD triple point (Fig. 3–20).

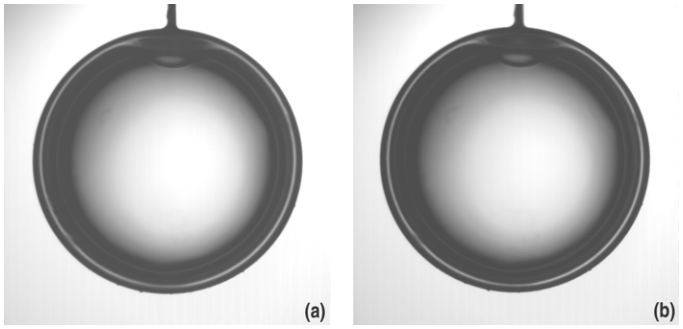

Fig. 3–20. (a) A uniform 50 μm thick HD layer formed near the triple point and (b) the same layer cooled to 1.5 K below the triple point. The layer was formed inside a 40 μm thick and approximately 1 mm outer diameter D-GDP shell with an attached fill tube. The volumetric heating rate in this case was $Q_{IR} = 30Q_{DT}$.

3.3.3. Enhanced Cryogenic Layering

3.3.3.1. DT Layering. The experimental apparatus used for β layering has been modified to permit IR enhancement of DT layers. The goal of this effort is to replicate the success of the IR enhanced layering effort on HD and D_2. It is desired to produce layers at temperatures as cold as 18 K, to produce smooth layers faster than what is possible with pure β layering, and to improve the layer quality. The development of IR enhanced DT layers is a joint effort with J. Sater (LLNL).

The greatest technical challenge for this effort has been to find a DT or D_2 adsorption line that does not excessively heat the polymer capsule. This was not an issue for the IR experiments on HD. The HD adsorption lines are in a region of the IR spectrum where deuterated polymer (D-GDP) does not have appreciable absorption. The IR adsorption lines of DT and D_2 are shifted from those of HD due to the difference in nuclear masses.

The adsorption of IR energy in the capsule can cause a number of problems. Excess heating of the capsule implies a larger ΔT between the capsule and the thermal boundary of the experiment. Since the capsule is cooled by gas conduction, this excess heat may increase nonuniform cooling effects due to convection. Also, any low mode variations of the polymer thickness will imprint onto the DT layer. Finally, the excess heat limits the amount of IR that can be used to enhance the layer smoothness since the total cooling capacity is finite.

For D_2 and HD, there is one primary absorption line each that is suitable for volumetric heat generation. In the case of DT, there are several absorption lines from which to choose. None of the lines is an obvious choice. We are using redistribution time constant measurements to determine which absorption lines are optimal for IR heating experiments in DT. Redistribution time constant measurements determine how well IR power is coupled into the solid. The more IR absorbed by the solid, the faster the solid redistributes and the shorter the redistribution time.

A simple model shows the IR redistribution time to be inversely proportional to the incident laser power. The volumetric heating rate generated by the IR in a weakly absorbing ice layer is given by

$$Q_{IR} = \alpha I_0 \quad ,$$

where α is the absorption coefficient and I_0 is the incident IR flux intensity. The time constant is then given by

$$\tau_{IR} = \rho l/Q_{IR} = \rho l/\alpha I_0 \quad ,$$

where l is the latent heat and ρ is the solid density. Since the ice is weakly absorbing, most of the IR power, P, losses occur in the 4% absorbing integrating sphere of area A_{IS}, out viewport openings, etc. Combining these corrections into a scale factor constant, C, one gets the time constant expression

$$\tau_{IR} = (\rho l/\alpha)(CA_{IS}/P) \quad ,$$

or

$$P*\tau_{IR} = CA_{IS}\, \rho l/\alpha \quad .$$

At a particular wavelength, the product $P*\tau_{IR}$ is a constant. As the incident wavelength is changed, the absorption coefficient will change. The goal is to illuminate the DT ice with IR at wavelengths where the ice absorption, and absorption coefficient, α, is as large as possible. A large α means a low $P*\tau_{IR}$.

Since DT has a β decay driven volumetric heating rate, Q_{DT}, the total volumetric heating rate generated under IR illumination is $Q_{TOTAL} = Q_{DT} + Q_{IR}$. The measured time constant is

$$1/\tau_{meas} = (Q_{DT} + Q_{IR})/\rho l = 1/\tau_{DT} + 1/\tau_{IR} \quad .$$

This expression can be rewritten as

$$\tau_{IR} = \tau_{meas}\,[1 - (\tau_{meas}/\tau_{DT})]^{-1} \quad ,$$

to extract the time constant associated with the IR illumination.

Time constant measurements were performed at various wavelengths over the range from 3.14 to 3.51 μm. Measurements were made both on and off absorption peaks. Periodic β heating time constants measurements were made and used to determine τ_{DT}. The compiled results from all experiments are plotted in Fig. 3–21. At wavelengths where multiple time constant measurements were performed, the $P*\tau_{IR}$ results were averaged. The error bars are an estimate of the error in determining the time constant. For the β heating time constant measurements, the solid layer interface was usually well defined and the variation in time constant was typically less than 10%. However, in some cases, the solid layer interface was difficult to track and resulted in a relatively poor time constant fit to the data. The estimated error for these data sets and the value used for the results in Fig. 3–21 is ±20%.

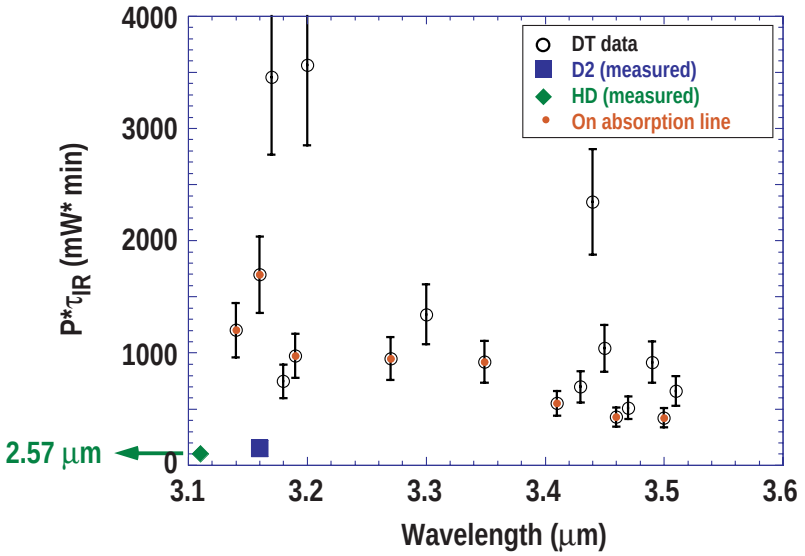

Fig. 3–21. Plot of $P^*\tau_{IR}$ versus wavelength. Measurements made on absorption lines are indicated by a red dot. For reference, $P^*\tau_{IR}$ for the HD (2.57 μm) and D_2 (3.16 μm) lines are also shown.

The results, to date, indicate that several absorption lines are potential choices. Near the D_2 line $P^*\tau_{IR}$ minima occur at 3.18 and 3.19 μm. Based on the available relative absorption data,[5] we expected $P^*\tau_{IR}$ to be larger at 3.18 μm than at 3.19 μm. The lowest $P^*\tau_{IR}$ values are at 3.46 and 3.50 μm. These results must then be compared to the absorption coefficients for the shell materials. Table 3–1 lists absorption coefficients[6] for H-GDP, D-GDP, and H-polyimide along with the absorption coefficient in D_2 and the estimated coefficient for DT. Ideal conditions require maximum ice absorption and minimum shell absorption. For example, in the case of D_2, if one has a capsule with the same volume in the H-GDP shell as in the ice layer, then there can be up to 2.5 times as much heat generated in the H-GDP as in the ice. The yellow highlights indicate the shell material with the minimum shell-to-ice absorption at the specified wavelengths. Additional experiments are planned to extend the wavelength range of our measurements to access DT absorption lines out to 3.9 μm.

3.3.3.2. IR Layering of HD in Hohlraums. Previous IR heating experiments were performed by injecting an IR laser beam into an integrating sphere. Since the integrating sphere wall was a diffusely scattering surface, the laser light was simply injected through one of the viewports or through an optical fiber. The primary constraint was to make sure the light did not hit the capsule before first hitting the integrating sphere wall. The symmetry of the integrating sphere provided the necessary illumination symmetry at the capsule. This is not the case for hohlraums. The nonspherical symmetry of the hohlraum complicates the IR injection scheme. This has required a significant modeling effort in addition to setting up the characterization and developing an understanding of how to make suitably rough hohlraums.

[5]Clark Souers, P., Hydrogen Properties for Fusion Energy, (University of California Press, 1986), pp. 328-330.
[6]Cook, R., A. Nikroo, and S. Letts (private communications).

R. London, B. Kozioziemski, and R. McEachern, all of LLNL, have contributed significantly to our joint effort on this project.

TABLE 3–1
ABSORPTION COEFFICIENTS FOR SHELL MATERIALS AT SELECTED WAVELENGTHS
(Shell Absorption Data from Cook et al.)

	Wavelength (μm)	Shell	a_{shell} (1/mm)	a_{ice} (1/mm)	a_{shell}/a_{ice}
D_2	3.160	H-GDP	1.0	0.4	2.5
	3.160	D-GDP	2.3	0.4	5.8
	3.160	H-polyimide	5.4	0.4	13.5
D–T	3.190	H-GDP	0.7	~ 0.1	7
	3.190	D-GDP	2.0	~ 0.1	20
	3.190	H-polyimide	9.1	~ 0.1	91
	3.464	D-GDP	2.3	~ 0.1	23
	3.464	H-polyimide	4.1	~ 0.1	41
	3.464	H-GDP	72	~ 0.1	720
	3.503	D-GDP	1.2	~ 0.1	12
	3.503	H-polyimide	3.0	~ 0.1	30
	3.503	H-GDP	65.2	~ 0.1	652

Last fiscal year, we reported on our initial hohlraum experiments.[7] Over the past year, we made improvements to the hohlraum experiment. We primarily investigated IR injection through one laser entrance hole (LEH). We incorporated optics at the front end of the IR laser (Fig. 3–22) allowing us to split the output beam into two beams and to couple each beam into an optical fiber for transport to the experiment. To be able to provide flexibility in adjusting the relative amounts of power between the two beams, we have inserted IR polarizers in both beam paths. We acquired four IR polarizers to determine which ones are most suitable for our application (one from Optics for Research, two different types from Optometrics, and one from Molectron). The wire grid polarizer from Molectron and the holographic polarizer from Optometrics had the lowest transmission losses. Of the two polarizers, the Optometrics holographic polarizer was significantly lower in price. Over the past year, neither polarizer has shown any apparent degradation due to the incident IR.

A new lower absorbing hohlraum with a roughened interior surface[8] was installed in the experiment. The new hohlraum has a 4 μm rms surface and infrared absorption reduced to between 10% to 15%. This new hohlraum performs well in the experiment, coupling the IR into the ice more efficiently than the previous hohlraum. The ice can be heated to higher

[7]Project Staff, "Inertial Confinement Fusion Annual Report," General Atomics Report GA–A23852 (2001), pp. 3-90–3-92.
[8]Project Staff, "Inertial Confinement Fusion Annual Report," General Atomics Report GA–A23852 (2001), pp. 3-55–3-57.

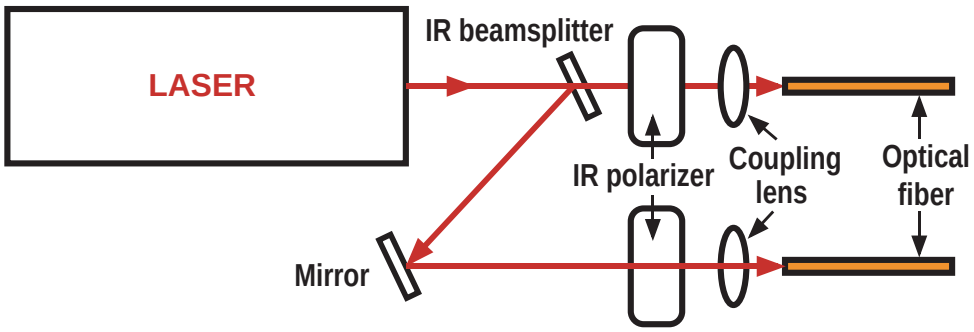

Fig. 3–22. Sketch showing how the IR beam is split and injected into fibers for transport to the IR injection optics. IR polarizers in each beam path allow for independent power adjustments.

powers since less energy is coupled into the hohlraum and the temperature drop between the hohlraum and cryostat cold tip is greatly reduced. To improve our diagnostics, cernox thermometers have been added. There is now a thermometer mounted at the center of the hohlraum barrel, a second thermometer near one LEH, and a third thermometer at the bottom of the copper support (Fig. 3–23). Thermometers placed in the center and one end of the hohlraum as well as the base of the copper support structure allow us to compare the heat conduction to models.

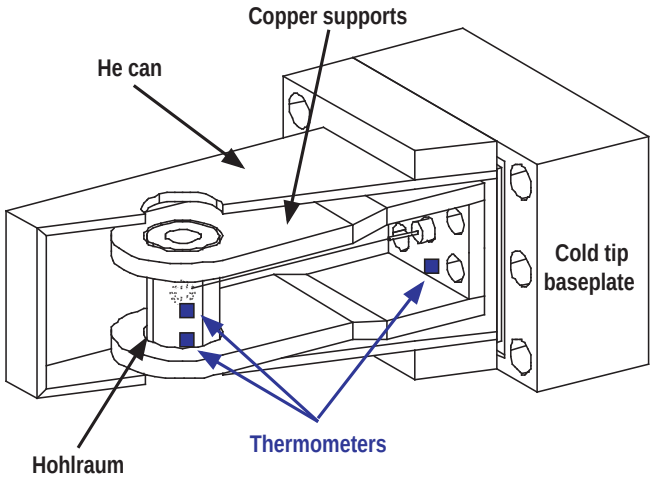

Fig. 3–23. Sketch indicating the relative locations of the cernox thermometers on the hohlraum assembly.

Beam shaping and positioning provide for control of the P1 and P2 modes in the solid layer. The beam shaping is done by taking the two fiber outputs (Fig. 3–22) and passing each beam through a metal axicon. The axicon consists of a pair of cylindrically symmetric mirrors that produce a focused ring of IR. The ring-shaped beams provide for cylindrically symmetric injection so that the IR scatters off the inner hohraum wall before passing through the capsule. By moving the beam radially about the hohlraum axis and adjusting the beam intensity, one is able to control P1 about the hohlraum axis. P2 control is produced by

moving the focal point of the beam along the hohlraum axis as well as adjusting the relative intensity of the two injected beams. Figure 3–24 shows P2 control by adjusting where the injected IR beam hits along the hohlraum wall. Experiments this past year have demonstrated P1 and P2 control of the ice layer.

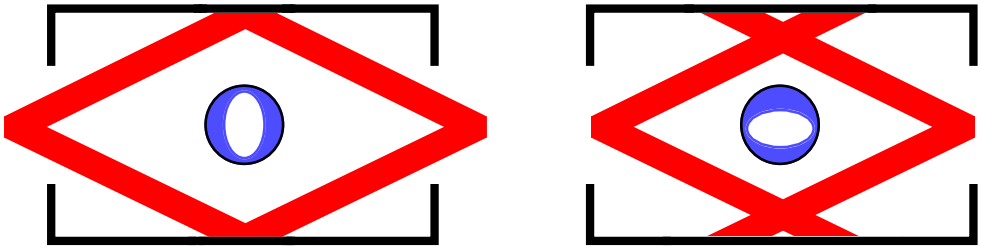

Fig. 3–24. IR pointing along the hohlraum axis controls P2 in the ice.

3.4. CENTER FOR TARGET COMPONENT FABRICATION AND FABRICATION DEVELOPMENT

Center head: James Kaae (GA)

Scientists: James Kaae, Joe Smith, and Emilio Giraldez (GA)

Technicians: Clyde Shearer, David Woodhouse, and Jason Wall (GA)

Overview

In FY02, fabrication of target components was our major activity. We produced a range of ICF target components for LLNL, LANL, SNL, and UR/LLE using combinations of high-precision micromachining, physical vapor deposition, and electroplating. Altogether in FY02, we produced 1851 very precise ICF target components.

Although some development is needed to fabricate many of the new orders for components, a significant advance this year was the incorporation of machining with our Kern high-precision milling machine into many of our fabrication processes. This effort is discussed in Section 3.4.2.

3.4.1. LLNL, LANL, and SNL Deliveries (Jim Kaae)

Near-term fabrication and delivery of target components of many different designs and made of many materials is critical for the success of the DOE ICF program. We provided this important support for experiments by LLNL, LANL, and SNL scientists.

3.4.1.1. LLNL Deliveries. Nine hundred and fourteen (914) components were produced for LLNL in FY02. Foremost among these were 264 gold-plated copper cylindrical hohlraum mandrels of 12 different geometries. These components ranged from 1.6 to 6.0 mm in diameter and from 1.2 to 10.0 mm in length. Dimensions were typically controlled to within ±2 µm. (Similar dimensional control was achieved in all of the components that we produced.) An example of a hohlraum with 25 µm thick walls formed when the copper mandrel was leached out is shown in Fig. 3–25.

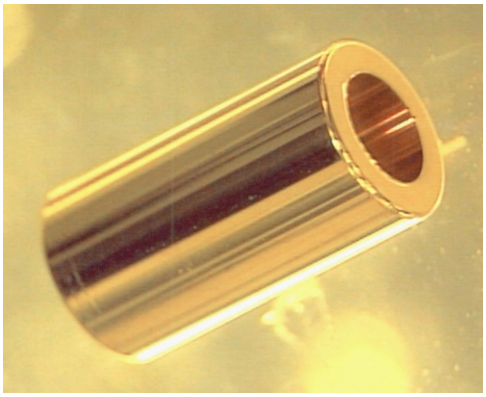

Fig. 3–25. A gold hohlraum with 25 µm thick walls.

One set of 10 similar copper hohlraum mandrels and two sets of 54 cylindrical mandrels of two different designs were coated first with a thin (2 µm) layer of gold and then with a thicker (100 µm) layer of epoxy rather than a single layer of gold. A photograph of one of these hohlraums is shown in Fig. 3–26.

Fig. 3–26. A 1.6 mm diameter hohlraum which is 2.55 mm long with a wall made up of 2 µm of gold and 100 µm of epoxy.

We also produced 26 pure aluminum cylindrical mandrels of two different geometries. An example of a similar aluminum hohlraum mandrel is shown in Fig. 3–27. They are used for coating with mixed elements to form "cocktail" hohlraums.

Eighty-three (83) of seven different types of gold coated cylinders also were produced. Some of these were half-round cylinders, some were square cylinders, and some were round cylinders. A photograph of a square cylinder with the copper leached out is shown in Fig. 3–28, and an example of a half-round cylinder with the gold leached out is shown in Fig. 3–29.

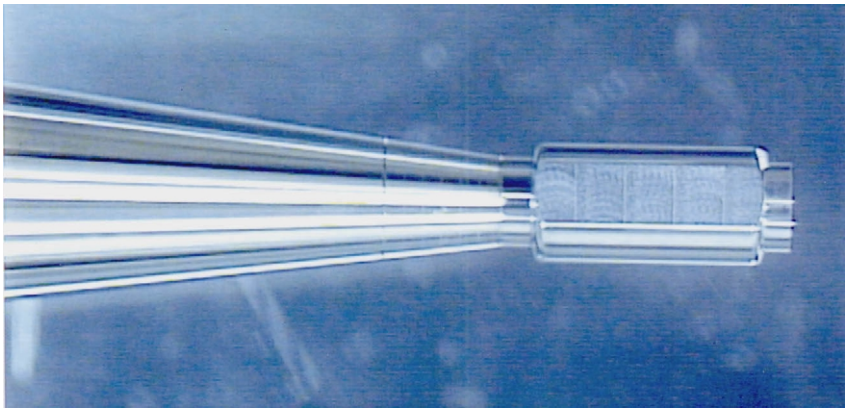

Fig. 3–27. An aluminum mandrel that will be used to form a cocktail hohlraum. A flat runs the length of the hohlraum. The small diameter regions at each end of the mandrel will become the laser entrance holes.

Small gold truncated cones similar to the one shown in Fig. 3–30 were another type of component that we produced. Altogether, we made 35 of these in three different geometries. As with the cylindrical hohlraums, these were made on copper mandrels.

Yet another gold-coated copper component that we produced this year was a small cup. One hundred and forty-two (142) of these cups in eleven different designs were fabricated. Examples of the gold cups are shown in Fig. 3–31.

Fig. 3–28. A 0.6 mm square gold cylinder that is 2 mm long. The wall thickness is 25 µm.

Fig. 3–29. A half round gold cylinder. The diameter is 1.6 mm; the length is 2 mm; and, the wall thickness is 25 μm.

Fig. 3–30. A small truncated gold cone used as part of an ICF target component. The cone is sitting on a dime.

Two hundred and thirty-three (233) square pure aluminum or copper witness plates of eleven different designs also were produced for LLNL. Examples of some of these designs are shown in Fig. 3–32.

Other components that we produced for LLNL in FY02 were: gold trapezoidal shields (16), sine-wave profiles in aluminum (33) and copper (1), NIF gold cryogenic hohlraums (16), gold disks (7) with controlled roughness and gold washers (27).

Fig. 3–31. A set of gold cups of different diameters and lengths. The diameters range from 0.64 to 0.16 mm and the lengths range from 0.6 to 0.15 mm.

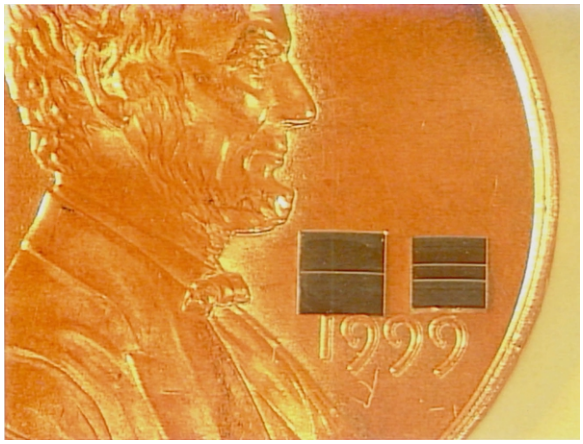

Fig. 3–32. Square pure aluminum witness plates shown relative to a penny. The plate on the left has a single step in it while the plate on the right has two steps.

3.4.1.2. LANL Deliveries. The LANL deliveries in FY02 consisted of precisely machined cylinders and disks.

One set of gold cylinders had a parallel circular cross section and a conical section but were of various lengths; another set of gold cylinders were circular in cross section with different diameters and lengths; and a third set were copper with circular cross sections and were in special holders.

The disks had precisely defined thicknesses and very smooth surfaces. Twenty-eight (28) were of copper, and 28 were of gold of four different geometries. An example of one of these disks is shown in Fig. 3–33.

Fig. 3–33. A gold disk 5 mm in diameter and 1.0 mm thick. The surface is very smooth.

3.4.1.3. SNL Deliveries. Of the 252 components produced for SNL in FY02, 46 were conventional gold hohlraums similar to the one shown in Fig. 3–25. Another 39 were gold hohlraums that were split in half; half of these had a small hole in the body of each hohlraum. Accompanying each pair of halves was a small thin gold disk that was to be inserted in the assembled hohlraum as a shine shield.

Ten (10) stepped aluminum witness plates similar to the one on the left in Fig. 3–32 were produced, characterized and delivered to SNL in FY02.

We also produced a variety of miscellaneous components for SNL. Among these were: two quasi-spherical gold shells, two aluminum crystal substrates, and eight large thin aluminum cylinders.

3.4.1.4. UR/LLE Deliveries. The UR/LLE deliveries consisted of two types of components. The majority were stepped aluminum witness plates of the type shown in Fig. 3–32. Three hundred and thirty-six (336) of these plates of seven different designs were produced, characterized, and delivered.

The second type of component produced for UR/LLE was gold cylinders. Eighteen (18) of these were produced for UR/LLE in FY02.

3.4.2. Components Produced by Micromilling (Emilio Giraldez)

The design of the target components for ICF is constantly changing and some designs require milling instead of turning to micromachine the target components. The Target Component Fabrication Group has a five-axis micromill shown in Fig. 3–34 which has been used to fabricate witness plates, flyer plates, disks, trapezoidal shields, flats, rectangular tubes, and slots and holes in hohlraums. Gold, copper, aluminum, and plastic have been micromilled into different shapes.

The cryogenic hohlraum, shown in Fig. 3–35, is a double wall hohlraum with a roughened inner surface fabricated by diamond turning and gold and copper electroplating. The micromill is used to machine the slots, notches, and a sight hole that are part of the hohlraum design. The outer hohlraum wall has sixteen slots 250 µm wide of two different lengths and at different angular orientations. The outer wall flange has two 250 µm radius notches 180 deg apart and there is a 125 µm hole in the inner wall. The machining of these three configurations is done using the same program. The micromill has the capability of storing tool diameter and tool height in a tool table that can be called within the program to change tools. In the program to machine the cryogenic hohlraum, the sight hole is machined first. The hole is machined through copper to a depth of about 1 mm to reach the inner wall of the gold hohlraum. With the axis of the hohlraum oriented horizontally, the hole is drilled with a 125 µm diameter drill. After the hole is drilled, the program stops allowing the operator to change tools. The drill is changed to a 250 µm diameter end mill to mill the 16 slots. The part is indexed around its axis to achieve the desired slot length and angular location. After milling the slots, the hohlraum is tilted vertically. The program stops for a second time and the tool is changed to a 500 µm diameter end mill. The two opposing notches are then milled.

Fig. 3–34. Photograph of the KERN five-axis micromill.

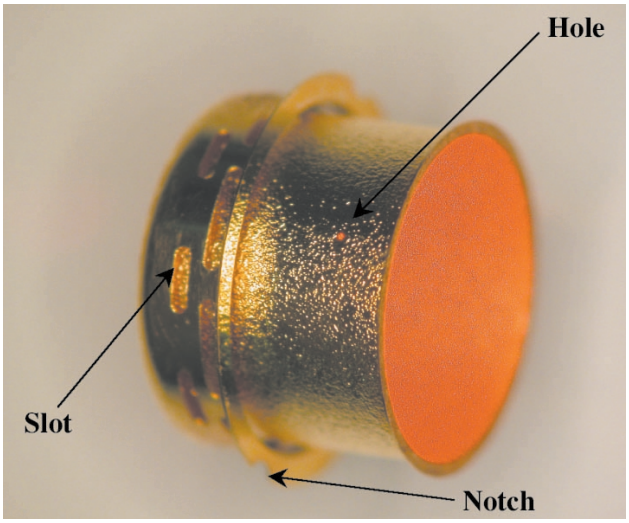

Fig. 3–35. Photograph of the cryogenic hohlraum. Arrows point to those areas that are micromachined using the KERN micromill.

Figure 3–36 shows a view of the setup utilized during the milling of 10 mm diameter by 2 mm thick gold flyer plates. The nozzle to the right of the spindle sprays the lubricant-coolant during the milling process. A carbide or high-speed steel mill is used to roughen out the shape. The flyer plate is finish machined with a diamond tip mill to meet the size and tolerance requirements.

Figure 3–37 shows a schematic of a type of trapezoidal shield that has been fabricated using the micromill. The shield is 6 mm long, 7 mm wide, and 2 mm tall with a 3×2.54 mm flat. Two of the sides of the trapezoid are at an angle of 135 deg with respect to the flat; the

side opposite the open end is at an angle of 150 deg to the flat. The trapezoidal shield is fabricated by first milling a copper mandrel 10 mm in diameter into the shape of a trapezoid. The copper mandrel is gold electroplated to the required shield thickness. The gold-plated mandrel is finish machined to its final dimensions using the micromill a second time. Figure 3–38 is a photograph of the finished trapezoidal shield.

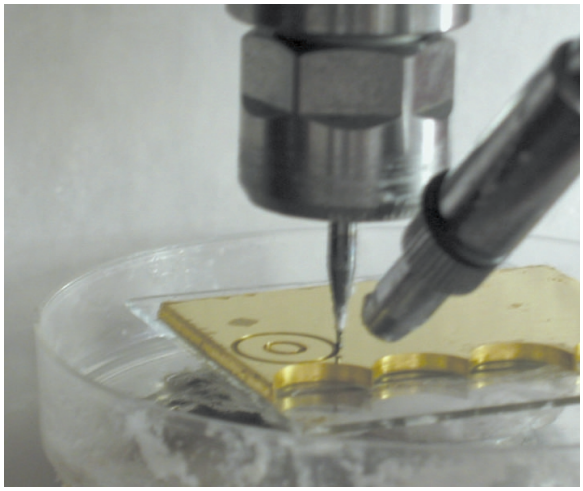

Fig. 3–36. Photograph showing the machining of a gold flyer plate in the KERN micromill.

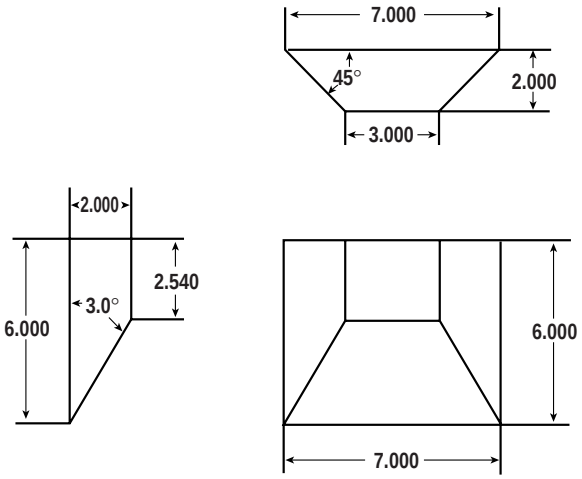

Fig. 3–37. Schematic showing the trapezoidal shield with dimension.

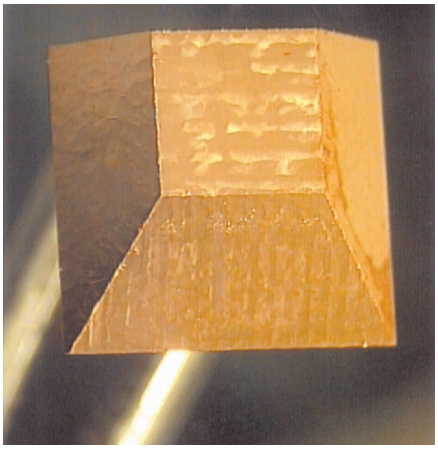

Fig. 3–38. Photograph of a finished trapezoidal shield.

3.5. CENTER FOR POLYMER AND COATINGS AND FOAM CAPSULE DEVELOPMENT

Center head: Abbas Nikroo (GA)

Scientists: Don Czechowicz, Barry McQuillan, Reny Paguio, Joe Pontelandolfo (GA), and Masaru Takagi (LLNL)

Technicians: Erwin Castillo, and Wes Baugh (GA)

3.5.1. Deliveries and Introduction

As in the past several years, the three-step depolymerizable mandrel technique (Fig. 3–39) was used to fabricate undoped or doped glow discharge polymer (GDP) shells for deliveries to UR/LLE. The depolymerizable mandrel technique is essential for fabrication of such shells. The delivery numbers are summarized in Table 3–2. These capsules were all provided in a timely manner in support of UR/LLE's laser fusion experimental program. In addition, many other capsules and targets were delivered as samples, which were not used in implosion experiments but rather for other developmental activities at UR/LLE. As part of the deliveries, we continued to supply significant numbers of thin-walled CH and CD capsules for use in cryogenic shots at UR/LLE in support of this important activity. We also performed extensive mechanical and permeation testing of such shells to provide valuable information for successful high pressure filling and cryogenic cooling (Section 3.5.2). We continued to fabricate batches of poly(α-methylstyrene) (PAMS) shells as needed, which serve as mandrels for UR/LLE shell fabrication depolymerizable mandrel technique to keep a fully stocked inventory of such. This allowed rapid and timely response to the various delivery requests from UR/LLE including several very short lead time requests (approximately two weeks). In FY02, we examined the dependence of the quality of the final GDP on the quality of the PAMS mandrel used more closely (Section 3.5.3). We continued delivery of multi-layered targets containing buried doped diagnostic layers such as titanium or chlorine-doped CH as well as examining the confinement of these dopant atoms to the desired position within the shell (Section 3.5.4). Also, a problem involving premature mass loss of PAMS shells at lower than expected temperatures was examined and solved (Section 3.5.5).

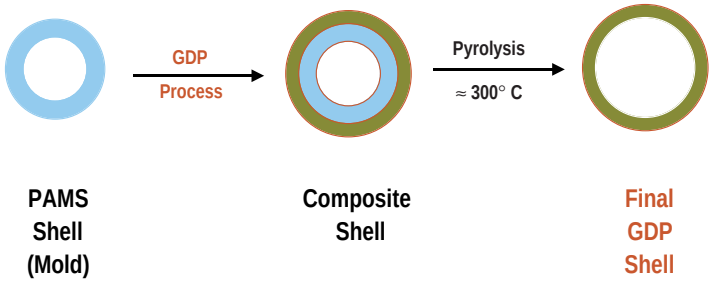

Fig. 3–39. Depolymerizable mandrel technique is used extensively in capsule fabrication for UR/LLE. PAMS mandrels are overcoated with GDP and after pyrolysis of the PAMS mandrel, the final capsule is a pure GDP shell.

TABLE 3–2
UR/LLE DELIVERIES FOR FY02

Polymer Capsules		Glass Capsule Orders	
Orders	Capsules	Orders	Capsules
58	1033	1	47

We embarked on a developmental effort to fabricate foam shells for future use at UR/LLE with direct financial support from the University of Rochester which was beyond the DOE base contract. We were able to fabricate such shells using several foam chemistries. Resorcinol-formaldehyde (RF) was chosen as the chemistry of choice because it leads to transparent foam, which allows optical characterization of shells for both fabrication purposes and cryogenic layering purposes. Developmental runs were performed to produce shells with good sphericity and wall uniformity. The progress on this task is reported in Section 3.5.6.

3.5.2. Cryogenic Capsule Development and Mechanical Testing

Thin-walled shells are needed for cryogenic experiments at OMEGA. These shells have been made at GA for the past several years. These shells are filled at the OMEGA cryogenic facility with ~1000 atm of D_2 and cooled cryogenically to freeze the D_2. In the last two years, a developmental effort led to routine fabrication of shells with superior strength and permeation properties, which allows more reliable and rapid filling of shells at the OMEGA cryogenic facility. These shells are made using a modified GDP coating process and are dubbed “strong” shells in contrast to those made by traditional GDP deposition that are called “standard” shells. Part of the successful developmental effort was aimed at reliable and reproducible fabrication of these thin-walled shells. Knowledge of buckling strength and permeation properties of these shells is essential for a proper filling schedule to ensure survival of shells during the high pressure fill. To obtain much needed data, extensive buckle testing of shells was undertaken in FY01 which was reported in the FY01 annual report.

In FY02, further testing of shells was performed; in particular, extensive burst testing of shells was done for the first time. This became necessary as some thin-walled shells were failing the cooldown step in the OMEGA facility in what appeared to be a bursting mode. Due to differential cooling rates within the different parts of the cryostat used at OMEGA and the shell itself, the shells may experience a bursting pressure during cooldown. Also, there appeared to be excessive and unexpected variability in the survival of shells even within the same batch shells. Therefore, the need for obtaining burst strength data on these shells became urgent.

In response to this urgency, we obtained extensive burst test data on 3–4 μm CD shells, which is the typical thickness currently used on OMEGA, from five different production batches. Due to limitations of the burst testing apparatus, the highest burst test pressure was 200 psi. The burst testing sequence was monitored in real time as the test apparatus allows

direct optical access to the shells under examination. The surviving shells were all tested for gas holding capability by measuring the argon permeation time constant to eliminate the possibility of unseen micro-cracks. All shells that survived the burst tests had a measurable argon permeation time constant typical of CD shells indicating the absence of micro-cracks. Figure 3–40 summarizes the data. Figure 3–40 shows both the failure and last survival pressure of the shells. In particular, all 89 shells tested survived 100 psi, establishing a lower limit for burst strength of shells of this wall thickness range. This is most likely well beyond any burst pressure the shells may experience during the OMEGA cooldown step. The spread in the data shows the variability of the burst strength of various batches made in different coating runs. This data alleviated the concerns regarding shells in two respects. It is unlikely that the shells are subjected to such high burst pressures during cooldown. Also, while there is some spread in the data, since the burst strengths of most shells tested lie in a very tight range, batch-to-batch variations were shown to be minimal.

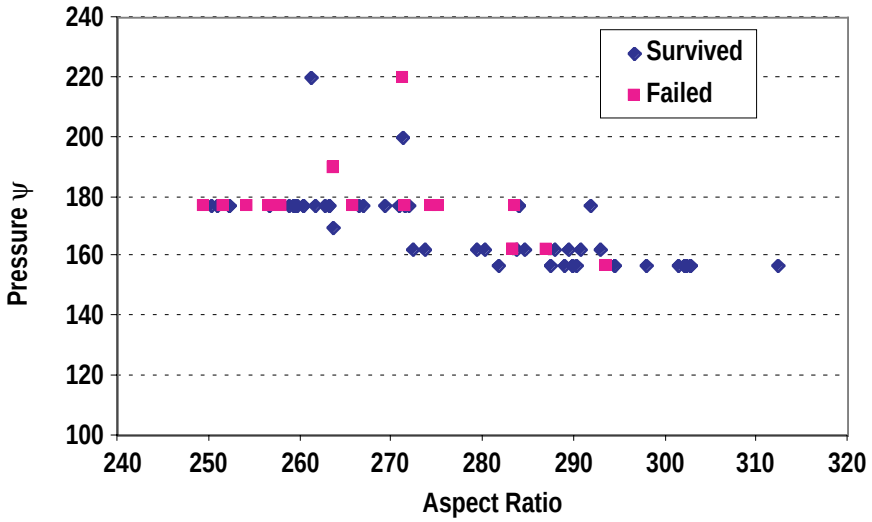

Fig. 3–40. Burst testing results for over 80 thin-walled (≈3–4 μm) CD shells from five different batches. All shells survived at least 100 psi burst test. As can be seen, most shells burst in a rather narrow range indicating minimal shell-to-shell and batch-to-batch variability in the strength of shells.

We also further studied the general mechanical properties of thin-walled shells of various types currently used at UR/LLE for cryogenic experiments, including “strong” CH and “standard” CH, to build a database on such frequently needed properties. In particular, we examined the effect of wall thickness variation on the strength of shells. A matrix of experiments was performed where shells of thicknesses in the range of 2 to 5 μm were fabricated using both the “standard” GDP technique and the “strong” technique. All shells had diameters of ~920 μm to within <5%. Batches of shells were made for buckle and burst testing and the values reported are averages of at least 10 shells. Shells were tested in a system with direct optical access, which is essential, especially for the buckle testing

measurements since some shells actually bounce back after buckling. The optical window arrangement limited the maximum pressure obtainable in the system to 19 atm.

Figure 3–41 shows the buckle strength of "strong" CH shells as a function of shell aspect ratio (AR). Buckle strength of an *ideal* thin shell is related to its dimensions and the material elastic modulus by

$$P_{buckle} = \frac{8E}{\sqrt{3\left(1-\nu^2\right)}}\left(\frac{1}{AR}\right)^2 \quad . \tag{1}$$

Where E and ν are the Young's modulus and the Poisson's ratio of the shell material and the AR is the ratio of the shell diameter to its wall. For the strong shells, the buckle pressure does vary linearly with the AR as expected for ideal thin-wall shells. However, the same is not true for "standard" shells. This is shown in Fig. 3–42 where the Young's modulus is calculated using Eq. (1) as a *figure-of-merit* for shell strength, which factors out the differences in AR. The first observation is that this figure-of-merit for "standard" CH shells varies with AR unlike the "strong" shells. It means that in practical terms, "standard" shells become weaker in buckling as the wall thickness decreases faster than that expected for an ideal thin-wall shell. Therefore for "standard" shells, it is not correct to make strength extrapolation based on Eq. (1) for varying thicknesses. The calculated Young's modulus for "standard" shells reaches a plateau at about 2 GPa for thicknesses beyond ≈5 μm as evidenced in our previous unpublished measurements. The second observation from Fig. 3–42 is that the "strong" shells are indeed stronger in buckling as evidenced by the larger Young's modulus.

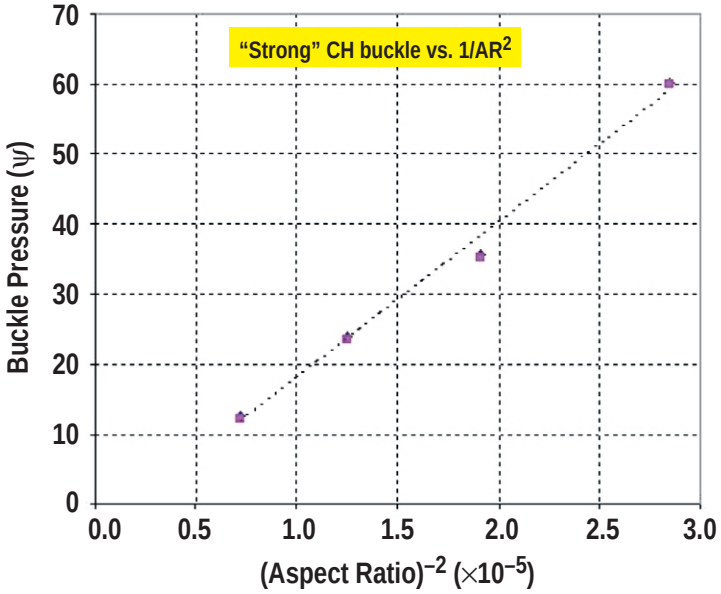

Fig. 3–41. The "strong" shells follow the expected ideal thin shell behavior in buckling as described by Eq. (1) in the text.

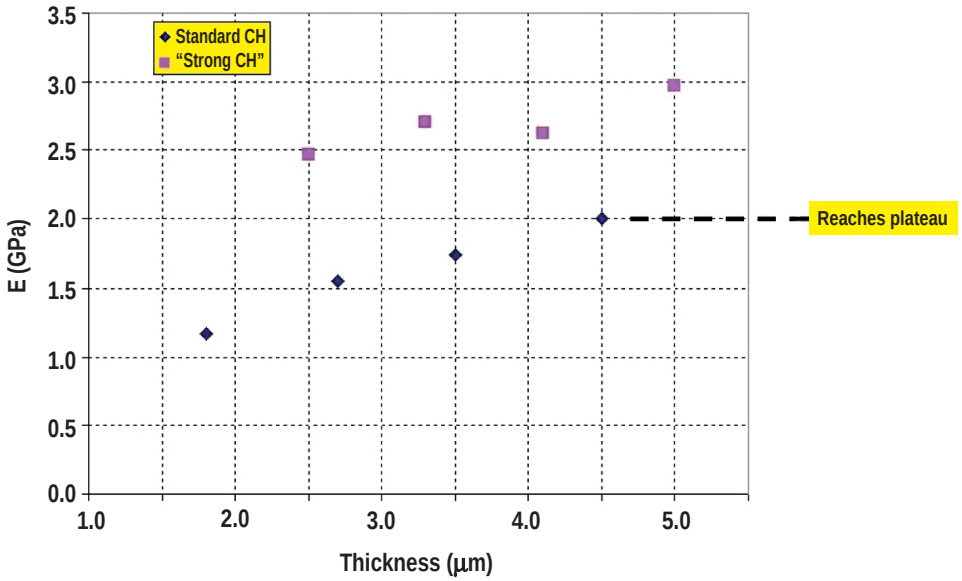

Fig. 3–42. Plot of the calculated Young's modulus of thin "standard" and "strong" shells as a function of shell AR using Eq. (1) as explained in the text. The Young's modulus of "strong" shells is indeed higher than "standard" shells. In addition, unlike "strong" shells, "standard" shells deviate from the ideal shell behavior, as the calculated Young's modulus is AR dependent.

The burst strength of the two types of CH shells was also examined for the various wall thicknesses. The burst strength of an ideal thin shell is inversely proportional to its AR:

$$P_{burst} = \frac{4\sigma}{AR} \quad , \tag{2}$$

where σ is the tensile strength of the material. In the same spirit as in Fig. 3–42, Fig. 3–43 shows the calculated tensile strength of the two types of shells. The tensile strength of "strong" shells is similar to that of "standard" shells for the thinnest shells examined (≈2 μm); however, unlike the "standard" shells, it appears to grow larger with wall thickness. Unfortunately, the safety limit of our apparatus did not allow us to increase the pressure enough to burst ≈5 μm "strong" shells. So, it is difficult to deduce a definite trend for the "strong" shell burst strength with increasing wall thickness. The "standard" shells on the other hand, had a constant tensile strength, as expected, from Eq. (2). We hope to extend these measurements in the future; in particular, by performing them at both higher and lower temperatures.

3.5.3. GDP Shell Low-Mode Surface Finish Dependence on PAMS and Pyrolysis

It is well-known that PAMS mandrels which are not round, have rough surfaces, or have nonuniform walls yield final GDP shells which are similarly not round, have rough surfaces, or nonuniform walls. A concern which had been raised in the previous years in production of PAMS shells was that some batches of shells exhibited an unwanted semi-regular low-mode wrinkling of the surface, the so-called "mode 10" problem. While some theories have been

presented to explain this wrinkling behavior of the shell surface, the exact cause is still not known for certain. Significant effort has been expended in removing such surface defects. However, there was no systematic study of whether such features were directly transferred to the final GDP shell. This question is especially justified given that the final step of GDP shell production involves a heating and cooling cycle of the GDP over-coated PAMS mandrel (300°C for typically 8 h followed by cooling over several hours). During this process, the GDP shell shrinks by as much as 5% in diameter and wall thickness. Such a treatment can alter the surface topology of the GDP shells rendering it very much unrelated to the original PAMS mandrel, especially in lower modes (~2–20), and potentially introduce new undesirable low-mode features even on GDP shells produced from very smooth PAMS shells. That would nullify the efforts expended on making smoother PAMS shells. Therefore, we performed a study on the effects of the low-mode PAMS mandrel surface finish on the low-mode surface finish of the final GDP shells for both thick and thin coatings.

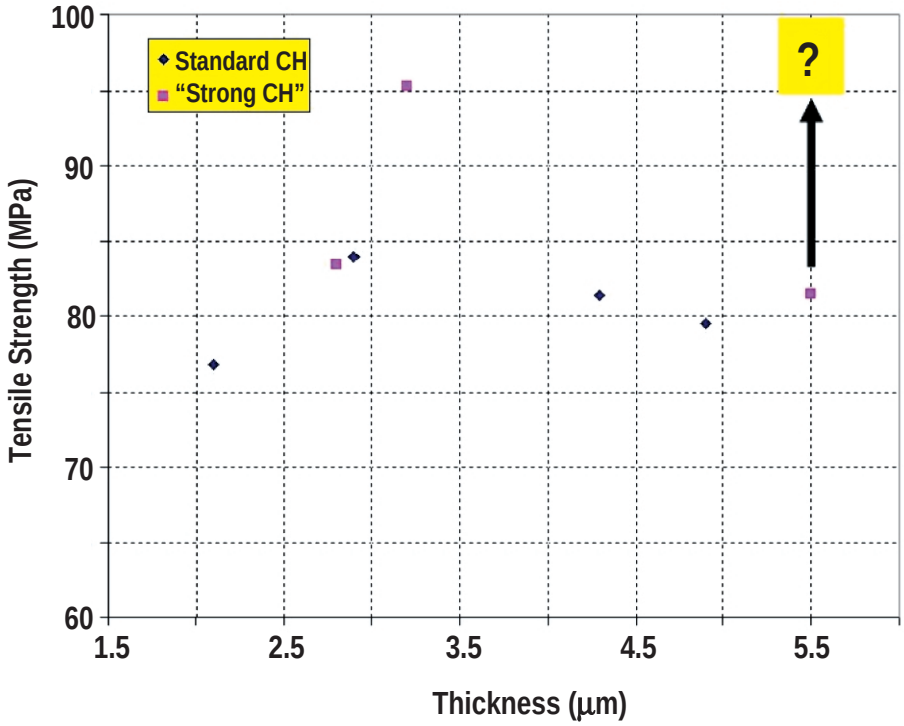

Fig. 3–43. Plot of the calculated tensile strength of thin "standard" and "strong" shells as a function of shell AR using Eq. (2) as explained in the text. The tensile strength of "standard" shells is comparable to the "strong" shells for the thinnest shells (highest AR). In this burst mode, unlike "standard" shells, the "strong" shells deviate from the ideal shell behavior with their tensile strength varying with AR. The burst strength of the thickest "strong" shells (≈5 μm, pointed at by the arrow) exceeded the maximum pressure attainable in our test apparatus (19 atm).

To examine this, we coated shells from two batches, one in which the PAMS shells had low-mode wrinkling and another in which the shells had smooth surfaces. Five shells were spheremapped from each PAMS batch prior to coating. These same shells were coated

together in the same coating run. Although, the shells from the two batches were mixed and lost their identities during the bounce coating, they could be distinguished post-deposition by the difference in their diameters. This procedure was initially done for thicker 20 μm coatings, typical of noncryogenic targets. The final GDP shells were spheremapped after the pyrolysis step. The resulting spheremapper traces are shown in Figs. 3–44 and 3–45 along with the "NIF standard" (smooth curve) on each plot. For the 20 μm coating, the low-mode surface structure was faithfully reproduced on the GDP shells. Smooth PAMS shells led to smooth GDP shells (Fig. 3–44) and wrinkled PAMS shells led to wrinkled GDP shells (Fig. 3–45).

We then repeated the same procedure to examine thinner GDP coatings ≈5 μm, typical of cryogenic targets. However, we chose only smooth PAMS shells for this test to examine whether smooth mandrels result in smooth GDP shells. The concern regarding introduction on low-mode wrinkling is higher for these thinner shells. We performed the test using both "standard" and "strong" CH coatings. The spheremap traces and the power spectrum of a typical PAMS shell used for these tests are shown in Fig. 3–46. Figure 3–47 shows the traces and power spectrum of a typical ≈5 μm "standard" CH shell resulting from the smooth mandrels. For thin "standard" coatings as can be seen from the figure, the final GDP shells developed wrinkled surfaces from pyrolysis. This points out the important fact that smooth PAMS mandrels do not necessarily result in smooth "standard" CH shells when the shell thickness gets below a certain value, most probably due to expansion and shrinkage effects during pyrolysis. It is important to point out that in all the different cases cited here, the shells were also examined after the coating step prior to pyrolysis and the surfaces were virtually identical to the PAMS shells. So, it is indeed the pyrolysis step that causes any new surface wrinkles. The results were different for thin "strong" CH shells. The traces and the power spectrum of a typical ≈5 μm "strong" shell made using the smooth PAMS batch is shown in Fig. 3–48. The pyrolysis induced wrinkling in the ≈mode 10 region is not apparent in these shells and the power spectrum remains below the NIF curve. The "strong" shells apparently do not change shape due to their increased stiffness, which is an additional serendipitous property for such shells. This lack of "mode 10" wrinkling has been observed in "strong" shells as thin as ≈3 μm.

3.5.4. Shells with Doped Layers

In the past, chlorine-doped polymer using GDP had proven to be difficult to fabricate due to the migration of chlorine atoms from the doped layer into adjacent undoped layers. Also, the pyrolysis step led to liberation of nearly 90% of the chlorine atoms from the doped layer. In FY02, we were asked to provide a series of targets involving a chlorine-doped layer as the inner layer followed by an undoped CH layer. Because the Cl-doped layer was to be the innermost layer of the shell, it necessarily needed to go through a pyrolysis step and most of the chlorine would be lost.

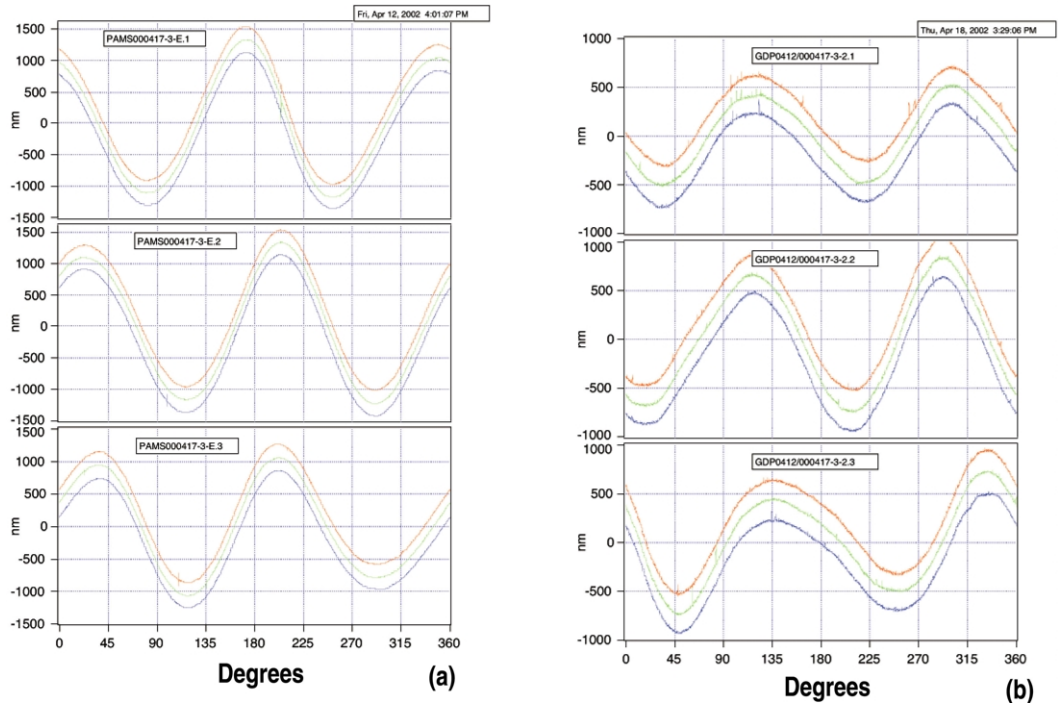

Fig. 3–44. Spheremapper traces of a typical "smooth" PAMS shell (a) without a "mode 10" problem from a batch used to make the final ≈ 20 µm GDP shell. (b) As can be seen, the "smooth" surface (especially in the low modes) of the PAMS is reproduced in the GDP shells.

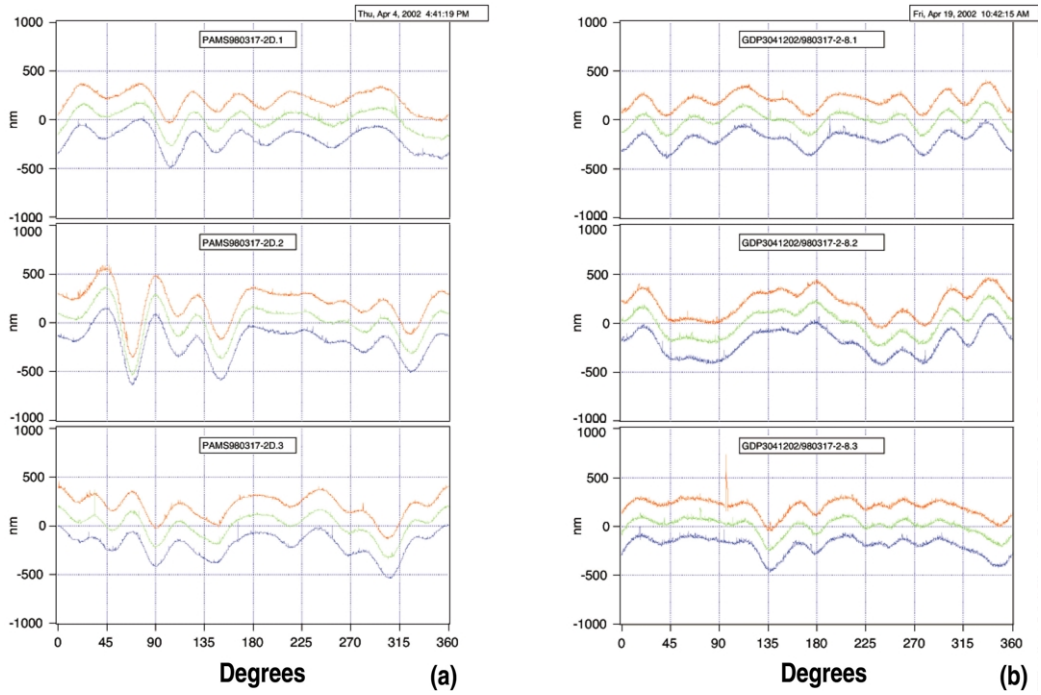

Fig. 3–45. Spheremapper traces of a typical PAMS shell (a) with a severe "mode 10" wrinkling problem from a batch used to make the final ≈20 µm GDP shell. (b) Again the PAMS surface is reproduced faithfully in the GDP shell with the wrinkling directly transferring through the pyrolysis step.

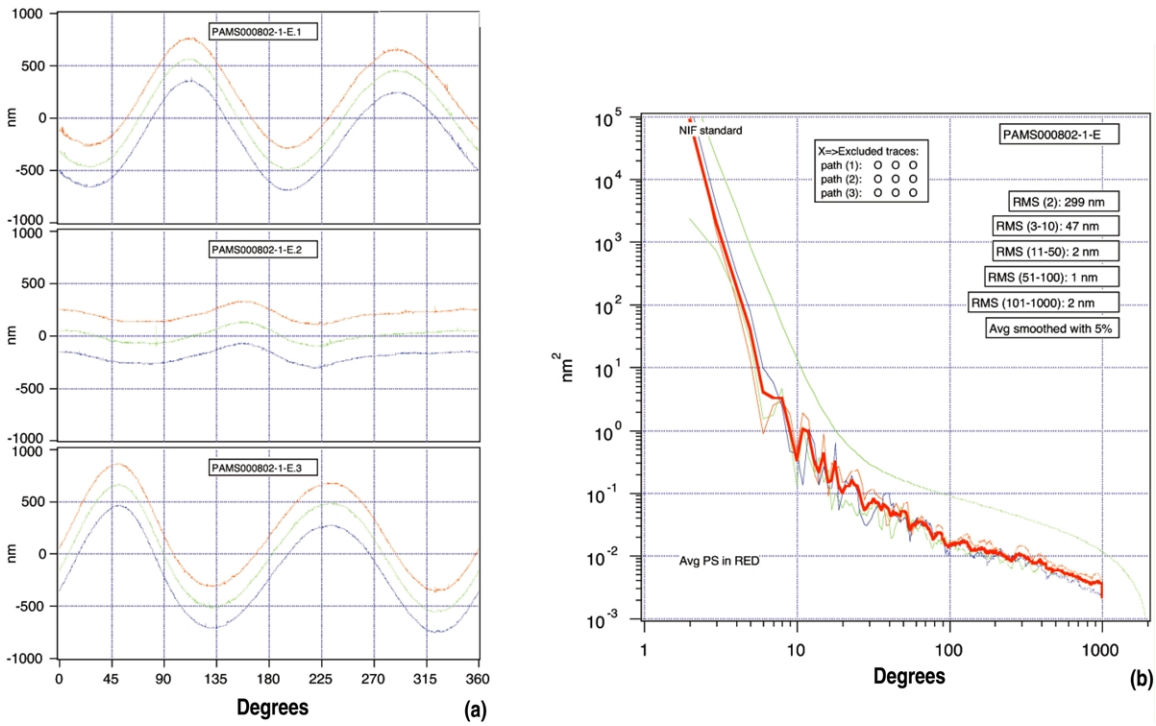

Fig. 3–46. Spheremapper traces and power spectrum of a typical “smooth” PAMS shell from a batch used to fabricate the thin-wall shells shown in Figs. 3–47 and 3–48.

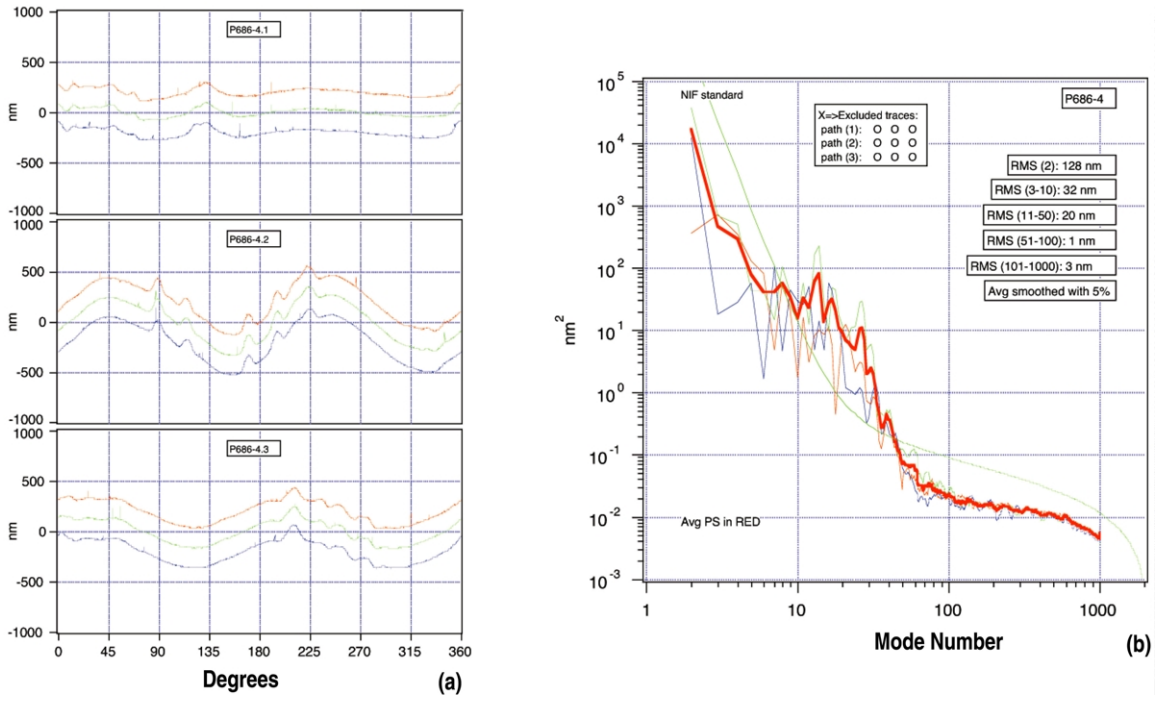

Fig. 3–47. Spheremapper traces and power spectrum of a typical “standard” CH made using the PAMS batch shown in Fig. 3–46. Wrinkles on the shells surface introduced in the pyrolysis can be clearly seen leading to a “mode 10” problem which was not present on the PAMS shell. Note that the very high modes are similar to those of the PAMS shells.

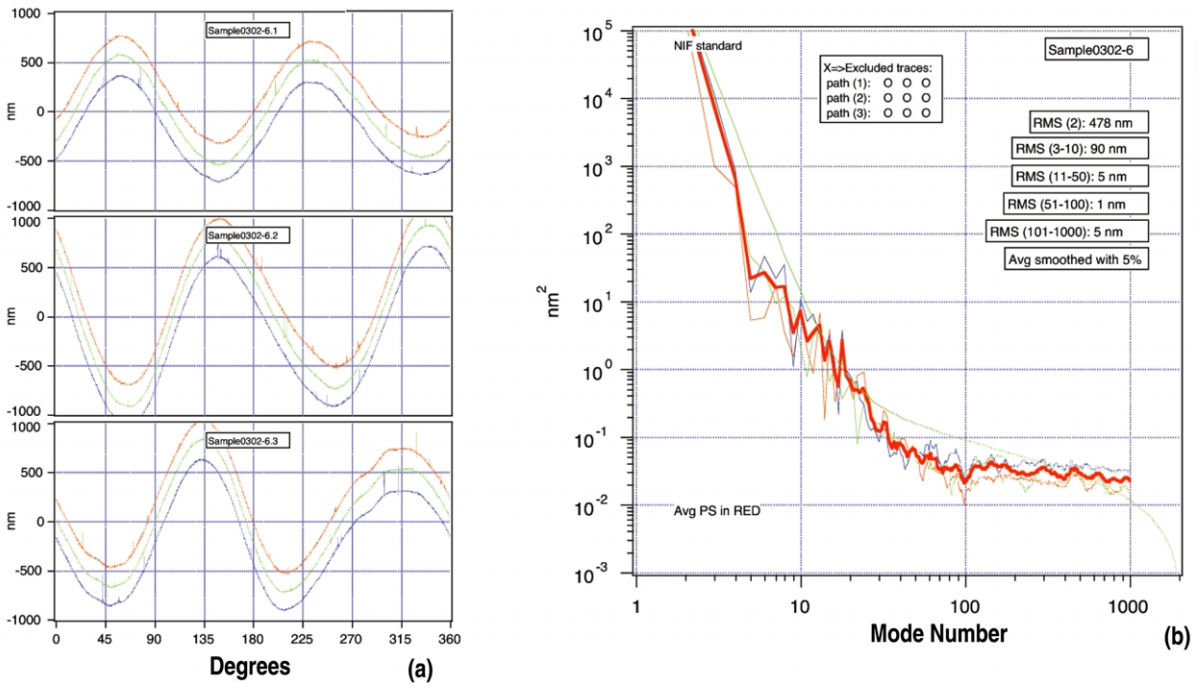

Fig. 3–48. Spheremapper traces and power spectrum of a typical "strong" CH made using the PAMS batch shown in Fig. 3–46. The strong shells did not exhibit a wrinkled surface and had power spectra that more closely resembled the original PAMS shells in the low modes. There is enhanced high mode roughness in these shells, typical of "strong" shells.

We pursued two avenues to make such shells. One was the GDP route to make shells with a relatively low atomic percent of Cl of a few tenths of a percent. To achieve this, Cl-GDP was deposited at ~5 at.% using chlorobutene as the coating gas. Pyrolysis of the PAMS mandrels indeed resulted in Cl-GDP shells with ~0.4 at.% Cl content. These were then overcoated to produce the final target. For these targets, we examined possible migration of the Cl dopant into the undoped layer during the overcoating step, which had been observed previously in shells with sandwiched Cl-GDP layers. In those cases, the dopant layer had not gone through the pyrolysis step. A shell was cross-sectioned and examined by scanning electron microscopy (SEM) in the backscatter configuration and for elemental analysis by energy dispersive x-ray analysis (EDAX). Figure 3–49 shows the SEM backscatter image, which enhances regions containing higher atomic number elements. As can be seen in Fig. 3–49, only the inner 7 µm of the shell shows enhanced contrast indicating that there is unobservable migration and chlorine is indeed confined to the desired position in the shell. The cross section was then probed by EDAX in the numbered areas in Fig. 3–49. The EDAX data is presented in Fig. 3–50, again showing that a chlorine signal is only present in the inner 7 µm of the shell as desired. Therefore, it appears that the chlorine remaining in the doped layer after pyrolysis is stably bound and remains in the intended position during the overcoating process.

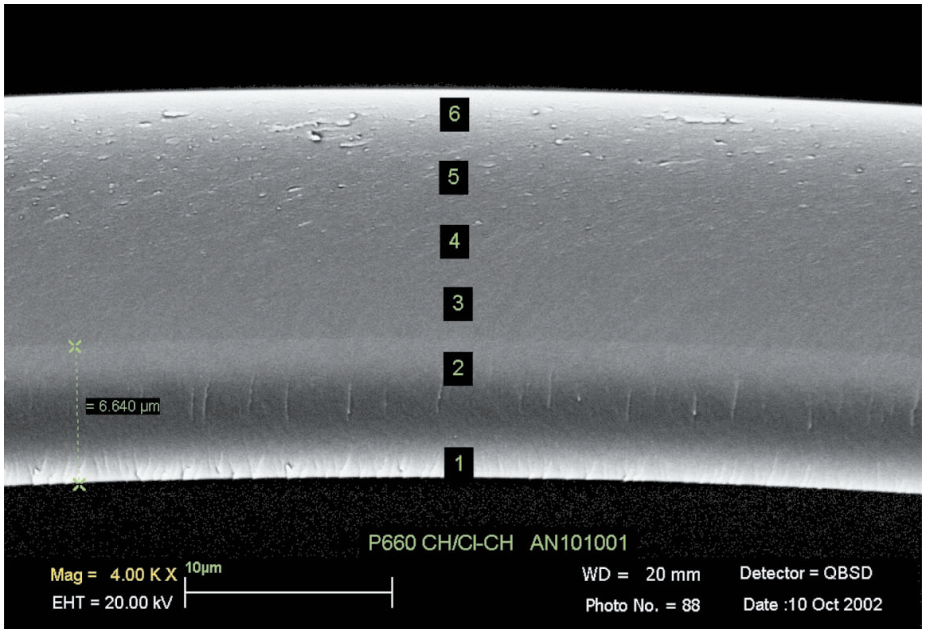

Fig. 3–49. Backscatter SEM image of a ≈20 µm thick shell containing an inner ≈7 µm thick Cl-GDP layer. The inner 7 µm does indeed exhibit an enhanced contrast as would be expected from a chlorine-doped layer. The numbers correspond to areas probed by EDAX as discussed in the text and in Fig. 3–50.

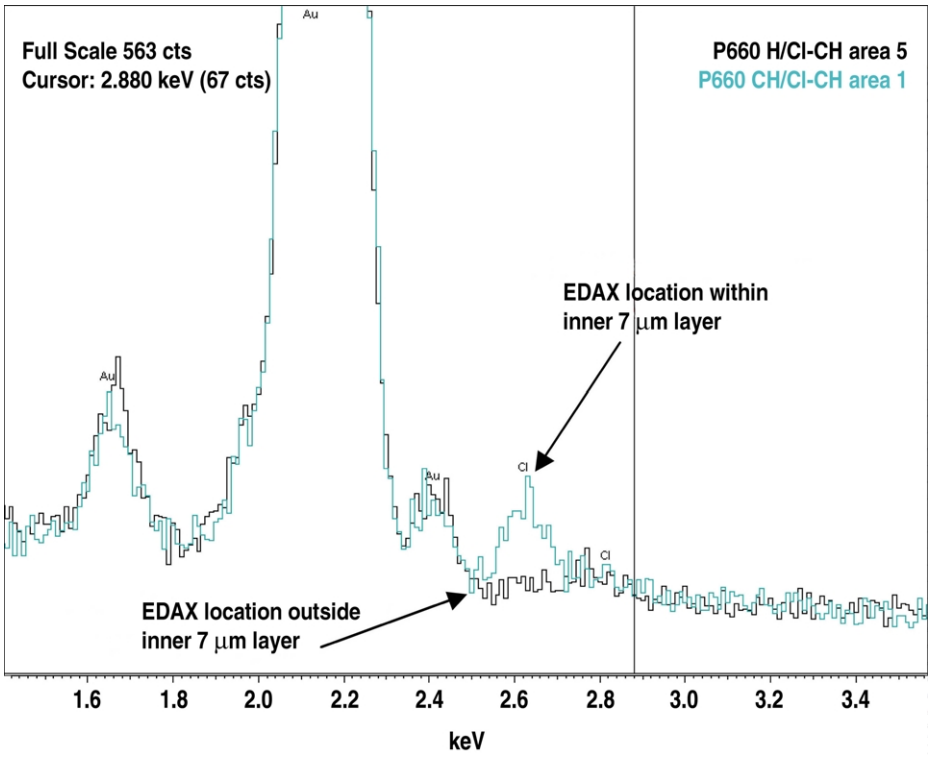

Fig. 3–50. EDAX response of an area within the inner ≈7 µm of the shell and one of an area outside that region. A chlorine signal is only seen within the inner 7 µm of the shell, as desired, indicating confinement of the dopant to the desired layer.

The other route was micro-encapsulation of a chlorinated polystyrene (Cl-PS) blend with ~ 1.0 at.% chlorine content to serve as the Cl-doped layer. Some of the specifications were loosened to allow fabrication of such shells. The desired thickness of the chlorine layer was less than 5 µm; however, this was increased to ~7 µm to increase the chances of making shells via micro-encapsulation. This increased AR resulted in successful fabrication of Cl-PS shells in the very first attempt, but at a very low yield. This method did, however, provide enough shells for the delivery. These shells were also overcoated with undoped CH as was required by the specifications. The concern about Cl dopant migration was negligible here since the chlorine atoms are stably bound in this polymer.

The question of possible migration of another dopant, titanium, also came up in FY02. We were asked to examine shells with very thin (≈0.5–2 µm) Ti-CH layers by the methods used for Cl-GDP described above. Figure 3–51 shows the backscatter SEM image of the cross section of a ≈20 µm thick shell containing a ≈0.5 µm Ti-CH layer. The enhanced contrast due to the titanium dopant is again only seen within the narrow region where the Ti-CH was intended to be. EDAX measurements were also done similar to the chlorine case and verified the backscatter SEM image data. Therefore, it appears that the desired dopants are indeed confined to the desired layers.

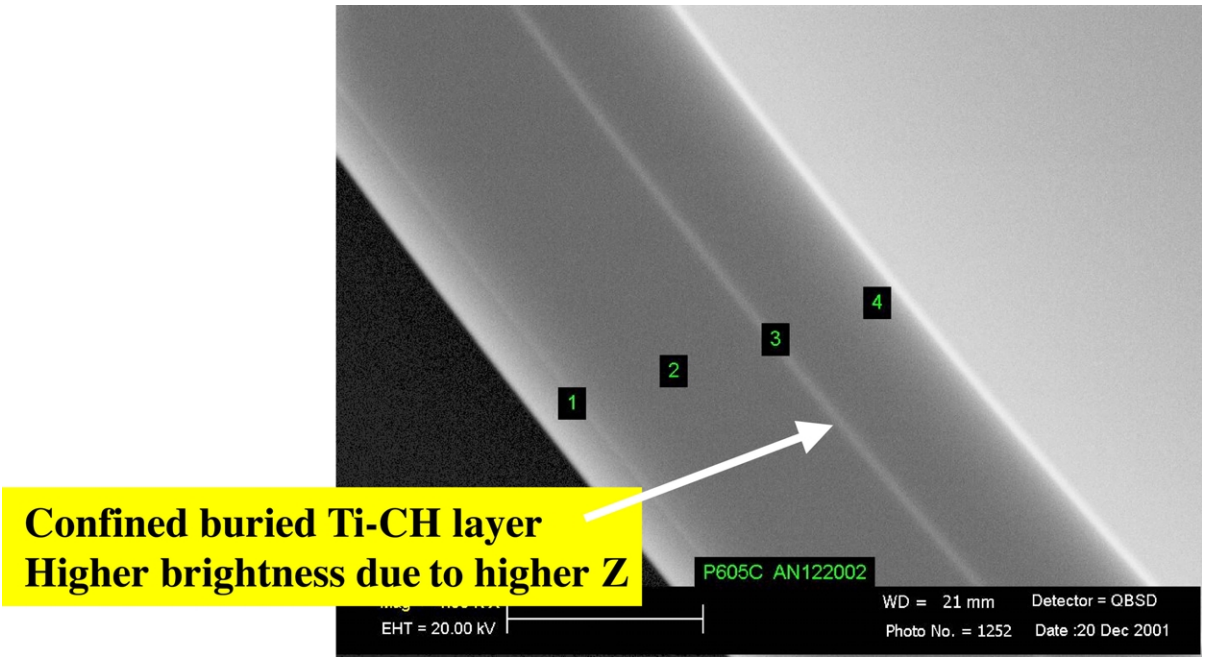

Fig. 3–51. Backscatter SEM image of a shell ≈20 µm thick containing a very thin (≈0.5 µm) buried Ti-CH layer. Again the enhanced contrast in the image due to the titanium dopant atoms is confined to the thin layer at the desired position.

3.5.5. Premature PAMS Mass Loss

Thin-wall polyimide shells for possible use in cryogenic experiments at OMEGA are made by vapor deposition of polyamic acid. The vapor deposition technique uses PAMS

shells as mandrels as is done in the GDP process. To convert the deposited polyamic acid to polyimide and remove the PAMS mandrel, the coated shells are heated to 300°C, imidizing polyamic acid while simultaneously pyrolyzing away the PAMS mandrel. In this step, the depolymerization of the PAMS mandrels can generate excessive internal pressures inside the polyamic acid coating leading to significant expansion of shells. In most severe cases, this would lead to bursting of shells especially when fabricating shells thinner than 3 μm. To avoid this problem, thin-walled PAMS shells (~7 μm) from several batches produced in 1998 at GA had been used at UR/LLE. In addition, the heating schedule was designed so that the temperature is ramped slowly (0.1 to 1 deg per minute) from 180°C, where PAMS shells soften, to 300°C. When a newer batch of PAMS shells manufactured in 2000 was used due to depletion of the batches made in 1998, more early and rapid expansion and subsequent explosion of polyamic acid-coated shells was observed in the imidization/pyrolysis step at UR/LLE, even when using the slowest ramp rates. A thorough set of experiments at UR/LLE showed that it was indeed the new PAMS shells that were the source of the problem and it was inferred that the PAMS shells made in 2000 decompose more rapidly beginning at lower temperatures than those in 1998. Therefore, we were asked to find a solution to this problem.

We initially investigated possible differences in the starting material used in PAMS shells fabrication at GA in 1998 and later in 2000 to find a possible cause for the difference seen in decomposition. While differences in the molecular weight and its distribution were a natural suspect, it was found that there were no appreciable differences between the starting materials used in the two different years. To examine the mass loss behavior of the shells made in different years with temperature, samples of shells from a batch made in 1998 and one made in 2000 were sent out for thermogravimetric analysis (TGA). The results are shown in Fig. 3–52. There was clearly more weight loss at lower temperatures in the 2000 batch than the 1998 batch in agreement with shell expansion observations made at UR/LLE. To investigate what exactly was happening to the PAMS shells, bare PAMS shells were pyrolyzed in an oven with optical access for direct observation of shells during pyrolysis at GA. These direct observations showed dramatically different behavior between the batches made in 1998 and 2000. Figure 3–53(a) shows two shells from a 1998 batch and two shells from a 2000 batch in the oven prior to start of the heating schedule. Figure 3–53(b) shows the same shells after the temperature was raised to ~190°C. The 2000 shells expanded significantly, while the 1998 shells did not exhibit any major expansion. Note that both sets of shells have softened as the small circular features in the center of shells indicates a flat spot on the shells when the glass transition temperature of PAMS, ~180°C, has been exceeded. The diameter of these shells as a function of temperature is plotted in Fig. 3–54, demonstrating the excessive earlier expansion of the 1998 batch. These results seemed to indicate the presence of a volatile impurity within the shell wall that led to the observed expansion when the PAMS glass transition temperature was exceeded. To avoid this problem, we prebaked the 2000 shells for an extended length of time (~3 days) at ~140°C, below the PAMS glass transition temperature. The heating results are shown in Fig. 3–55. As can be seen, prebaking avoids this undesired early expansion of the PAMS shells. Spheremaps of these PAMS shells taken prior and subsequent to the 140°C baking showed

no degradation of shells due to the treatment. It is most likely that the main source of this impurity is residual fluorobenzene, used as PAMS solvent, remaining in the shell wall. This is reasonable since fabrication techniques in 2000 differed from those in 1998, mainly in the addition of extra fluorobenzene to the process. A TGA combined with mass spectrometry also showed liberation of fluorobenzene from the 2000 shells. Polyimide shells made using these prebaked PAMS shells survived the pyrolysis step as desired. This prebaking treatment has provided a simple solution to this problem.

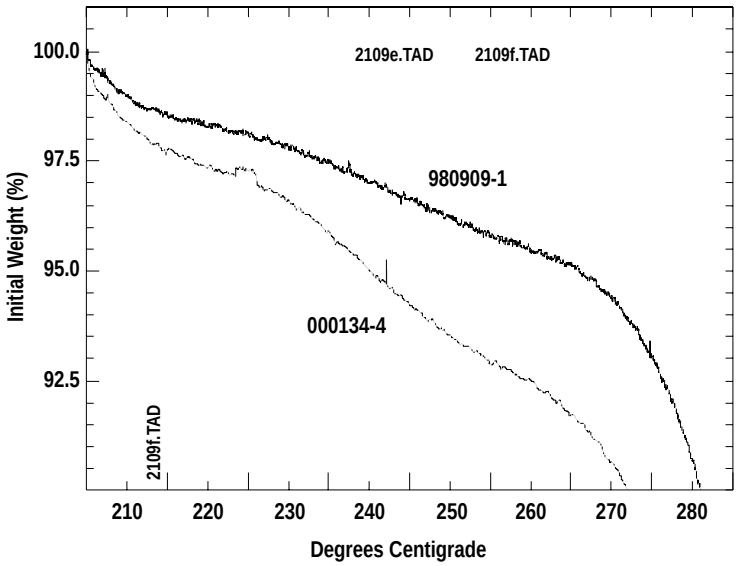

Fig. 3–52. TGA of PAMS shells made in 1998 (980909-4) and those made in 2000 (000134-4). The shells made in 2000 begin losing weight earlier than those made in 1998.

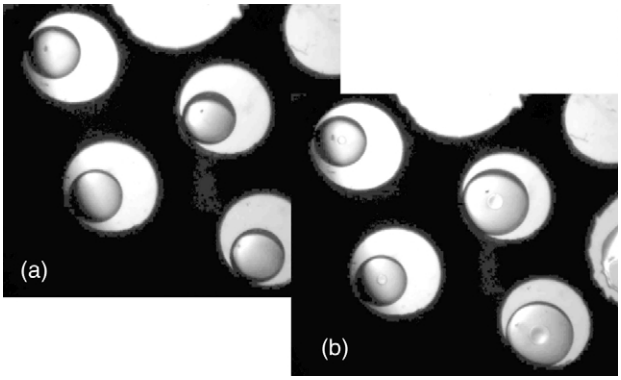

Fig. 3–53. Two shells each from a 1998 PAMS batch and a 2000 batch were heated in an oven with real-time optical access. (a) These shells are shown in the oven in (a) at room temperature at the beginning of the heating cycle. The 2000 shells are on the right hand side. (b) The same shells as in (a) but when the oven temperature has reached 190°C. The PAMS shells from the 2000 batch have expanded significantly, while the 1998 batch shows little expansion. Note that both batches have softened as can be seen by the enlarged contact spots at the center of the shells.

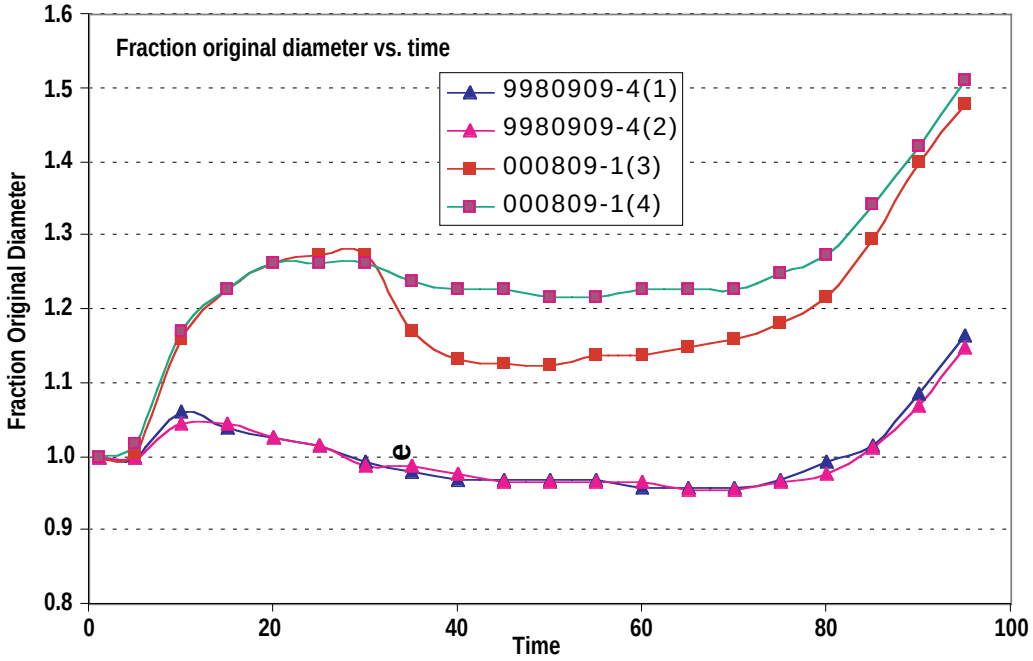

Fig. 3–54. The diameters of the shells shown in Fig. 3–53 are plotted as a function of oven temperature showing the excessive expansion of the 1998 PAMS shells, which caused failure of polyimide shells during the pyrolysis step.

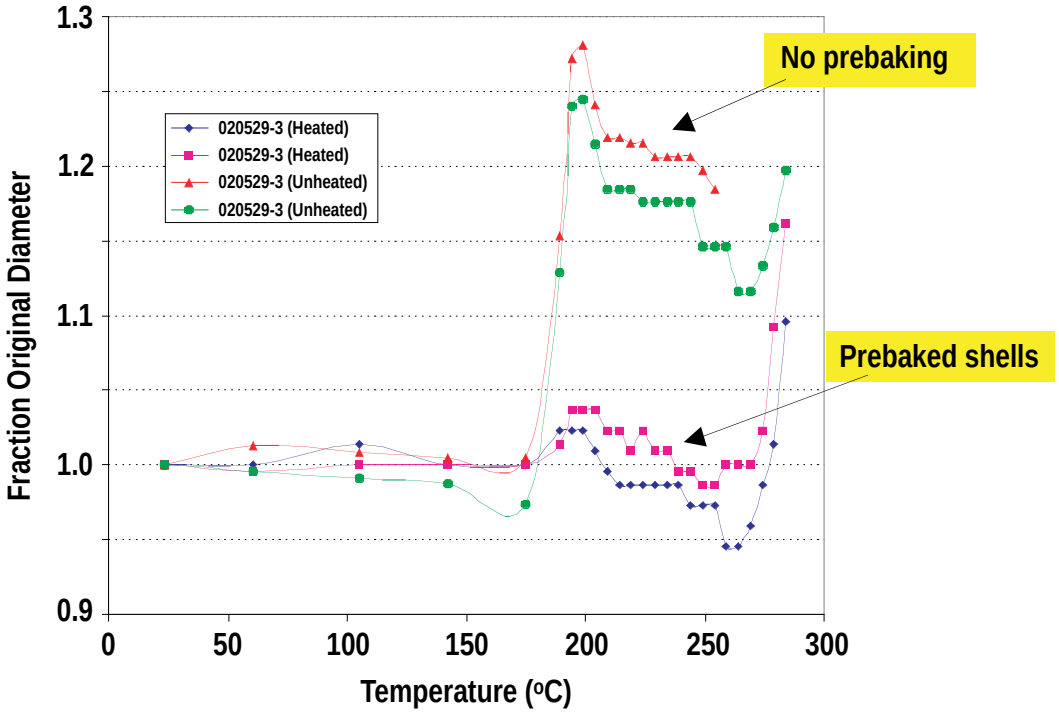

Fig. 3–55. Prebaking of shells from the 2000 batch at ~140°C for several days virtually eliminated the early unexpected expansion of PAMS shells. The use of these shells, which had gone through such treatment, led to much improved survival of thin polyimide shells during the pyrolysis step.

3.5.6. Progress Report for FY02 Foam Fabrication for UR/LLE[9]

The following is a short progress report on the foam work performed so far at GA under the first phase of this contract. Support for this work was provided by UR/LLE beyond the base DOE target fabrication support contract. The goal of the project was to develop shell foam fabrication suitable for use at UR/LLE. The specifications for the foam shells were simply to add a foam layer of densities ~30 to 140 mg/cc and wall thicknesses ~30 to 100 μm on the inside of the full density CH shells currently made (see Section 3.5.2). The full density layer in this case would be deposited after production of the foam shells and act as a permeation barrier to keep the fuel contained. The composition of the foam was to be CH with as much as 30 at. % of oxygen allowed. A major goal was to produce large batches with the yields similar to as what is achieved in PAMS fabrication.

We began the project by a thorough review of the previous work on foam shell fabrication in the ICF community. This work is summarized below, categorized by the various foam systems used:

- TMPT/EGDM — Main work was performed at Institute of Laser Engineering (ILE) in Japan. ≈10 to 30 μm thick, ≈500 to 800 μm diameter shells were made which reportedly had enough transparency for optical characterization. Overcoating was achieved by chemical means. Shells were used in cryogenic experiments at ILE. Contain ≈12 at. % oxygen. Involves "usual" water/oil/water micro-encapsulation system.
- Divinylbenzene (DVB) shells — Fabrication development is in progress by Schafer Corporation under a contract in the IFE area. This foam is currently the main candidate for IFE applications, which has many similarities to the UR/LLE experiments. These shells are expected to be too opaque for characterization due to large cell size (microns). No samples were available at the time our contract began. It is a pure CH foam as it contains no oxygen. Involves "usual" water/oil/water system.
- RF — Shells fabrication demonstrated at LLNL. Reproducibility of sphericity, concentricity and yield were potential problems. Overcoating was not achieved by chemical means. Plasma coating achieved but no data on gas retention properties of shells coated as such. Some samples available from LLNL courtesy of Bob Cook. Contains 14% oxygen. Involves "reversed" oil/water/oil system.

A foam workshop was planned at GA in mid-February 2002 shortly after receipt of funds for the task (January 2002) to lay out a road map for the present effort based on the previous experience in the ICF community. In preparation for the workshop, some preliminary work was performed at GA to gain some additional and more direct data on the previously used systems. That work is summarized below.

A dedicated droplet generator was assembled, tested and made operational at GA for this task in the first two months after receipt of funds (Fig. 3–56). A GA-owned droplet generator was used to commence actual shell fabrication work during that period of time. Other

[9] The work described in this section was supported by contract 411876-001G with the University of Rochester.

available instrumentation and setups were used for further processing of shells after fabrication.

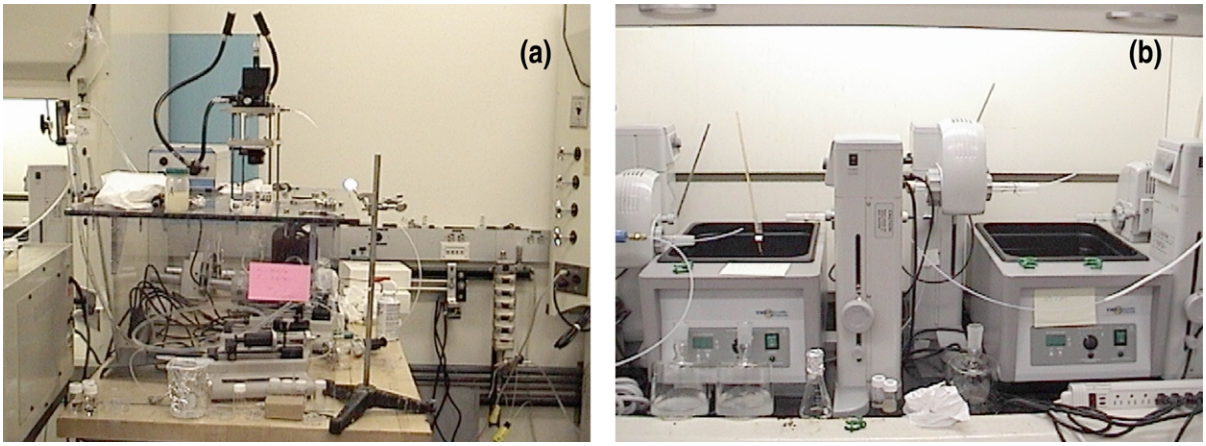

Fig. 3–56. A dedicated droplet generator and shell curing equipment were constructed for the foam work for UR/LLE.

- M. Takagi reproduced the TMPT/EGDM work he had performed at ILE. These shell fabrication runs were performed using the shake-and-toss technique designed to duplicate the previous successful work that was performed in Japan. This initial work demonstrated that fabrication of batches containing hundreds of "good" shells was far from trivial.
- DVB — Shells were successfully made using the droplet generator using standard techniques used for PAMS shell fabrication. While there were several issues in the few runs made, the process appeared to be one that could be fine-tuned quickly. Shell and flat samples were made to allow optical transparency study of these foams.
- The basic and prompt conclusion of the above work was that shells made using TMPT/EGDM or DVB would not have enough transparency for practical optical characterization. *Flat* samples of these foams were transparent at thicknesses of interest to UR/LLE (≈ few hundred microns). However, since a shell of the same material has two walls separated by a substantial gap (the inner void in the shell), it acts as a double diffuser and the shells are very much opaque.
- RF — no work was done on fabrication of these shells prior to the workshop mainly because it involves a reverse system and it was not possible to use the same droplet generator for these types of foams. Due to their very small cell size structure, RF shells are very transparent in the visible and no work was needed on examining their transparency. Thus, the work concentrated on the samples received from LLNL and possible overcoating using plasma deposition of GDP used extensively in ICF capsule fabrication. This work showed that a thin (as thin as 3 μm or even fewer) GDP coating could be placed on the shells which appeared to hold gas based on observed buckling of shells.

Over 20 foam fabrication experts from around the world were present at the workshop, which was held at GA February 14–15, 2002. The basic conclusion of the meeting was that shell fabrication effort should be focused on RF foam due to its superior optical transparency. Also, the GDP overcoating would initially allow fabrication of shells that could be tested for filling and layering in the UR/LLE cryogenic facility more rapidly than the other schemes.

After the workshop, work began on fabrication of RF shells which included procurement of chemicals and setup for the "reversed" system. After an initial trial and error period, RF shells were fabricated (Fig. 3–57) before the next designated review in late April (during the semi-annual review of the ICF contract at GA). These shells were still in the processing liquid, isopropanol (IPA).

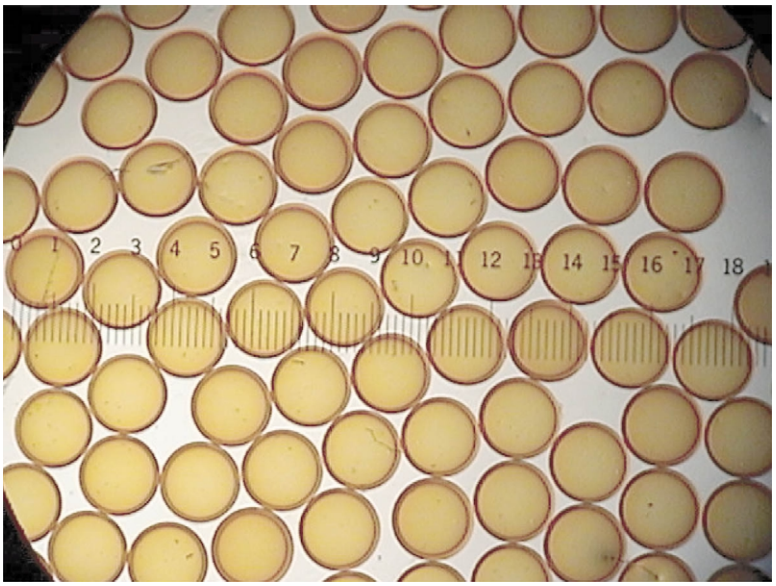

Fig. 3–57. Many batches of successful RF shells have been made. Shells shown in the photo are ~1300 µm diameter, ≈80 µm wall thicknesses, 90 mg/cc density. The shells are shown while still in IPA prior to drying.

Drying of foam shells involves a slow process (minimum of two weeks) and is done in a critical point drier to avoid detrimental shrinkage of the foam. Therefore, it is important to only dry batches that are expected to yield good shells. Characterization techniques developed in the early part of the year were used to make measurements on these shells while still in IPA to determine whether a batch was worthy of drying. This avoided wasted effort on poor batches.

Proper drying proved to be a challenge until early May, at which time a batch of shells was dried properly and measured. The measurements indicated nonconcentricities of dry foam shells of ≈ less than 10% with most shells having values under 5%, which is the typical value for CH shells currently manufactured for UR/LLE. The sphericity of these shells was typically better than 99.5% (5 µm out-of-round) which was high enough to allow spheremapping of shells. These shells were overcoated with GDP to thickness of ≈5 µm.

The overcoated shells were tested for argon holding capability and were found to have a time constant similar to what would be expected of the GDP coating (Fig. 3–58). Not all shells examined held gas, which indicated that each shell must be tested before it can be used for filling in the OMEGA cryogenic system. Two shells were selected and sent to UR/LLE in mid-May for testing at UR/LLE. One of these shells was indeed filled with D_2 and the fuel was frozen and some layering experiments were performed. Further detail on this can be obtained from UR/LLE personnel. Other batches were also sent to UR/LLE for testing.

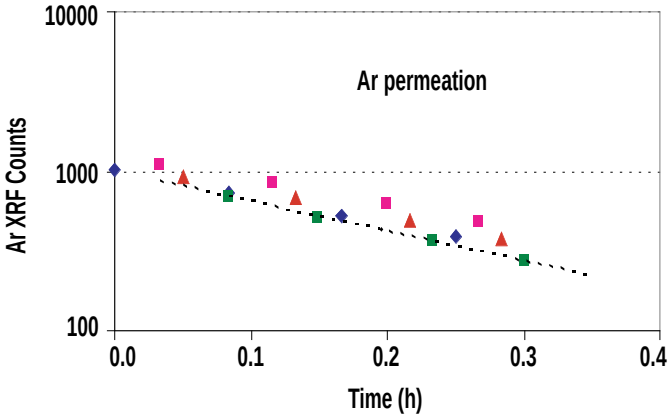

Fig. 3–58. Argon permeation data provided direct evidence of gas retention of GDP-coated shells. Shells were filled with argon and the argon content of shells as a function of time was measured after the fill using x-ray fluorescence. Data for four different shells is presented. The rate of loss of argon from these GDP-coated RF shells is similar to that of pure GDP shells.

Overcoating using chemical techniques proved difficult and unsuccessful in the LLNL work on RF in the 1990s. We have just begun examining the possibility of such coatings, which have the promise of smoother surface finish and more predictable gas retention for coated shells. The chemical coating will be followed with GDP coating to thicken and strengthen it. The shells coated in the first trials of this work do not exhibit the cracking observed at LLNL and they are currently being dried.

Currently, foam batches are made on a weekly basis to provide shells for drying and coating. Current work involves developing the chemical overcoating and gaining an understanding of the critical parameters that would eventually allow nearly 100% success in fabrication runs and concurrent production of shells with continued improvements in sphericity and nonconcentricity.

3.6. CENTER FOR FOAM DEVELOPMENT AND PRODUCTION

Center head: Diana Schroen (Schafer)

Scientists: Jon Streit, and Kelly Youngblood (Schafer)

Technicians: Pat Collins, Scott Faulk, Chris Russell, and Dave Tanner (Schafer)

The Center for Foam Development and Production is responsible for the development and delivery of low-density foam components used as precision target and diagnostic components. These targets are requested primarily by SNL, but occasional requests are also made by NRL, LANL and LLNL. Two facilities and groups of staff are responsible for this work. On-site at SNL are Jon Streit and Diana Schroen. In Livermore are Kelly Youngblood, Pat Collins, Mike Droege, Steve Gross, Ed Hsieh, and Brian Motta. This combination of people and facilities gives us the ability to produce five foam types: polystyrene, resorcinol-formaldehyde aerogel, silica aerogel, DVB, and TPX (1-methyl-4-pentene). The foams can be molded, machined, doped, cast with embedded objects or coated with thin metallic coatings. The foams we produce and their properties are listed in the Table 3–3.

TABLE 3–3
FOAMS AND THEIR PROPERTIES

Foam	Density Range (mg/cc)	Pore Size	Dopants	Chemical Composition
HIPE Polystyrene	15–700	1–10 µm	Halogens Physical dispersions Embedded objects	CH
Resorcinol-formaldehyde aerogel	20–850	nm	Chemical modification Physical dispersions	65 wt%C, 38 wt% O&H Carbonized 93 wt%C
Silica aerogel	10–700	nm	Chemical modification Physical dispersions	SiO
DVB	15–200	1–2 µm	Deuterated	CH
TPX	3–250	1–15 µm	Physical dispersions	CH_2

For SNL we produced 113 foams in FY02. That number is down from previous years, but that number is deceptively simple when the requirements are considered. In previous years, the foams tended to be simple geometries and the majority were hole-closure foams as opposed to target foams. Hole-closure foams have simple shapes and tolerances that are much more forgiving. In FY02, hole-closure foams were rare and often one foam was used in situations that required several (Fig. 3–59). One foam is used to cover the entire end of a 19.2 mm o.d. hohlraum (a hot wire tool was used to cut the required clearance holes).

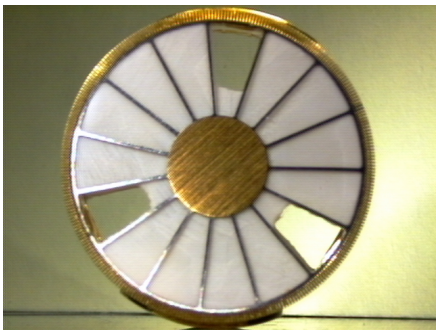

Fig. 3–59. Photo of one end of a double-sided pinch hohlraum. This is an example of one foam doing the work of 15.

Many target foams requested required advanced fabrication and characterization techniques. Most of the development was an extension of work begun in the previous year. Foams with embedded capsules were a common target last year. Throughout the year, the tolerances were tightened on capsule placement and density non-uniformities. Radiographs showing the improvement achieved are shown in Fig. 3–60. The foam is 14 mg/cm^3 TPX.

In support of LANL experiments on Z, a coated foam target was developed. (This target was funded from the SL02 task). The target is an extension of the embedded capsule target shown above, but with increased geometry issues and gold coating. The change in geometry was to cast a hole-closure foam at each end of the target foam. The gold coating was placed as a 2 mm band directly over the capsule (Fig. 3–61).

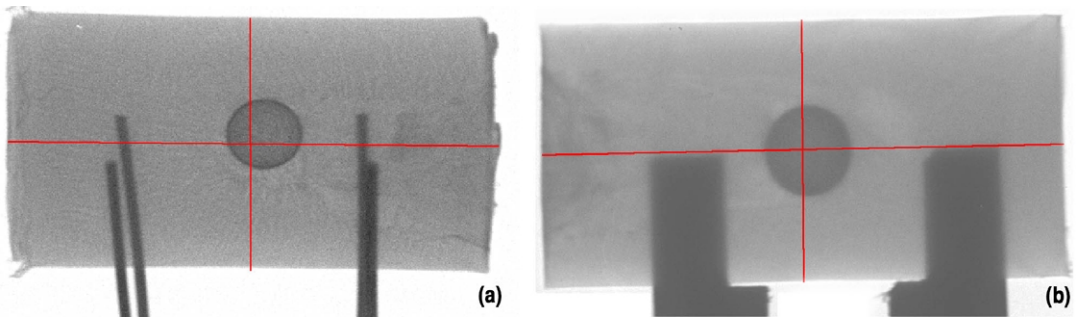

Fig. 3–60. (a) The typical capsule placement and foam density uniformity of a target shot in a January 2002 series. (b) A typical target from a September 2002 series. The red lines indicate the radial and axial centers of the foam. Clearly the foam from the September series has better capsule placement and density uniformity.

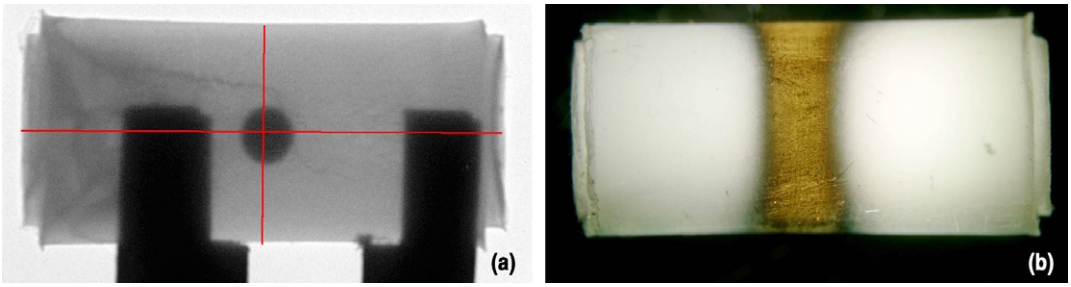

Fig. 3–61. (a) A LANL target before the gold coating. The radiography is done first to confirm the capsule placement. (b) The gold band is placed directly over the capsule. Approximately 0.4 mm of gold is used in the coating.

We also produced foams for Defense Threat Reduction Agency (DTRA) experiments that contained particle doping in TPX foams (Fig. 3–62). The density of the foams produced were 20, 35, 40 and 45 mg/cm^3. The doping was 25 wt% titanium with the actual particles being TiC. The stated particle size from the manufacturer was 4 µm but due to agglomeration the effective particle size was much higher. Another complication of the target request was the geometry required: these targets were cylinders 20 mm tall by 2 mm in diameter.

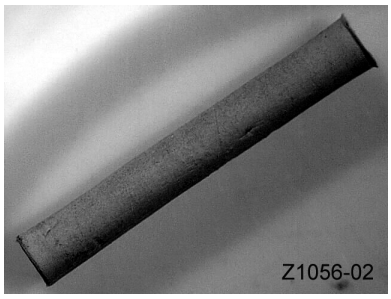

Fig. 3–62. A DTRA foam shot on Z. It is TPX foam but appears gray in color due to the heavy TiC doping.

In addition, a new type of foam was requested in FY02. These foams were used as "ride along" experiments to study the behavior of foams in the Z environment. The concept involved having a very low-density TPX foam, 5 mg/cm^3, captured in a frame with either a metal foil or metal coating on one side of the foam. The first attempt was done using a holder that already had the foil in place and the foam was cast directly into the holder. The second attempt used a coated stepped foam with another stepped foam placed over the top. This made the foam a constant thickness while the metal diagnostic was at four discrete thicknesses (Fig. 3–63).

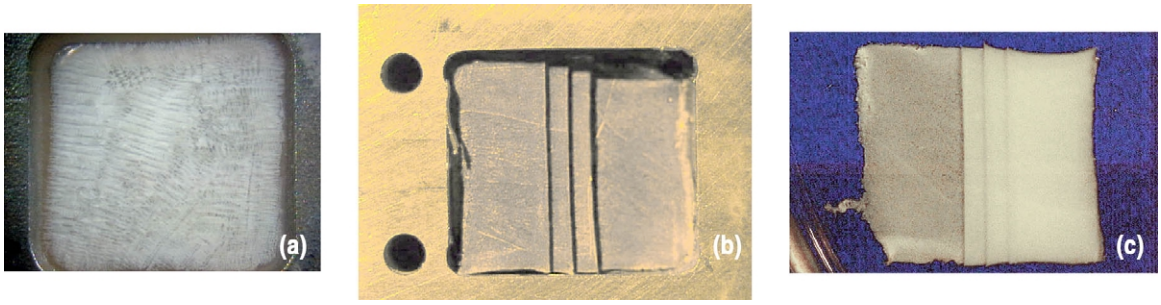

Fig. 3–63. (a) A 5 mg/cm^3 foam cast over a metalized foil. (b) A stepped foam in the same holder after gold coating. (c) The far right image is of just a stepped foam. This foam would be laid over the coated stepped foam to produce a constant foam thickness.

FY02 required fewer foam components than previous years, but the funding level was slightly increased to cover the effort required. There were four reasons for the increased effort required. First, a single foam often replaced what would have been several foams in FY01 or earlier. This single foam was larger or had a complex geometry, either of which is more difficult to produce. Second, the complexity of the targets increased. For example, target foams often required complex shapes, embedded capsules, and high foam uniformity. Third, new technologies were developed such as gold coating and particle doping. Fourth, the on-site personnel assumed all the responsibility for radiography of the foam targets. The radiography system is described in Section 3.9.3 but this labor-intensive characterization cannot be ignored when considering the level of effort required to produce a foam target. The result of all of these factors is that the cost per foam is greatly increased over previous years. Figure 3–64 highlights the situation. In FY98 and FY99, the foams had very simple

shapes and the majority were the "easy to fabricate" hole closure foams. By FY02, the situation was very different.

The situation in FY02 was especially interesting because SNL severely under-predicted its needs for FY02 (Table 3–4). The success of the Z machine led to a very strong demand for more shots, thus more targets.

SNL was able to compensate for the difference between expected and actual costs for FY02 by transferring $600,000 directly from SNL program funds to the DOE/SNL/GA/Schafer contract. Without that additional funding, the GA/Schafer team could not have met the needs of SNL and we are very grateful for their support.

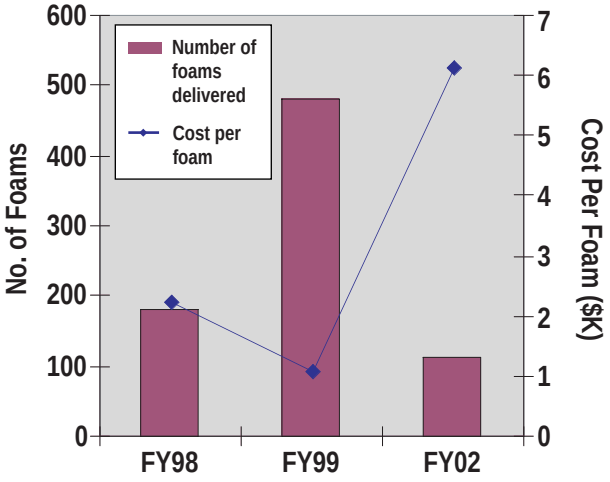

Fig. 3–64. The cost per requested foam initially dropped when we developed the technique for casting TXP foam but has since escalated with the new designs, new techniques, and new characterizations required.

TABLE 3–4
THE EXPECTED AND ACTUAL NEEDS FOR FY02 AND FY03 EXPECTATION

	FY02 Expected Need	FY02 Actual Need	FY03 Expected Need
Capsules	70	126	240
Micromachined parts	100	187	314
Target foams	85	113	176

In summary, FY02 was a very interesting and successful year for the development and fabrication of foam components. The GA/Schafer team has made significant contributions to foam technology, leading to advances in foam characterization and foam production techniques.

3.7. INERTIAL FUSION CAPSULE PRODUCTION

Center head: David Steinman (GA)

Technical Group

Supervisor: Martin Hoppe (GA)

Scientist: Salvacion Paguio (GA)

Technicians: Stephen Grant and Ron Andrews (GA)

Deliveries Group

Supervisor: Annette Greenwood (GA)

Scientists: Jane Gibson and Dale Hill (GA)

OVERVIEW

The Center for Inertial Fusion Capsule Production is principally concerned with fabricating and characterizing capsules and components for current ICF experiments. This year, we delivered 125 orders comprising 2200 characterized target-quality capsules to the ICF program. We expanded our capabilities in glass shells and coating large capsules with a permeation barrier. In glass shells, we made shells ranging in size from 2 mm diameter with 22 μm walls down to 400 μm diameter with 43 μm walls. We deposited metal coatings onto glass shells and developed characterization methods to quantify the coating thickness and uniformity. We are developing "spin coating" to uniformly coat a PVA permeation barrier onto 2-mm GDP capsules. In addition, we fielded GDP capsules having a composite aluminum/PVA permeation barrier that enhanced their deuterium fill half-lives.

3.7.1. LLNL, LANL, and SNL Capsule Fabrication Highlights

Our major effort is the fabrication of plastic capsules and glass capsules for near-term testing, evaluation, and experiments by the ICF laboratories. This section will highlight the wide range of targets that are requested by the ICF laboratories with only a few weeks lead time before delivery is needed.

3.7.1.1. Hemishell Production and Characterization. In FY02, the ICF laboratories made requests for a wide variety of new types of targets. Dave Hanson, an experimenter at SNL, made a request for eight 2 mm diameter hemishells with 60 μm walls. This was the first time such targets were requested from us. Later in the year, Russell Wallace likewise requested similar hemishell targets for experiments to be conducted by LLNL scientists.

To make the requested hemishells, we fabricated GDP capsules using the standard decomposable mandrel technique. We then used our diamond point micromachining capability to cut the capsules in half at their equators. The shells were measured before and

after machining, giving us confirmation that no distortion had occurred in the machining and cleaning processes (Fig. 3–65).

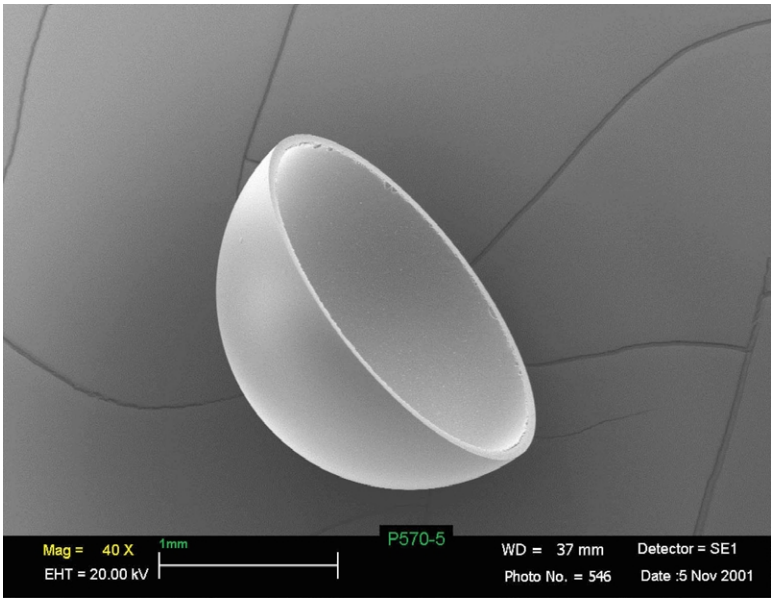

Fig. 3–65. 2 mm × 60 µm wall hemishell fabricated for SNL experiments by cutting a capsule at the equator using diamond point micromachining.

3.7.1.2. New Application for the WYKO Interferometer. We found we could use our WYKO interferometer system to measure the quality of the edges of the GDP hemishells fabricated for SNL and LLNL. We also used it to characterize PAMS hemishells that we fabricated to evaluate the "machinability" of the two materials.

The SEM and WYKO interferometer photos (Figs. 3–66 and 3–67) show and quantify the differences between the machined cuts obtained using GDP and PAMS shells. The SEM qualitatively shows that the PAMS shell machined substantially better than the GDP shell. The GDP is chipped along the surface of the cut while there are smooth groves in the PAMS surface. Though the WYKO does not have the lateral resolution of the SEM, it can quantify the depth of the groves or pits on the lip of the hemishells.

In the processing of subsequent FY02 hemishell orders, we found machine settings that resulted in GDP cuts approaching the quality of those made in PAMS shells. In general, the higher the lathe rotation rate and the slower the tool feed rate, the smoother the hemishell edge became. We expect to further improve hemishell quality as we gain experience fabricating these types of targets.

3.7.1.3. Gas in Capsule Walls. In October and November of 2001, we prepared a group of targets for Jim Bailey of SNL. His targets consisted of 1.6 mm GDP capsules with approximately 50 µm walls, coated with PVA and filled with a variety of gases.

One of the diagnostic fill gases requested was sulfur dioxide (SO_2), a gas never before used in experiments by the ICF community. With this in mind, we performed a trial permeation fill to confirm that there would be no surprises. We found that the PVA-coated shells turned very dark in color after the high temperature (142°C) fill. To verify that we had reached fill equilibrium, we used our x-ray fluorescence (XRF) system and weighing to determine how much gas the shells contained. Surprisingly, the shells had gained about nine times more weight than they should have implying that it was likely that the sulfur dioxide

was forming chemical bonds with the GDP wall. We had included an uncoated GDP witness shell in the fill. It too darkened like the PVA-coated shells, indicating that the GDP was reacting with the gas. Both types of shells lost an equivalent amount of weight overnight revealing that PVA was not a good permeation barrier for sulfur dioxide. After consultations with Bailey, we performed more permeation trials with other gases to field in his campaign.

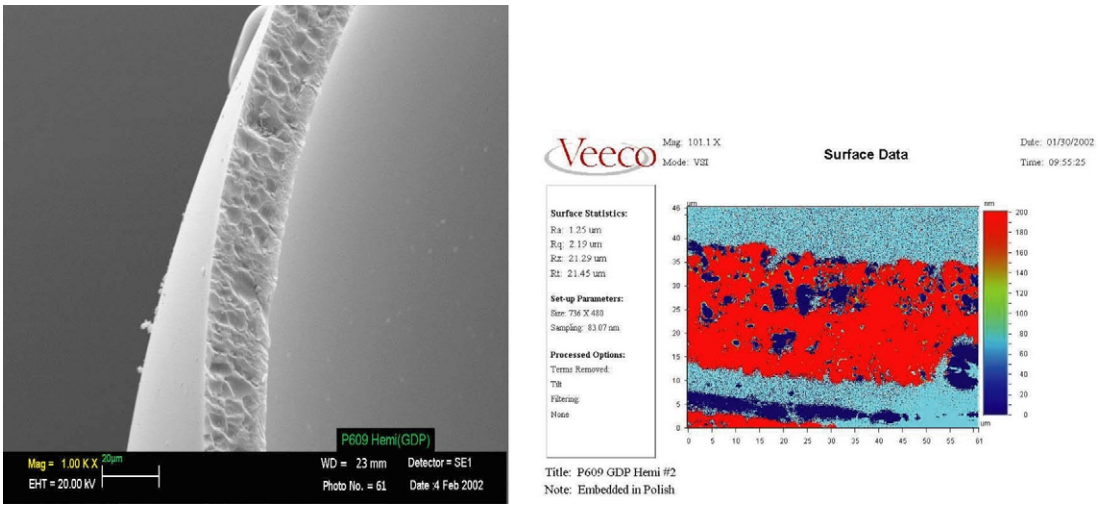

Fig. 3–66. SEM and WYKO images of the lip of a micromachined GDP hemishell. SEM images have better lateral resolution than those obtained from the WYKO.

Fig. 3–67. SEM and WYKO images of the lip of a micromachined PAMS hemishell. The WYKO can readily measure the depth of the grooves produced by the diamond tool bit while the SEM cannot.

Dichloromethane (CH_2Cl_2) and carbon disulfide (CS_2) were tried and found to be unacceptable. Both were well entrapped by the PVA permeation barrier but the capsules' weight gain indicated that most of the gas was being held in the GDP wall as found using SO_2.

Tetramethylsilane (TMS) was next tried with silicon being the diagnostic element of interest. Our first attempt to fill a bare GDP capsule with TMS at 142°C proved unsuccessful

as weighing and XRF showed only a trace amount of gas had entered the capsule. We then filled the capsule overnight at 250°C and found that both weighing and XRF agreed that the bare capsule held this gas. We burst tested one of the shells and the pressure measurement showed that the proper amount of TMS gas was present. Thus, for the campaign, we filled uncoated GDP shells with TMS at 250°C, then applied the PVA coating to allow for filling the capsules with deuterium at ~90°C.

Other requested capsule fill gases (argon and deuterated methane) were permeation filled through the PVA permeation barrier at ~140°C. At room temperature, the argon and deuterated methane filled capsules have half-lives of many months, so out-gassing of these gases was not a concern.

Because we had little experience with deuterated methane fills, we performed burst test experiments on some capsules to determine their fill half-lives for CD_4 at that elevated temperature. These tests gave us some unexpected results. Immediately after the first shell was burst, the pressure measurement apparatus confirmed that the pressure rise in the chamber was consistent with the expected fill pressure of the shell void. However, the system pressure continued to climb over the next several hours indicating that there was a substantial amount of CD_4 in the thick (~68 μm) GDP wall. The plot on the following page shows how the shell wall out-gassed over time (Fig. 3–68).

In response to the needs for better capsule fill gas pressure measurement, capsule half-life determination, and an understanding of the quantity of gas(es) in shell walls, we have begun a series of experiments to address these concerns.

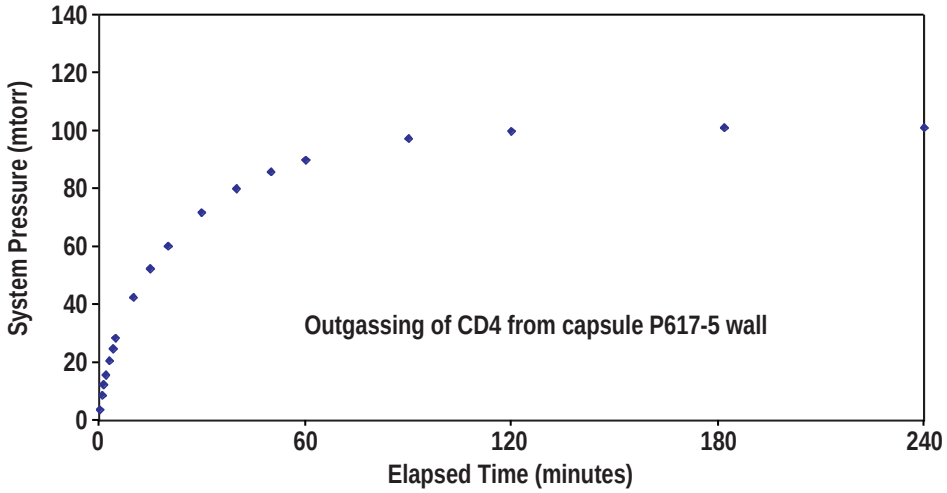

Fig. 3–68. This plot shows out-gassing from the GDP wall of a PVA-overcoated 1600 μm capsule filled with 6 atm of CD_4 after it was burst tested. The density of CD_4 in the shell wall was calculated to be ~1.4 times that of its density in the shell void.

3.7.1.4. Witness Plate Measurements. In early FY02, in response to a request from Russell Wallace, we improved our technique for witness plate thickness measurement. Our original method of determining witness plate thickness employs a fixture having three stainless steel

balls glued to the surface of an optically flat glass block. The balls are approximately the same size (400 µm) and arranged in a triangular array to support the witness plate (Fig. 3–69).

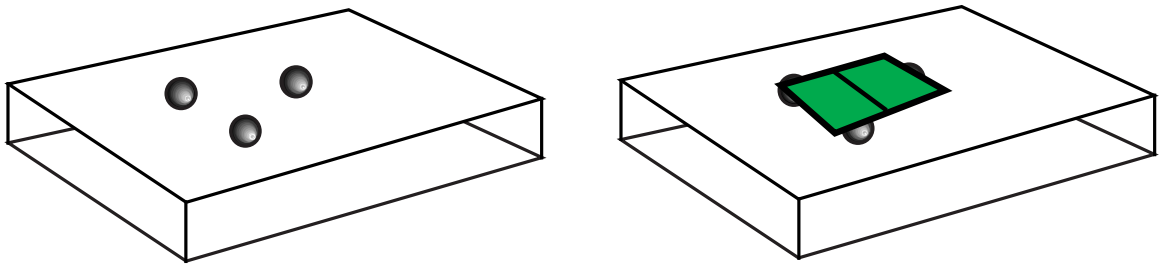

Fig. 3–69. In our original method, three stainless steel balls were glued to an optically flat glass block to support the witness plate for interferometric measurement.

White light interferometric microscopy is used to identify reference fringes reflecting off the top surface of the balls and off the glass block. The height of each ball is thus precisely determined from the measure of the distance the stage moves up and down when locating the reference fringes with the microscope. After the witness plate is positioned on top of the balls, its thickness at the points above each ball is found by measuring the distance from the glass block to the upper surface of the witness plate. The witness plate thickness at that point is then determined by subtracting the height of the appropriate ball from the measurement (Fig. 3–70).

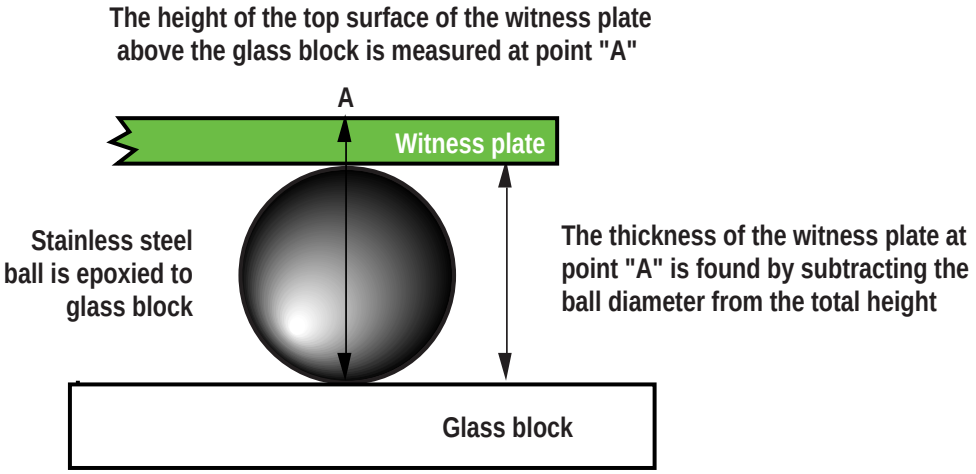

Fig. 3–70. Modified glass block used for revised measurement procedure.

Our modified measurement technique makes use of an array of six stainless steel balls epoxied to the surface of a glass block (Fig. 3–71). Four of the balls support one side of the witness plate as they are balanced on the “measurement ball,” the one from which all the measurements of the witness plates are made. Using only one “measurement ball” eliminates the errors associated with multi-ball measurements.

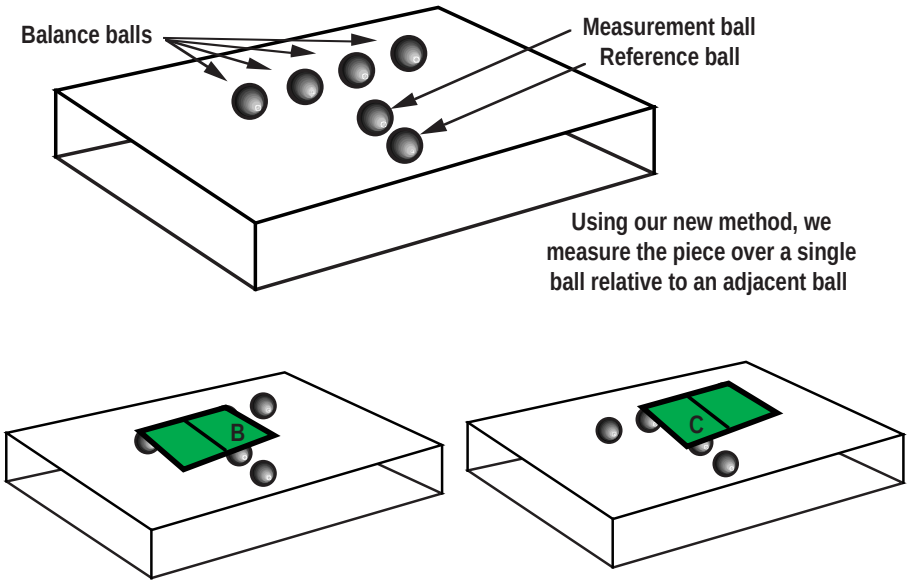

Fig. 3–71. Witness plate thicknesses at points B and C are measured by positioning the plate so that those points rest on the measurement ball. Then the plate thickness is measured using the adjacent reference ball.

Further, we positioned a "reference ball" next to the measurement ball. Rather than measuring the distance from the top surface of the witness plate to the glass block, the distance to the top of the reference ball is measured. In this way, ~400 μm of stage travel is eliminated with a corresponding increase in accuracy of the measurement.

To measure the thickness of a witness piece at selected locations, the piece is slid down the row of "balance balls" until the desired point rests on the measurement ball.

Using the revised procedure, we improved our thickness measurement error by a factor of 2 down to ~0.3 μm for a typical 50 to 200 μm thick witness plate.

3.7.1.5. NIF Quality GDP Capsules. In response to a LLNL concern that recent batches of 2 mm GDP shells have not met the NIF Power Spectra curve, in FY02 we began a study to address the issue. We started with 20 batches of NIF size shells produced by GA personnel under the technology transfer task involving Masa Takagi. The best five of the 20 batches (based on optical inspection) were selected for further testing. Five shells from each of these batches, in addition to one of Masa's best batches, were spheremapped. The results are displayed in Table 3–5.

We began fabricating batches of 2 mm GDP shells from one the best new batches above. Included in the coating run were shells from Masa's PAMS4027 that served as controls. The GDP-coated PAMS shells had essentially the same power spectra as the PAMS shells that were used as the mandrels. The low modes remained unchanged while the high modes (>100) were elevated as the coating process increased the height of isolated surface features.

TABLE 3–5
AFM SPHEREMAP RESULTS OF NEW NIF PAMS BATCHES

PAMS Batch	Mode 2 (nm^2)	3–10 (nm^2)	11–50 (nm^2)	51–100 (nm^2)	>100 (nm^2)
PAMS020107-B	409	96	20	4	7
PAMS020107-C	134	77	7	2	4
PAMS020114-C	170	99	24	4	8
PAMS020121-A	190	79	9	2	5
PAMS020121-C	255	167	10	3	4
PAMS4027	81	20	11	3	5

After the shells were pyrolyzed to remove the PAMS inner mandrel, we spheremapped four or five shells from each of the two batches.

3.7.1.6. Develop Methods to Characterize Metal-Coated Glass Shells. We were also tasked by LANL to develop methods for characterizing metal coatings on glass shells. In addition to using weighing techniques to deduce the average amount of metal coating on the shells by the weigh gain of the shells, we investigated both optical and XRF characterization.

We had on hand a small stock of poor-quality gold electroplated glass shells. We broke one of the shells and placed some of the gold-coated glass shards on a mirror, gold side down, for interferometric examination. We found we could measure the thickness of the glass as well as the thickness of the gold coating to the resolution of our system (~0.2 μm). Figure 3–72 illustrates how this was done. A typical shard we measured had a glass thickness of 3.5 μm and a gold thickness of 7.9 μm.

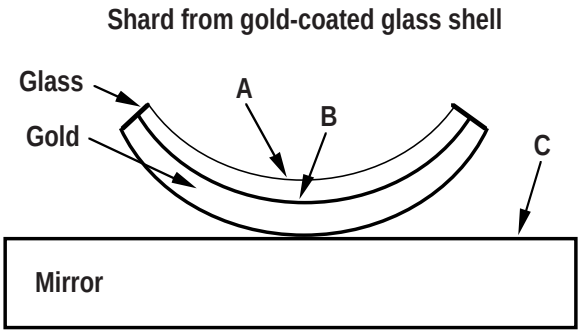

Fig. 3–72. Gold coating thickness is measured on the shard of a broken witness shell. Both the height of the glass shard's inner surface above the mirror (from A to C) and the glass wall thickness (A to B) are measured using interferometry. The gold thickness (B to C) is the difference between the two measurements.

3.7.1.7. Enhanced Interferometric Wall Thickness Measurements. We developed an interferometric technique to improve the measurement precision of thick walled (>50 μm) shells.

The method we normally employ to precisely measure capsule wall thickness is independent of the index of refraction of the shell wall material(s). An interferometric microscope is used to measure the inner and outer diameters of the shell. These two values are then used to calculate the average wall thickness. The interference microscope is used to find precisely the inner and outer surfaces of the shell and the surface of the glass block upon which the shell rests. This is done using white light so that a specific reference fringe can be

identified (by its color/contrast) and used as a marker. Thus, the reference fringe is found on the glass block, then the microscope stage is lowered until the reference fringe is found on the top surface of the shell. The distance the stage has been lowered (measured by laser optics to ~0.1 μm) is the shell outer diameter. The inner diameter of the shell is measured in similar fashion using the reflections off the inner upper and inner bottom wall surfaces.

Optical dispersion causes the measurement of thick walled shells to be less precise because the interference fringes coming from the inner wall surface reflections have less contrast as a result of dispersion caused by the thick wall. We overcame this problem when measuring the shells' inner diameter by inserting an ~100 μm thick plastic sheet in the reference arm of the interferometer (Fig. 3–73). The plastic insert effectively cancels out most of the dispersion and fringe contrast is restored.

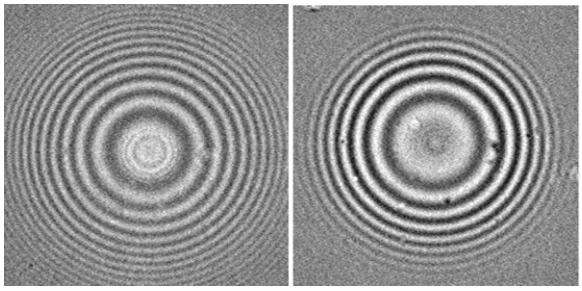

Fig. 3–73. The interferometric image on the left shows the transmitted fringe pattern of a thick-walled shell. Dispersion makes identification of the highest contrast reference fringe extremely difficult. We inserted a sheet of plastic in the reference arm of the interferometer to cancel out dispersion giving us the image on the right. The darkest reference fringe can now be identified and used for wall thickness measurement.

Using this technique, we measured the wall thickness of shells for a LANL order consisting of 400 μm diameter shells having ~80 μm thick walls. The measurements listed in Table 3–6 illustrate the efficacy of the new method.

TABLE 3–6
SHELL WALL THICKNESS MEASUREMENT ACCURACY

Measurement	Shell 1 Wall Thickness (μm)	Shell 2 Wall Thickness (μm)
1	80.7	82.1
2	80.8	82.0
3	81.0	82.1
4	80.8	82.1
5	80.9	81.8
Average =	80.8	82.0
St. Dev. =	**0.1**	**0.1**

The standard deviation of these ~80 μm thick capsules was only 0.1 μm.

3.7.2. Glass Shells from Doped GDP

Perhaps one of the most significant target fabrication breakthroughs in recent years was our discovery of a method to make high-quality glass shells[10] by adding a step to the decomposable mandrel technique developed by Letts.[11] In FY02, using the new method, we continued to expand the wall thickness range for glass shells. At the larger diameter size, we increased the maximum thickness of 2 mm shells from 14 to 20 μm. At the middle diameter range, we increased the maximum thickness of 500 μm shells from 35 to 43 μm. Thus, we now have fabricated Si-GDP derived glass shells having aspect ratios (diameter divided by wall thickness) ranging from 11 (480 × 43 μm shells) to over 300 (800 × 2.5 μm shells).

In order to field Si-GDP glass shells for implosion experiments at the laboratories, we conducted experiments to determine permeation, buckle and burst strength characteristics of these capsules.

3.7.2.1. Glass from Doped GDP Procedure. In step one of the new process (Fig. 3–74), doped GDP is deposited on decomposable PAMS shells made by the droplet generator technique.[12] The PAMS shells are then coated in a plasma polymerization system based on a helical resonator and piezo bouncer described by previous authors.[13,14] In this case, the GDP must be doped with an element that forms a suitable oxide, such as silicon or titanium. For making SiO_2 glass, tetramethylsilane, trans-2-butene, and hydrogen are used as feed-stock gases for the plasma coater. The silicon-doped GDP contains about 0.26 g/cm^3 silicon dopant.

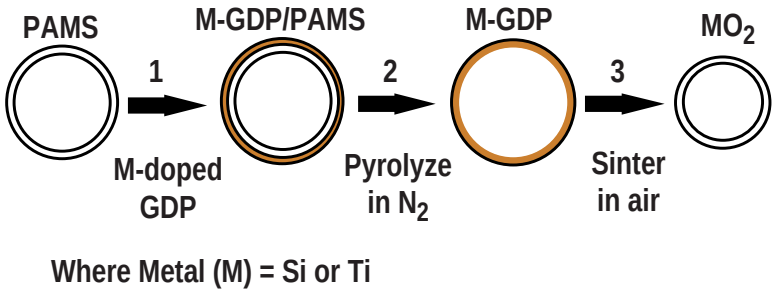

Fig. 3–74. In step one of the GA process, doped GDP is deposited on decomposable PAMS shells. The dopant needs to be one that forms a suitable oxide, such as silicon or titanium. In step two, the shell is pyrolyzed at about 300°C in an inert gas, such as nitrogen, to remove the PAMS. In the final step, the doped GDP shell is pyrolyzed in an oxygen-containing atmosphere to convert it into a glass shell.

[10]Hoppe, M.L., Fusion Technol. **38**, 42 (2000).
[11]Letts, S.A., et al., Fusion Technol. **28**, 1797 (1995).
[12]McQuillan, B.W., et al., Fusion Technol. **31**, 381 (1997).
[13]Letts, S.A., et al., J. Vac. Sci. Technol. **19**, 739 (1981).
[14]Ferguson, S.W., et al., J. Appl. Polymer Sci. **54**, 107 (1994).

After the Si-GDP coating step, the PAMS inner mandrel is removed by a controlled heating process in which the temperature is slowly ramped to 300°C under nitrogen to decompose and volatilize the PAMS polymer and create a Si-GDP shell.

In the final step, the Si-GDP shell is converted into a glass shell by slow pyrolysis in air up to 580°C followed by sintering in air or argon to 1050°C. Larger diameters or thicker walls required progressively slower ramps and significantly longer hold times in order for shells to survive the pyrolysis procedure. This progression was necessary in both the PAMS removal step under nitrogen and the glass conversion step in air.

3.7.2.2. Permeation Properties of Si-GDP Glass Shells. This year we performed a series of experiments to measure the gas retention characteristics of Si-GDP glass shells for helium and deuterium at a variety of temperatures. We are seeking to determine the correlation between the permeation time constants associated with those gases for Si-GDP glass shells. With that correlation, we will be able to quickly infer a capsule's deuterium fill half-life by testing it with helium, that will out-permeate from the capsule at room temperature in only a few hours or days. This will allow us to test production shells in a timeframe compatible with our target deliveries.

We measured capsule half-lives in a number of ways depending on the size of the shells and the gas used. For capsules over 1 mm in diameter, we used weighing techniques to measure the gas fill of the capsules while they out-gassed for both deuterium and helium. Interferometry was used when we measured deuterium half-lives of shells over 1 mm in size or of shells filled to high (>50 atm) pressure. We generally used destructive pressure testing to determine fill half-lives of smaller shells. The results for one of our first half-life tests on helium filled 1300 × 4 μm shells at room temperature are displayed in Fig. 3–75.

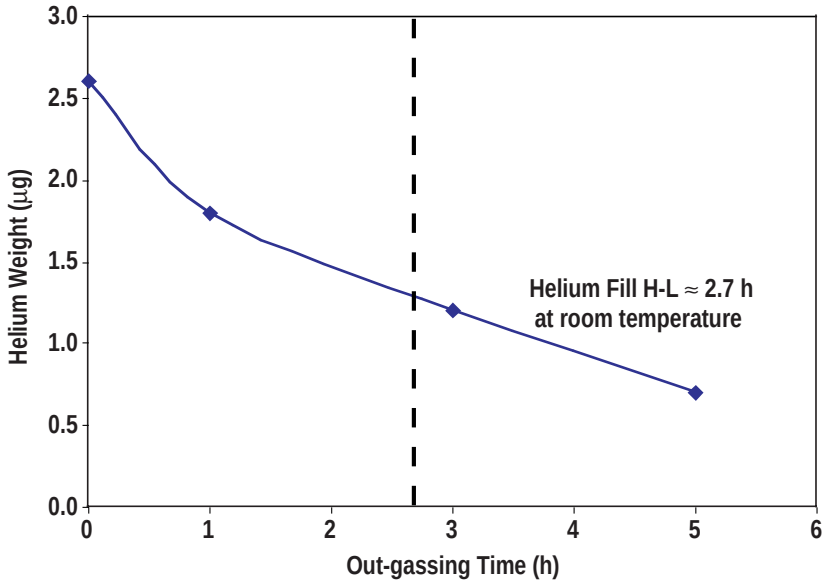

Fig. 3–75. Half-life of 1300 × 4 μm Si-GDP glass shells.

Some experimentalists specify Si-GDP glass targets with an overcoat of several tens of microns of GDP. To fill those targets, we had to determine the glass permeation characteristics at the maximum temperature that does not damage the GDP layer (about 150°C) but still allows the capsule to be filled in a reasonable amount of time. We did our first measurements with a 20 atm helium fill of 1300 × 5 μm Si-GDP glass shells. We found that the shells had a helium fill half-life at room temperature of about 4 h. To make our deuterium measurements, we filled the shells for ~18 h with a fill system pressure of 22 atm of deuterium at 145°C, a temperature at which a GDP overcoat would not be harmed. Using the weighing technique, we determined that the partially filled capsules' deuterium half-life at 145°C was ~30 h.

The capsules were then brought to fill equilibrium. As of this writing, we are monitoring their out-gassing rate at room temperature using interferometry and weighing techniques. After the first month of out-gassing, our measurements indicate that the deuterium half-life at room temperature for these 1300 × 5 μm Si-GDP glass shells is ~80 days. This value will be refined as time elapses. Additional shells are being fabricated and tested to learn if there is strength and permeability variation from batch to batch. Table 3–7 summarizes the preliminary results of this first set of experiments.

TABLE 3–7
RESULTS OF FIRST PERMEATION TEST RUNS ON SI-GDP GLASS SHELLS

Helium H-L at R.T. (used for production testing)	4 h
Deuterium H-L at 145°C (for filling GDP coated shells)	~30 h
Deuterium H-L at R.T. (for shot pressure determination)	~80 days

When we have tested a statistically significant number of shells and shell batches, we will prepare a report that summarizes the permeation studies.

3.7.2.3. Buckle and Burst Strength of Si-GDP Glass Shells. To measure strength properties of Si-GDP glass shells, we began by performing buckle and burst testing on 1300 × 3.9 μm shells using helium. Typical results of the buckle and burst tests are displayed in Fig. 3–76.

When we have tested a statistically significant number of Si-GDP glass shells and shell batches, we will prepare a report that summarizes the strength studies.

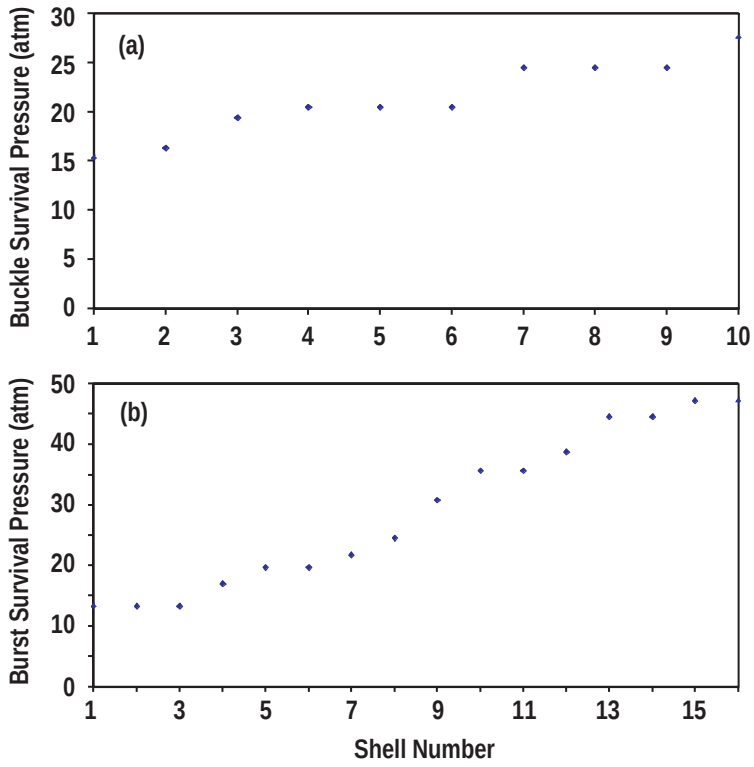

Fig. 3–76. Buckle and burst strength of 1300 x 3.9 μm Si-GDP glass shells.

3.7.2.4. Burst Strength of GDP Overcoated Si-GDP Glass Shells. During this year, we measured the strength of several "leftover" composite glass/GDP capsules fabricated for a recent LANL campaign. Those capsules consisted of ~1270 × 7 μm Si-GDP glass shells that were overcoated with 90 μm of GDP. From this small sample of leftover shells, we confirmed that the burst strength of the glass shells was enhanced by the addition of the GDP overcoat. Table 3–8 lists some of the properties we measured:

TABLE 3–8
GDP SHELL PROPERTIES

Bare 1270 x 7 μm Si-GDP Glass Shells		After Overcoat of 90 μm GDP
Buckle strength	~80 atm	Not enough shells to test
Burst strength	~60 atm	~110 atm
Deuterium Half-Life	~140 days at R.T. (~half that of drop tower shells)	

After years of testing, we have learned that the burst strength of drop tower glass shells is greater than their buckle strength. We find that the opposite is true of Si-GDP glass shells (as witnessed in Table 3–8), perhaps reflecting the different morphology of the two materials. In addition, Si-GDP glass shells are about a factor of two more permeable than drop tower

shells. This may be because the final sintering of those shells has been done only to 1050°C (the temperature limit of our box oven), resulting in less than fully dense glass. We hope to test this theory in FY03 by dropping Si-GDP glass shells through our glass tower at a similar temperature, ~1600°C, to see if this changes their permeation and strength characteristics.

3.7.3. PVA Coating Improvements

PVA has long been the permeation barrier of choice for polymer ICF capsules. In FY02, we improved upon our method of "spin PVA-coating" 2 mm GDP capsules for experiments on SNL's Z-machine.

In our previous efforts to field gas-filled targets for SNL, we "dip and flip" coated 2 mm GDP shells with ~ 4 μm of PVA. This coating technique consisted of holding a shell with a vacuum chuck, dipping it in a 7% PVA in water solution slightly past the equator, then inverting the shell so that the hanging PVA droplet flowed towards the equator more uniformly coating the shell. After the PVA-coating dried from the first dip, the shell was transferred to a second vacuum chuck, and then "dip and flip" coated to cover the opposing side with PVA.

Fig. 3–77. A hole was drilled through the rotor of a small 12-V dc motor so that a vacuum line could be attached to hold a 2-mm GDP shell to the other end of the rotor.

We developed "spin-coating" to more uniformly redistribute the PVA. In this method, the vacuum chuck holding the shell is motorized (Fig. 3–77) to rapidly spin so that the droplet of PVA hanging from the shell redistributes itself upward due to centrifugal force (Fig. 3–78). Of course, the key to this technique is to have the appropriate spin rate to uniformly spread the PVA. There are many parameters affecting this redistribution. They include the viscosity of the PVA solution, the diameter of the shell (affecting centrifugal force), temperature and humidity conditions to name a few.

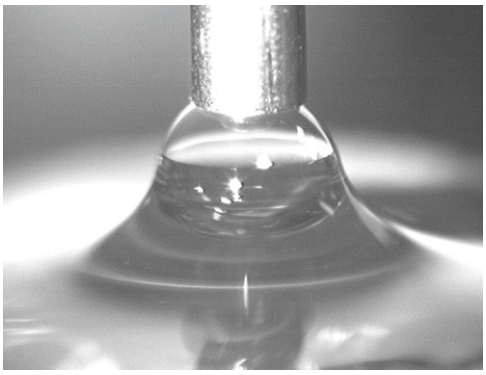

Fig. 3–78. Spinning the shell while it is withdrawn from a solution of PVA causes the PVA to redistribute itself uniformly around the axis of rotation. The shell takes about 10 minutes to dry while it spins.

To find the optimum spin rate(s), we adopted the use of methylene blue as a dye in the PVA solution to quickly visualize how uniformly the PVA coating was being distributed on the shells. The shade of blue around the PVA-coated shell is indicative of the thickness of the coating. Figure 3–79 illustrates how the dye reveals that the PVA will form a thick band around the shell's equator if the

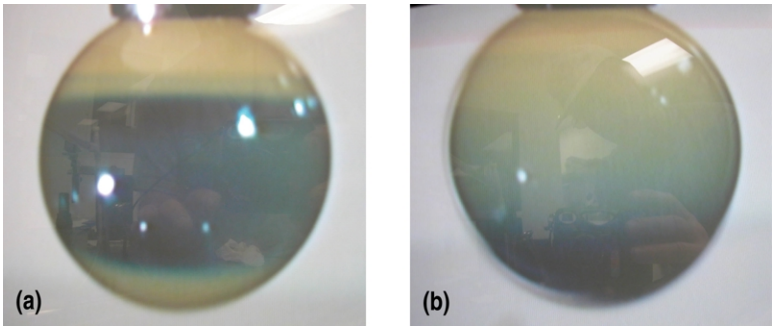

Fig. 3–79. (a) Dyeing the PVA solution with methylene blue allowed us to readily determine that the PVA was too thick around the equator if the shell was spun too fast. (b) Likewise, if the shell was spun too slowly, the PVA pooled at the south pole of the shell.

shell is spun too rapidly. Likewise, if the shell is spun too slowly, the PVA can pool at the bottom of the shell.

Based on our experiments, we determined that the most practical means of establishing the optimal spin rate in an open lab environment was to use methylene blue dyed PVA on witness shells. We then found the optimum spin conditions for the ambient humidity and temperature conditions and coated the production shells using those parameters. In the upcoming year, if no better PVA coating technique is devised, we'll investigate the feasibility of tightening controls on the aforementioned parameters that affect the uniform distribution of PVA using the spin-coating technique.

In some cases we found that rather than using a single rotation rate, it was easier to attain a uniform PVA coating by coating the shell twice; the first time with the spin rate set high so that the equator would be well coated, and the second time with the spin rate set low to coat the bottom half of the shell.

We also started a series of experiments to quickly determine the half-life of PVA-coated capsules for SNL (Table 3–9). We needed a means of measuring as many as 20 shells at a time (a typical production run quantity). Furthermore, since the capsule half-lives we hope to attain may approach a month at room temperature, we needed a method that would take no more than a few days to perform in order to meet schedule deadlines. This we are doing by correlating the gas fill H-Ls of shells at an elevated temperature to their H-Ls at room temperature. As of this writing, we have found that for a typical 2 mm shell overcoated with about 4 μm of PVA, the following estimates apply for a dry (<30% relative humidity) environment:

TABLE 3–9
EXPERIMENTS TO DETERMINE THE HALF-LIFE OF PVA COATED CAPSULES

2 mm Shell Type	Temperature	DD H-L
PVA coated shells	25°C	14 days
PVA coated shells	70°C	20 h
Al/PVA coated shells	25°C	28 days
Al/PVA coated shells	70°C	48 h

The follow-up experiments we will perform in the upcoming year will address the affect of humidity on shell fill half-lives. We will also measure how much protection from humidity is provided to the PVA layer by both an aluminum overcoat and by imbedding the PVA layer in the GDP wall.

3.8. ADVANCED PLANAR TARGETS

Center Head: Tom Walsh (Schafer)
Target Fabrication Scientist: John Varadarajan (Schafer)
Technicians: Derrick Mathews and Sue Carter (Schafer)

A major portion of ICF research involves planar targets. Planar targets are ideal for exploring material properties, hydrodynamic instabilities, and laser-target material interactions. The Nike Laser at the NRL is designed only for experiments using planar targets. The laser beam is very uniform and well characterized so experimenters can explore the effects of depositing a large amount of energy in a material without perturbations from anomalies in the beam. For experiments to have meaningful results, the quality of the targets must at least equal the uniformity of the beam and exceed the limits of the diagnostic equipment. Over the years, as diagnostic equipment and prediction codes have improved, the requirements for target surface finish, uniformity, flatness, and purity have increased. Additionally, the complexity of target designs has increased by the addition of material layers, dopants, intentional surface and mass perturbations, and foams. NRL has also developed a cryogenic capability requiring targets that are designed to work in the wall of a cryogenic Dewar.

Other ICF program lasers also use planar targets in addition to the spherical targets for which they were designed. The OMEGA laser at the UR/LLE is a regular user of GA/Schafer planar targets for laser imprinting studies and Rayleigh-Taylor instability experiments. There are also plans to use planar targets at the NIF located at LLNL when it becomes operational.

We discuss the activities of the Center of Advanced Planar Targets in delivering and developing targets for NRL and UR/LLE, especially:

- Flat CH Films of polystyrene and polyimide.
- Patterned CH Films with a wide range of sine wave periods and amplitudes. This year, we made advances in producing large amplitude patterns on polymer films by machining the film directly rather than using a machined mold.
- Coatings of various metals on polymer or polymer foam.
- NRL Foams of a variety of polymer types and densities. This year, we developed the capability to routinely produce high and low density RF foam and began development of DVB foam, higher density patterned RF foam, and patterned CH film-RF foam constructs. We also made foams with a rippled surface.
- Nike EOS Targets which come in several varieties, many of which required intricate assembly schemes due to their complicated designs.
- Characterization of these targets which required new developments in white light interferometry, a scanning surface profilometer, and an in-house ultraviolet (UV) microscope.

3.8.1. NRL and UR/LLE Deliveries

The past year has seen an increased emphasis on patterned films both for NRL and UR/LLE (Fig. 3–80). A large portion of the targets requested by both labs had a sine wave pattern on one surface with the opposite surface flat. The sine wave peak-to-valley amplitudes varied from 0.25 µm to over 3 µm. Periods for the patterns were generally between 20 and 60 µm. Both laboratories also requested and received flat targets (Fig. 3–80). Targets shipped to NRL during FY01 included targets with patterned surfaces, metal and metal-coated targets, and complex EOS targets in addition to simple smooth-surface flat films.

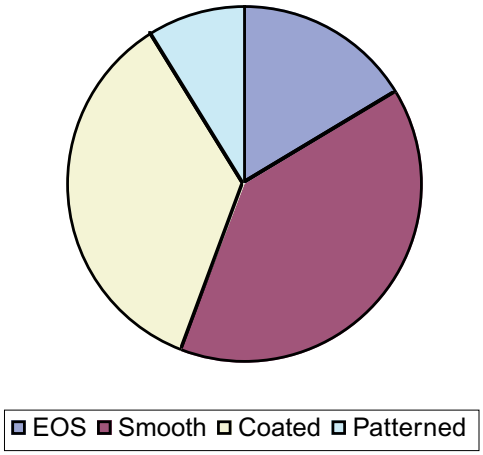

Fig. 3–80. We supplied a variety of films for experiments by NRL and UR/LLE.

We also provided NRL with EOS targets consisting of metal or polymer, sometimes with steps, mounted on a cryogenic target mount (CTM). A number of metal targets or metal-coated CH targets (both flat and patterned) filled out the NRL orders for the year.

3.8.2. Flat CH Films

We continue to deliver some classic flat-film polymer targets mounted on polycarbonate frames (Fig. 3–81) to NRL. Nearly all flat-film polymer targets are made with polystyrene that we cast to precise specifications. Target thickness is usually required to be within 1 µm of a nominal thickness that can range from 10 µm to well over 100 µm. The thickness of each target must be uniform over the entire area of interest and must be reported with a precision of 0.1 µm. The surface must be smooth with no accidental perturbations greater than 25Å measured peak to valley. The films must also be very flat when mounted with a maximum of 1 µm of curvature over 1 mm laterally. We are able to consistently produce flat, smooth films by casting polystyrene on a flat substrate, usually a silicon wafer. After the polystyrene dries into a stiff film, it is annealed at 100°C for about two days to remove stresses in the film. We were also able to make silicon-doped polystyrene films.

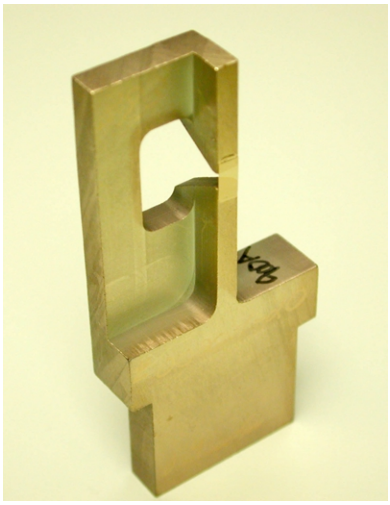

Fig. 3–81. Nike target frame with gold coated polymer film target.

Many of the targets NRL requires are designed to work in a cryogenic environment. The targets have various configurations, but usually have certain things in common. All the cryogenic targets we made for NRL during FY01 consisted of an aluminum CTM (Fig. 3–82) and most had a covering of polyimide film.

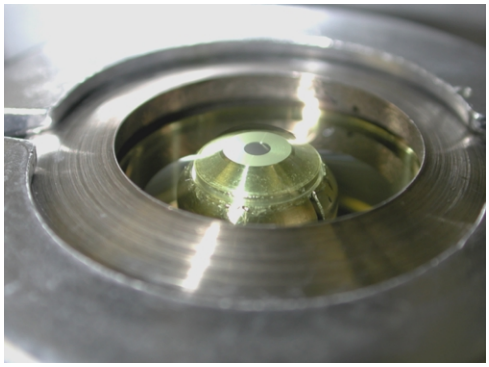

Fig. 3–82. Aluminum CTMs have a film of 1.5 µm thick Schafer-made polyimide stretched over them and sealed.

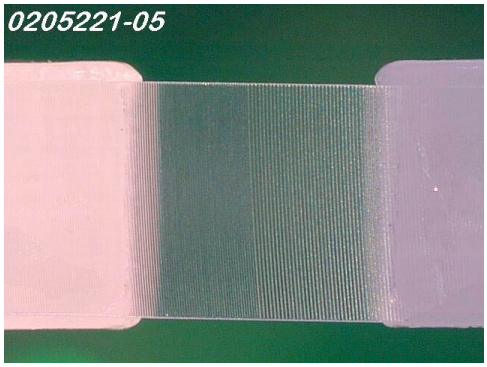

Fig. 3–83. For an NRL experiment, the ridges on a patterned polystyrene film had to be mounted parallel to the edges of the Nike target holder. This target has two different patterns machined side by side.

The simple polyimide films for the NRL targets have been obtained commercially or spin cast in our laboratory. The films we make are normally 1.5 µm thick, but have been as thin as 50 nm. Thicker films, usually 13 µm, are available commercially. These commercially available films often are not smooth and have imbedded impurities and flaws, but if the requirement is only for a cryogenic pressure seal, they are adequate and less expensive than the high-quality films we make.

Often, we have been asked to deliver flat CH films that are doped with an impurity. The most common example of this is the silicon-doped CH films we send to UR/LLE. Ideally, these films are made much like we make the normal dopant-free CH films. However, the raw material used to make these films is usually not as suitable for making thin films as the high molecular weight, monodisperse polystyrene we use for the undoped films. As a result, materials such as silicon-doped polystyrene, which we obtain from GA, or polycyclohexylmethylsilylene $C_7H_{14}Si$ (PCHMS) do not make robust, crack-free films. Because the doped films are usually not as cohesive as pure polystyrene films, we have difficulty lifting them from the casting substrate. We have been successful casting doped films on commercially available salt flats that can be dissolved away after the casting has cured. We are continuing to explore techniques and materials to improve the quality of our silicon-doped CH films.

3.8.3. Patterned CH Films

During FY01, NRL and UR/LLE requested an increased number of polymer films with a sine wave pattern impressed on them (Fig. 3–83). The normal method for making patterned films is to cast the film on a patterned substrate or mold.

We have obtained the best results casting patterned films on molds made of laser-etched fused silica. Fused silica has a very smooth surface, the pattern reproduces well on the film, and the film is easy to separate from the mold after it dries. These molds, however, do have a finite lifetime. After several years of use, we have noticed organic deposits on the molds that cannot be removed by rinsing with solvents. Since target surface finish is critical to the success of many experiments, we do not use mechanical cleaning on these molds. Several

times we have had to buy replacement molds for often used combinations of wavelength and amplitude.

As more of our patterned molds became unusable, it became evident that we needed some way to clean them. Consequently, we purchased a plasma asher. The March Instruments PX 250 (Fig. 3–84) has demonstrated an ability to return our silica molds to near new condition. The asher is flexible for use as a research machine as well as for preparing surfaces for sputter or evaporative coating and activating surfaces so that multiple layers of polymers may be cast into one target foil.

Fig. 3–84. March Instruments PX 250 Plasma Asher. This machine is used to clean silica molds, prepare surfaces for coating, and conduct materials research.

Both NRL and UR/LLE have also requested a number of patterned targets with larger amplitude perturbations. When the amplitude of the perturbations is above 1 µm, it is easy to machine a casting mold from a ceramic or plastic material such as Delrin. Usually, the surface finish for these targets is not as critical as it is for smooth targets or those with smaller amplitudes so single point diamond turning makes an acceptable surface on plastic. Polystyrene usually casts well on Delrin and can be lifted easily. Sometimes, however, especially with larger amplitude patterns, the polystyrene clings to surface features on the mold and cannot be lifted without tearing the film. To facilitate separating the casting from the mold, we coat the mold with a layer of sodium chloride before we cast (Fig. 3–85). The layer conforms to the shape of the mold's surface so the proper pattern is impressed on the polymer film. Separation is easy because the salt layer dissolves away when the mold with its casting is immersed in water.

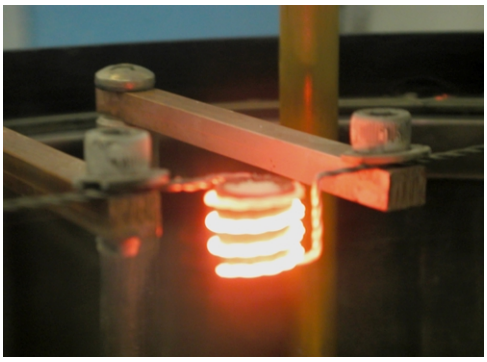

Fig. 3–85. This filament-heated crucible is part of a salt coater used to apply a release layer to some molds before casting.

We have also made patterned substrates of gold, copper, silver, and aluminum blanks using our precision micromachining capability. Unfortunately, it is difficult if not impossible to remove polystyrene from machined metallic molds after casting. We have not attempted to use a salt coating on metallic molds as a release layer, but the technique should work if the salt conforms to the smaller amplitude patterns as well as it does to those of the Delrin molds.

During the past year, we have developed a new technique for making patterned polymer foils: machining the pattern directly onto the polymer. We have used this technique on both polystyrene and polyimide with excellent results. Machining a pre-cast foil not only gives us the proper pattern, but we have better control over the thickness of the finished target.

For targets that have patterns with amplitudes less than a micron or so, etched silica still gives the best results. We have a number of silica molds in our inventory and can order more from our supplier. Table 3–10 is a list of the patterned silica substrates currently on hand at Schafer for casting.

TABLE 3–10
LIST OF THE PATTERNED SUBSTRATES CURRENTLY AVAILABLE AT SCHAFER FOR CASTING

Plate or Design	Surface Function	Period (μm)	Amplitude (μm)
Gnd Quartz #3	Ground with 3 μm grit		
Gentec #01B	Sin(x)	12.0	0.23
Gentec #01C	Sin(x)	12.1	0.28
Gentec #01D	Sin(x)	12.1	0.31
Gentec #06	Sin(x)	20.0	0.25
Gentec #10	Sin(x)	20.0	0.50
Gentec #11	Sin(x)	20.0	1.00
Gentec #08b	Sin(x)	30.0	0.25
Gentec #08a	Sin(x)	30.0	0.26
Gentec #07	Sin(x)	30.0	0.10
Gentec #08	Sin(x)	30.0	0.25
Gentec #09	Sin(x)	30.0	0.50
NPL01	Sin(x)	30.8	0.94
Gentec #03	Sin(x)	60.0	0.10
Gentec #04	Sin(x)	60.0	0.25
Gentec #14	Sin(x)	60.0	0.47
Gentec #15	Sin(x)Sin(y)	20.0	0.23
Gentec #12	Sin(x)Sin(y)	30.0	0.10
Gentec #16	Sin(x)Sin(y)	30.0	0.26
Gentec #13	Sin(x)Sin(y)	60.0	0.10
Gentec #17	Sin(x)Sin(y)	60.0	0.23

3.8.4. Coatings

This year, demand increased for targets made of polymer or foam with a metallic coating. Metal coatings have been primarily aluminum, gold, and palladium. We apply coatings to targets in one of two ways; sputter coating or evaporative coating. Our evaporative coater (Fig. 3–86) can use a variety of tungsten filaments or boats to melt and evaporate most metals. The film to be coated is mounted above the source. A shutter protects the target from excessive heat and a quartz crystal thickness monitor allows us to deposit the correct amount of material. Even with careful control, the heat radiated from the source is often too

much to be absorbed and reradiated by a polymer film, particularly if the film is thin. To protect the film from damage, we mount it on a heat-conducting material.

Fig. 3–86. The evaporative coater is used primarily for aluminum or gold coatings with thickness greater than 1000Å.

Fig. 3–87. Sputter coating facility at Schafer.

Sometimes, mounting film on a heat sink for coating is not practical. Additionally, coating layers of metal thinner than 500Å is difficult to control with the precision required for many experiments. In these situations we sputter coat the metal onto the film or foam (Fig. 3–87). The temperature in the sputter chamber is low enough to keep from damaging polymers and the coating rate is slower so it is easier to control for thin coatings. We have targets for sputtering made of a variety of metals and can order more with lead times of about 8 to 10 weeks.

3.8.5. NRL Foams

The primary ICF target design for NRL includes low-density foam. In the past, and to some extent in FY02, we provided polyimide-covered CTM to NRL and they would make and mount RF foam to complete the target. During FY01, we developed our own capability to make RF foam targets. Because our foam laboratory is in a clean room environment, the foams and foam targets we make are generally cleaner and of better quality than those made in a chemistry lab at NRL. The techniques we use are those that were developed at NRL and some of the equipment we use was supplied by NRL.

We also made foams with rippled surfaces. We form these foams against a mold of rippled polyimide or a patterned quartz substrate. The foam pattern matches the pattern on the mold fairly well; wavelengths match exactly and amplitudes are about two-thirds the mold amplitude (Fig. 3–88). We are starting work on making patterned foams directly on patterned polyimide that has been stretched onto a CTM. Thus, we will provide targets with flat polyimide and patterned foam, patterned polyimide and flat foam, and finally patterned polyimide with patterned foam.

We are routinely able to produce higher density RF foams (250 mg/cc) with desirable thickness (120–140 μm) towards the final goal of making patterned RF foam by single point diamond turning and also patterned polystyrene film-RF foam (250 mg/cc) targets. Further development is in progress.

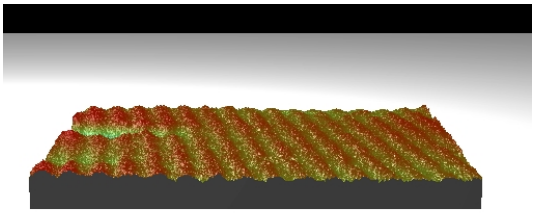

Fig. 3–88. Rippled surface on RF foam.

For making thin target components, we are developing DVB foam as an alternative to RF foam. DVB offers a unique combination of pure CH elemental composition, density as low as 10 mg/cm^3, and a cell size approaching a micrometer (Figs. 3–89 and 3–90). It has been easy to produce bulk samples, but difficult to mold due to the very fragile nature of the foams. The combination of low density and small cell size dictates that the walls must be thin. Removing foam from a mold and then handling it often results in the complete destruction of the foam. This is aggravated by nonreproducible properties in foam batches. One batch (shipped to NRL in July) released well and produced very promising atomic force microscope (AFM) traces when analyzed at NRL. Two more recent batches did not release as well and have been difficult to impossible to characterize by AFM. While these difficulties are not unexpected in a new foam system, especially when trying to produce a difficult geometry, the causes are not currently understood and are part of our ongoing research.

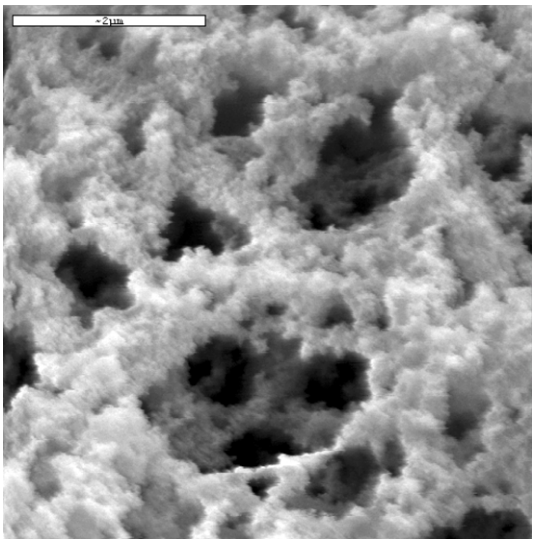

Fig. 3–89. This SEM micrograph shows the cell size and structure of DVB foam. There appears to be very little change in cell size as the density changes.

Additionally, some DVB foam has been used for wicking experiments with liquid D_2. The preliminary indications are that the foam survives the filling process and fills well but more analysis is required.

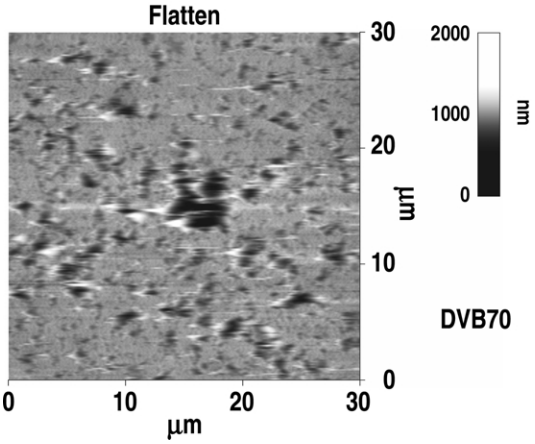

Fig. 3–90. This AFM trace of a DVB foam cast at 70 mg/cm^3 shows an average feature size of approximately 1.5 to 2.5 µm.

3.8.6. NIKE EOS Targets

This year we delivered a new type of EOS target for NRL. These EOS targets consist of a machined 60 µm aluminum plate with a 25 µm step and a pair of aluminum witness strips mounted 60 µm or 100 µm above the plate. The assemblies are mounted on a 13 µm polymer film attached to a CTM.

Figure 3–91 is a photograph of one of these targets. To implement the design, we machine a 60/85 µm thick aluminum plate with 60 µm or 100 µm high supports on each end, depending on the specification. The support walls are actually curved slightly because the plates are machined on a lathe and cut out from a circular piece. The base plates are attached to a CTM that has a 13 µm thick layer of commercially procured Kapton stretched over it. The aluminum witness stripes must be supported away from the base in order to provide a

diagnostic x-ray flash during the experiment when the shock wave reaches them. We support the aluminum with a 6 µm sheet of polyimide with a piece of glass cover slip for stiffening. A hole drilled in the center of the cover slip allows characterization without sacrificing rigidity (Fig. 3–92). The assembled witness plate is fastened to the target in the proper position using the support rails machined into the side of the aluminum base plate.

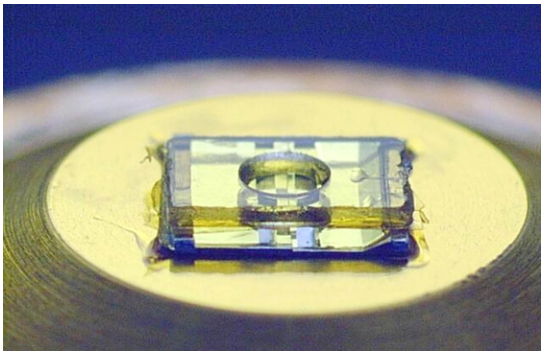

Fig. 3–91. Nike EOS step-witness target.

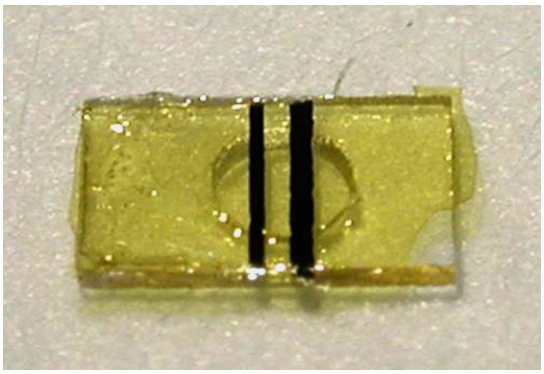

Fig. 3–92. Witness plate consisting of two aluminum strips, polyimide for support, and glass to stiffen the polyimide.

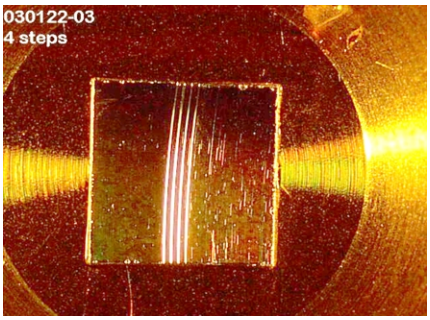

Fig. 3–93. EOS target consisting of a five-level aluminum plate mounted on a Kapton-covered CTM.

We also provided other types of EOS targets, some of machined metal and some of polystyrene. The metal targets were mounted on Kapton-covered CTMs or Nike frames and consisted of a piece of aluminum that was machined to a precise thickness. Many of the targets had from one to five precision steps machined into the top surface (Fig. 3–93).

3.8.7. Characterization

Making targets to precise specifications is critical to the success of ICF experiments — just as critical is characterizing the targets precisely. We have several methods of characterizing targets and target parts including white light interferometers, laser scattering setups, transmission photometers, optical microscopes, and surface profilometers.

3.8.7.1. White Light Interferometer. Most film thickness characterizations are performed with a white light interferometric microscope (Fig. 3–94). This instrument consists of a Nikon Optiphot microscope with a Michelson interferometer in the objective lens assembly. A mechanical probe measures stage displacement to a precision of better than 0.1 µm.

To measure film thickness, we use one of three techniques. When the thickness must be measured far from an edge and the film is attached to a reflective substrate such as a silicon wafer, we focus the microscope on the surface of the film using the interferometer for precision, and then refocus on the substrate. The thickness of the film is calculated by dividing the displacement measured by the mechanical probe by the index of refraction of

Fig. 3–94. By positioning the fringes from this white light interferometer, focus position and, therefore, film thickness can be measured precisely.

the material. If the thickness can be measured near an edge of the film and the film is over a reflective substrate, we focus the microscope on the substrate beside the film and then move the focus to the substrate below the film. Dividing the distance, the stage moves by the index of refraction minus one which gives the thickness of the film. Incidentally, for films with an unknown index of refraction, measuring the thickness using a combination of the preceding methods allows us to solve for both the thickness of the film and the index of refraction.

Sometimes the film is not attached to a reflective substrate and a third method must be used. In this case, we focus on the top surface of the film and then refocus on the bottom surface. As in the first method, the thickness is calculated by dividing the distance the stage moves during refocusing by the material's index of refraction. This method does not always work, especially with patterned films, because there may not be enough light reflected from the bottom surface of the film to allow precise focusing.

3.8.7.2. Scanning Surface Profilometer. The surface of complex objects can be measured with our scanning surface profilometer (Fig. 3–95). Like the white light interferometer, this machine has an interferometric objective that generates constructive and destructive fringes when the microscope is nearly in focus. The maximum constructive interference (brightest fringe) occurs when the microscope is focused precisely.

Fig. 3–95. Our Veeco RST–500 scanning surface profilometer is used to measure the surface of complex objects.

The scanning surface profilometer generates a three-dimensional map of a surface by scanning the focus through a preset range, up to 500 μm, and noting the position of maximum constructive interference for each pixel in the CCD. Thus, a planar image is formed of an entire surface with height information for each point on the surface (Fig. 3–96).

3.8.7.3. UV Microscope. In order to characterize the uniformity of RF foams, we built a UV microscope. The microscope has a strong UV light source that is aligned below the object to be examined (Fig. 3–97). One of two UV objectives collects light transmitted through the object. A UV-enhanced CCD forms an image of the transmitted light, which can then be

analyzed using Interactive Data Language (IDL™) software for data analysis, visualization, and cross-platform application development. This microscope was patterned after a similar machine at NRL. In addition to measuring the optical density of foams, the UV microscope can be used to characterize the uniformity of thin metallic coatings or examine other objects using transmitted light. The system is designed to work with visible light as well as UV.

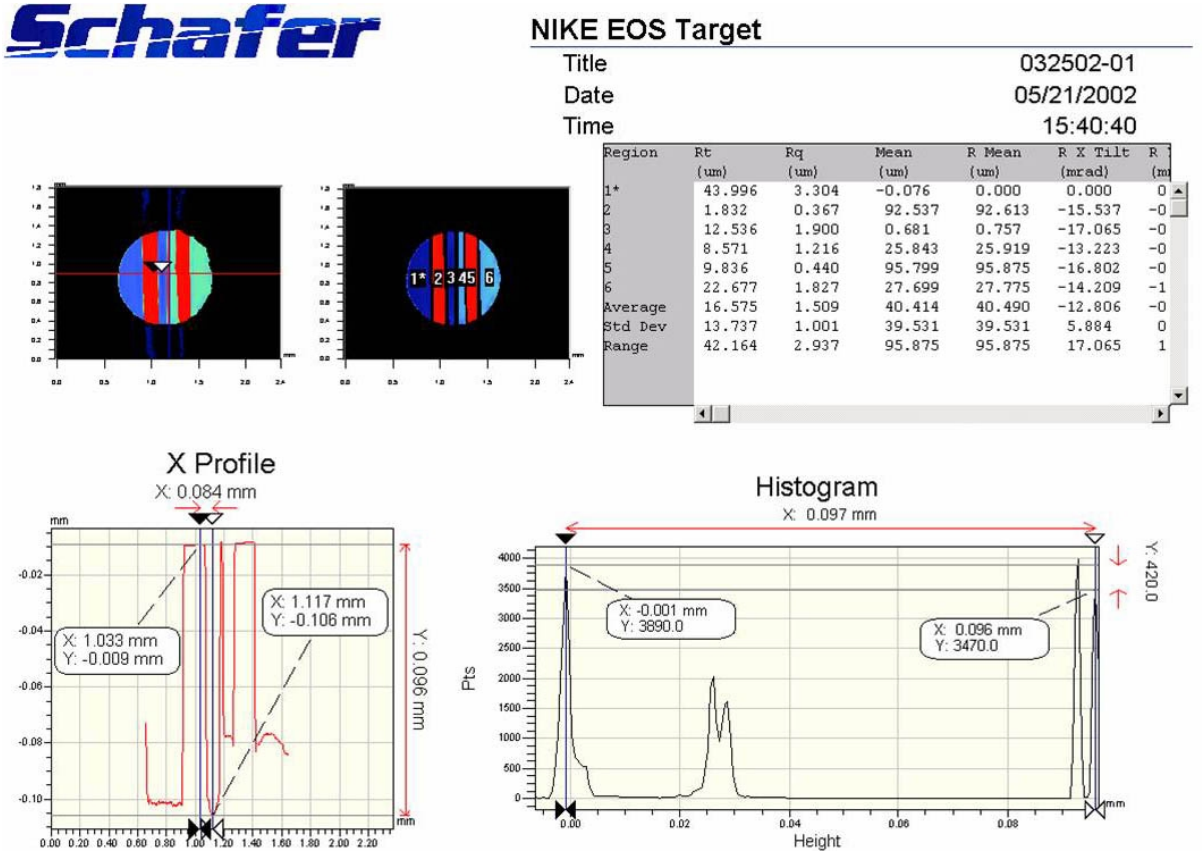

Fig. 3–96. The scanning surface profilometer measures the heights of points over a surface and reports the data in a variety of formats as shown by these characterization results from a foam EOS target.

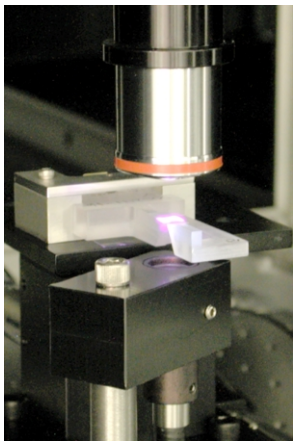

Fig. 3–97. A Nike target is examined by imaging transmitted UV light.

3.9. CHARACTERIZATION INNOVATION AND DEVELOPMENT

Office head: Richard Stephens

Overview

The characterization innovation and development office is responsible for anticipating and defining new characterization requirements within target fabrication and developing the required capability. The anticipating and defining part of the responsibility requires understanding the needs of our customers — in some cases even helping them to understand their needs.

Funding under the DOE contract was meager in FY02. Thus we report on two activities funded outside the DOE contract.

3.9.1. Next-Generation Spheremapper/Wallmapper[15]

We have designed, built, and delivered the next-generation spheremapper/wallmapper (SM/WM) to UR/LLE. It takes advantage of all our experience in production characterization at GA and embodies it in a more coherent, user-friendly design.

1. The workspace has been organized and made; monitors are clustered around the working area while the electronics boxes are off to the side [Fig. 3–98(a)].
2. The vibration isolation system has been redesigned to minimize low frequency vibrations that previously degraded performance in the mode 10 to 100 range (at some reduced sensitivity in modes >1000) (Fig. 3–99).
3. The AFM head has been redesigned to allow easier access to the rotating vacuum chuck tilt adjustments. [Fig. 3–98(b)].

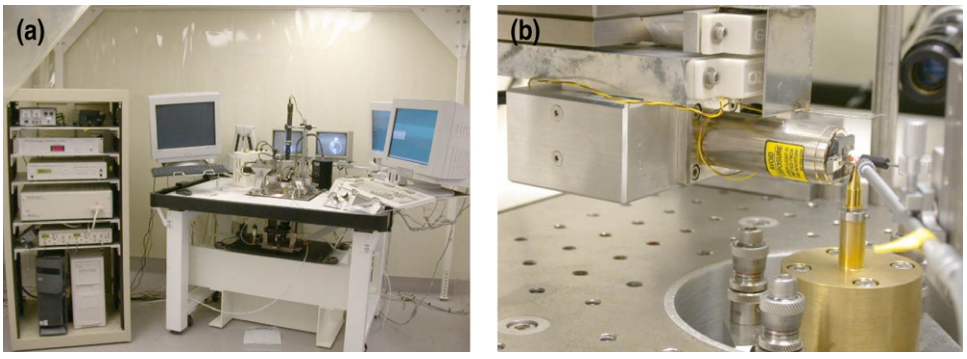

Fig. 3–98. (a) SM/WM installed in target fabrication area at UR/LLE. (b) View of the AFM head from direction of the operator showing clear access to the tilt control knobs on the rotating vacuum chuck.

[15]Work done for the University of Rochester under contract 411876-001G.

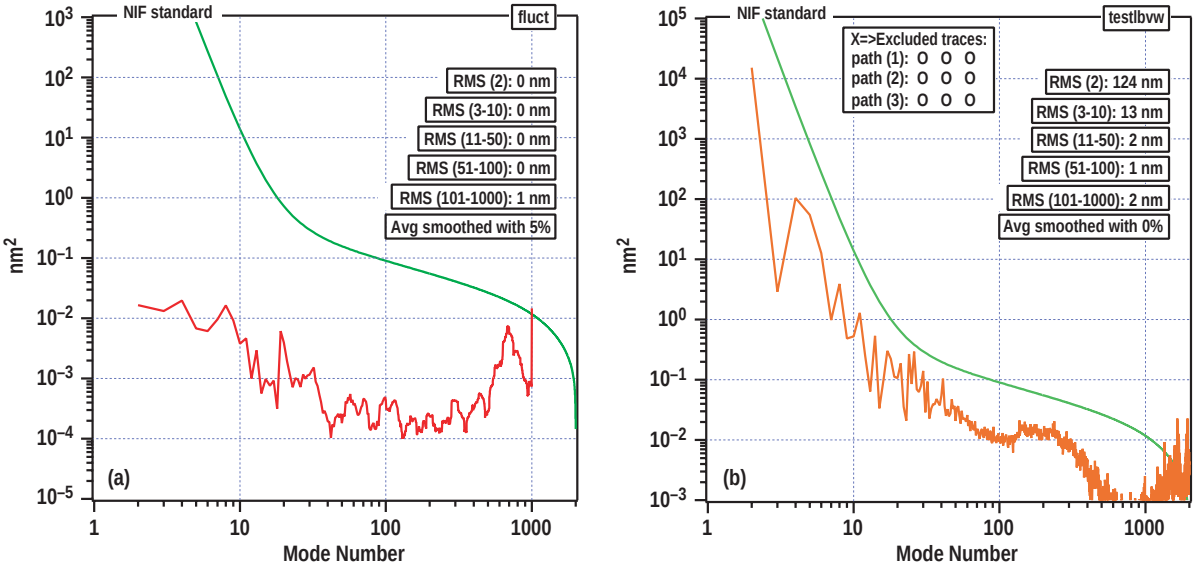

Fig. 3–99. (a) Nose power determined from height fluctuations recorded while the AFM tip is resting on a nonrotating shell. (b) Roughness power spectrum averaged from three parallel traces around a test shell.

4. The SM control system has been switched from a Mac to a PC computer allowing consolidation with the WM controls onto the same system (and eventual integration of those control systems).

5. A jig has been constructed to support flat samples in front of the AFM head, allowing easier calibration of the system.

For further information, contact R.B. Stephens.

3.9.2. Video Measuring Microscope[16]

This last year, we bought a NEXIV VMR from Nikon (Fig. 3–100) to automate labor-intensive batch characterization jobs. All aspects of this microscope — magnification, illumination, stage position — are under computer control, and the stage reproducibility is ~0.2 µm for short distances. The software includes edge detection and surface routines that allow analysis of images. One of the more convenient of these routines allows the microscope to trace out the edges of images that are larger than the field of view of the microscope (the stage is used to recenter the examination area whenever it gets close to the edge of the field of view); the result of those analyses can be automatically output to a formatted spreadsheet. Reproducibility of those measurements

Fig. 3–100. NEXIV VMR.

[16]Work supported by Internal Research and Development funds from General Atomics.

is excellent. The standard deviation for repeated measurements of 2 mm diameter shells (including find and focus steps between each measurement) is ~ 0.1 μm.

We have developed a jig and programs for initial batch measurements of PAMS shells. The jig is an array of Al dots on a thin hydrophobic plastic sheet. When the jig is dipped in water and blown (almost) dry, each hydrophilic Al dot retains a water drop that can temporarily and cleanly hold down a shell. When the dots are loaded with shells, the jig is placed under the microscope and the coordinates of two of the dots are located. Using those locations, the program will automatically find every shell in the array, for each one measuring its average diameter, out-of-round, wall thickness, and nonconcentricity, and create a spreadsheet with those values and the batch average. It takes about 10 minutes to characterize 16 shells.

Although the program described above works, our testing program revealed an asymmetric illumination or distortion that added ~1 μm to the out-of-round measurements. That was not present in the system we tested before purchase; Nikon is investigating the problem and will correct or replace our instrument. There is a further problem in calibrating the shell dimensions. Measured diameter varies nearly continuously with light intensity (Fig. 3–101), and the intensity dependence is different for our sapphire ball size standards and the hollow plastic shells; we expected a middle range of light intensity for which the diameter was insensitive to light setting. We suspect that this problem arises from the illumination asymmetry.

As soon as these problems are corrected, the microscope will be moved into the characterization lab and will replace one of our manual microscope setups. In the future, we expect to add the capability for batch characterization of stepped witness plates.

For further information contact: R.B. Stephens.

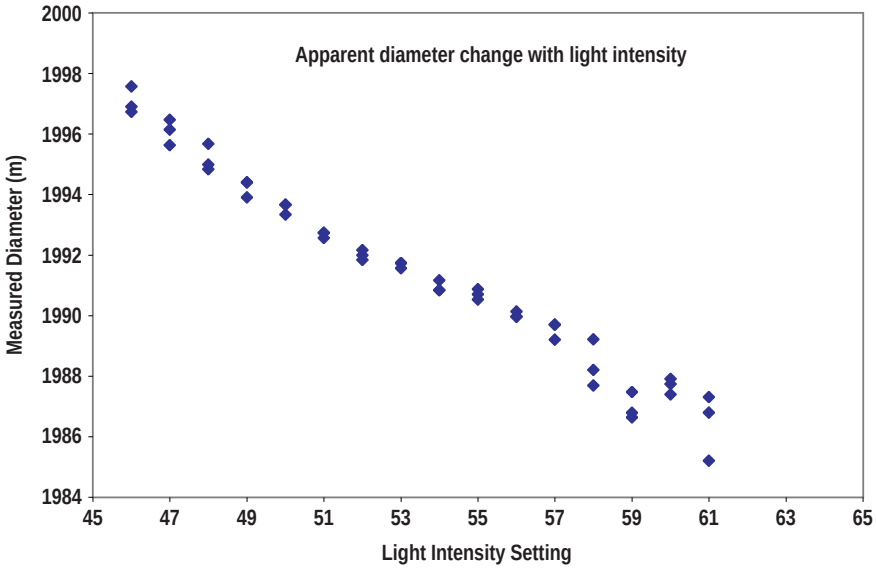

Fig. 3–101. Apparent change in shell diameter with light intensity setting.

3.9.3. Radiography System for Low Density Foam Components (Diana Schroen)

The Sandia on-site support was gifted a radiography system by Sandia National Laboratories (Fig. 3–102). This system had been an experimental system, designed and built by Larry Ruggles. Fortunately, it had many very desirable design features for our application (Fig. 3–103). First the x-ray source was an electron source with changeable anode and filter capability. This allows one to select the energy of x-rays that are going to be used. Second, the system was designed to have the samples analyzed under vacuum. For very low-density components, this is essential. Consider the problem of trying to analyze a 5 mg/cm^3 foam. The foam is composed of only carbon and hydrogen. The density of dry air is 1.2 mg/cm^3, but includes elements that are much more x-ray absorbing, oxygen for example. Unless the air around the sample can be removed, it is impossible to obtain any contrast in the radiographic image.

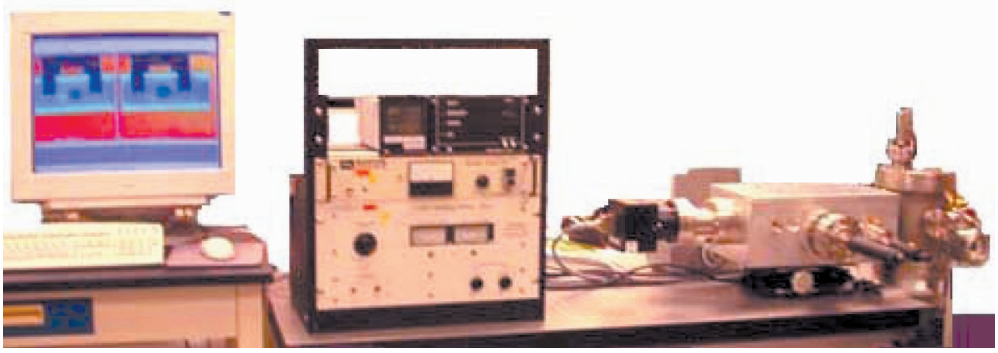

Fig. 3–102. This is the radiography system as it exists today. Two foam cylinders with embedded capsules are shown in false color on the monitor. The electronics include two vacuum gauges, power source and x-ray source control. The vacuum chamber and x-ray source are at the far right.

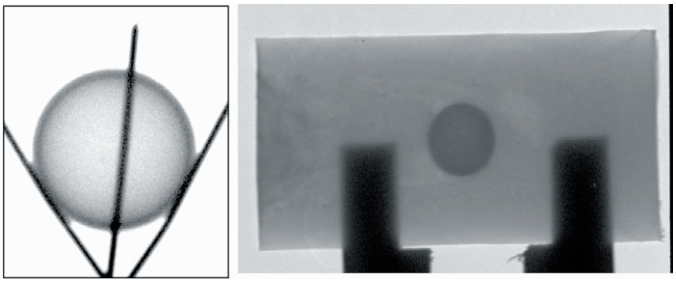

Fig. 3–103. These are two examples of radiographs collected by the current system. The first image is a 4 mm foam sphere, 100-mg/cm^3 density with about a 300 µm wall. The second image is that of a 12 mm long cylinder of 14 mg/cm^3 density foam with an embedded capsule.

We are in the process of optimizing this system for our application. We are going to add the ability place up to 11 samples in the chamber at a time and the ability to rotate the samples to get two orthogonal views. At some future date, we hope to build a second-generation unit with 10 µm resolution, but the current system is limited to about 28 µm.

3.10. OPERATIONS OFFICE FOR SCHAFER DIVISION OF INERTIAL FUSION TECHNOLOGY

Director and Head of Operations: Keith Shillito (Schafer)

Target Fabrication Technicians: Ron Perea, Craig Rivers, Chris Bostick, Steven Gloss, Dave Tanner, and Chris Russell (Schafer)

Overview

The Operations Office at Schafer's Livermore Laboratory is responsible for budgets, reporting, task coordination and personnel management for all activities related to Schafer's role in the ICF target fabrication program. It also serves as the link for those people who work on-site at LANL, LLNL and SNL under laboratory supervision. The work of our LLNL on-site employees is covered in Section 3.11.1.

3.10.1. On-Site Support at LANL

During FY02, Ron Perea built over 1000 targets for the Trident Laser Facility. In addition, he was directly involved in the LPI experiment with Dennis Paisley at LANL. This experiment has taken a great deal of extra time to build the targets, make fixtures for the fabrication process, order all the special materials (BK-7, sapphire, gold, copper, etc.). Perea met with different groups who specialize in different types of coatings to ensure that the parts would be coated to the highest standards and would be finished in a timely manner. He also had the task of finding companies that do high-quality precision machining. Throughout, Ron always managed to get enough targets to the experimenters so that no shot time was ever lost and the targets turned out near perfect quality every time. At present, Ron is still working on this experiment and hopes to have some results by December 2002. Laser-launched flyer plates are being developed to accelerate a 1-D plate to high velocities (100 to 1000 m/s) to impact 1-D targets as depicted in Fig. 3–104.

By recording the free surface of the shocked target, the dynamic response of the target to shock waves and release waves can be understood. This data is of importance for weapons programs, ICF target designs, and basic material properties. Trident experiments will use laser-launched flyer plates to collect spall data depicted below (Fig. 3–105).

Fabrication of substrates and flyer plates with precision and accuracy is required for quality experimental data. The quality of the flyer plates and targets determine the shot-to-shot variation.

3.10.2. On-Site Support at SNL (Schroen)

At Sandia National Laboratories we have an Assembly Technician, David Tanner, and a Production Engineer, Chris Russell. The group is managed by Diana Schroen. A portion of the Foam Center personnel are also on site to facilitate the production and delivery of foams to SNL, but their work is covered under Section 3.6.

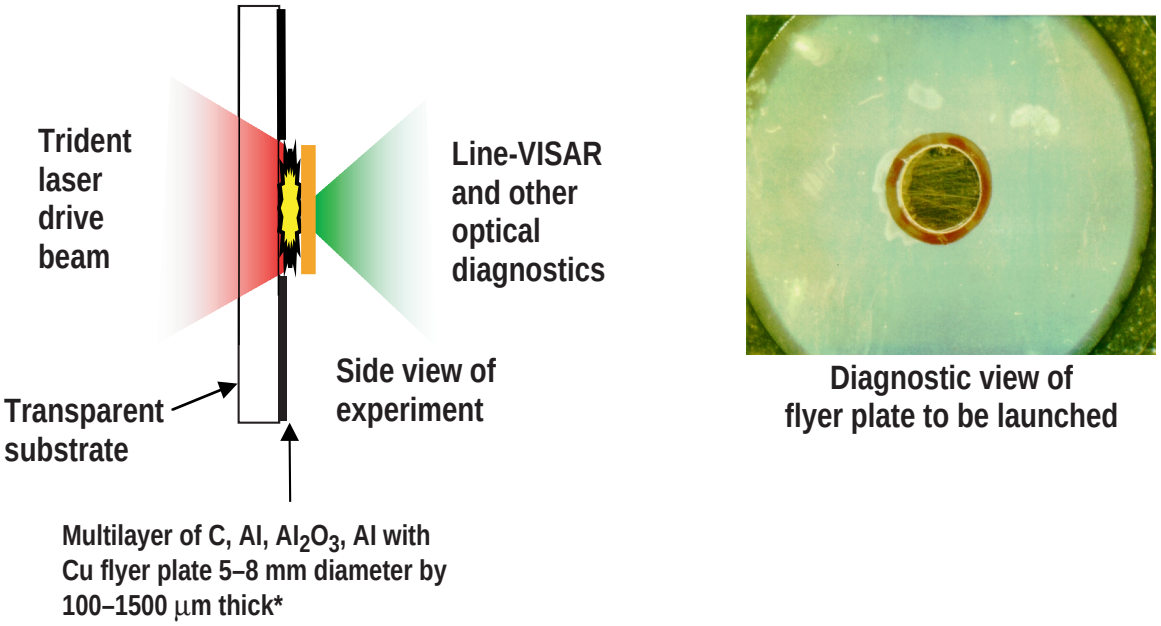

Fig. 3–104. The Trident laser can launch 1-D flyer plates of various thickness (2 to 1500 μm) and velocity (0.1 to 5 km/s).

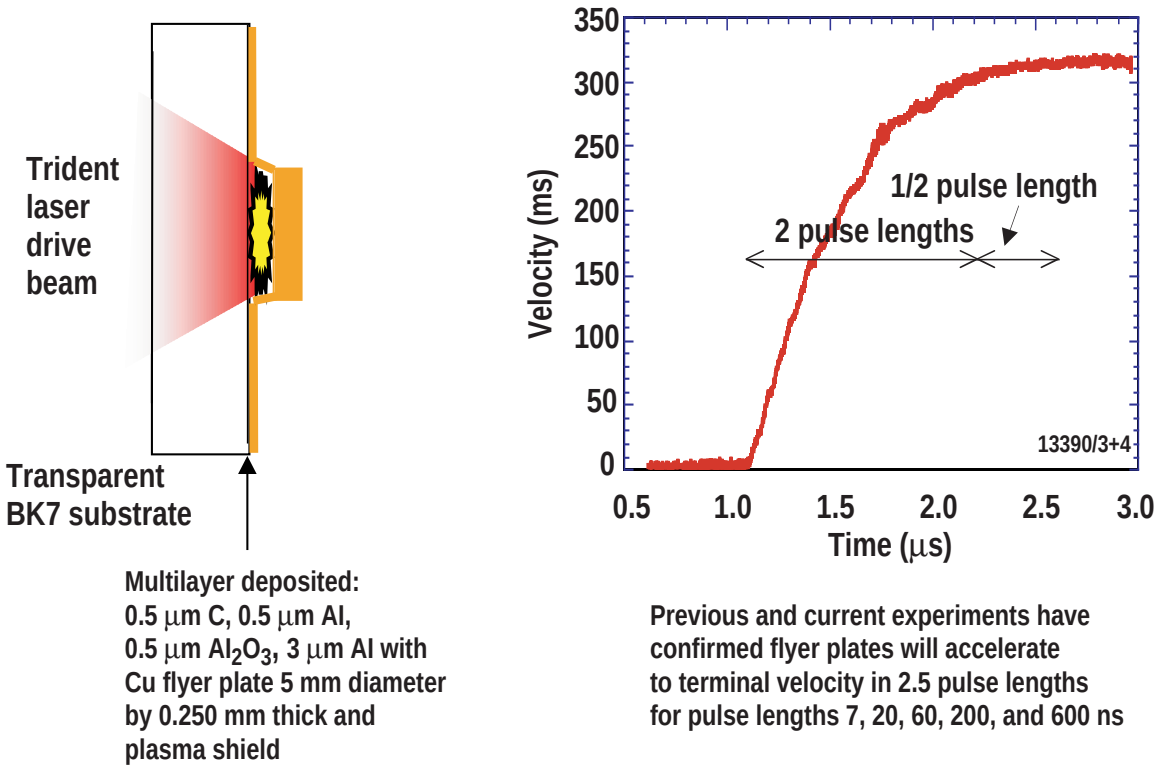

Fig. 3–105. Trident experiments will use laser-launched flyer plates to collect spall data.

The Target Fabrication Laboratory at Sandia supports five facilities: Z, Saturn, Star, Z-Beamlet and OMEGA. We have made a strong push this past year for increased documentation and quality control. As part of that effort, we have been using CAD drawings, generated by Mr. Russell, to procure and fabricate targets. Procedures are being documented stored in an electronic database. This will hopefully culminate in an ISO 9001 certification for this facility.

The assemblies provided include diagnostic assemblies, filters and targets. There are two basic types of targets: hohlraums and EOS assemblies. The hohlraums are used for experiments on Z and OMEGA (Fig. 3–106).

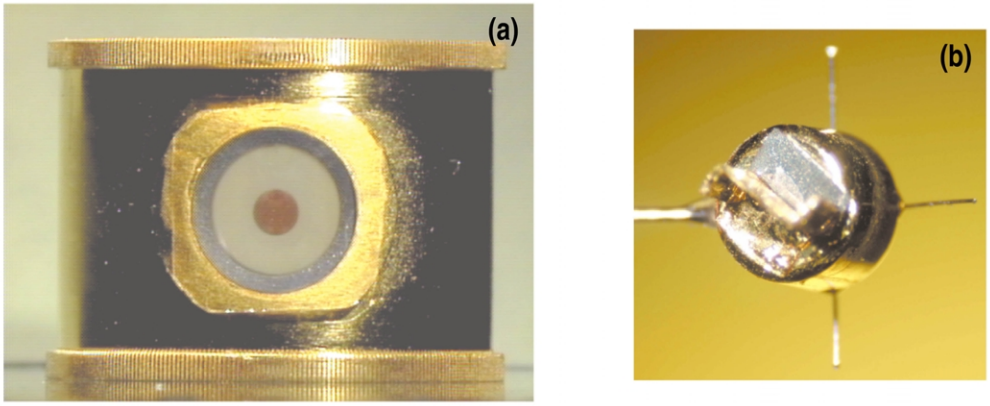

Fig. 3–106. (a) This hohlraum is typical for a Z experiment where the capsule would be backlighted by Z-Beamlet during compression. Hohlraum (b) was used on OMEGA this year.

The EOS assemblies require specialized characterization and assembly techniques (Fig. 3–107). The goal is to minimize glue bond thickness and fully characterize components for thickness and planarity. We are now making EOS assemblies for Z, Saturn, and Star. The components used have included depleted uranium, heaters (for melting samples), and cryo cells (for D_2 studies).

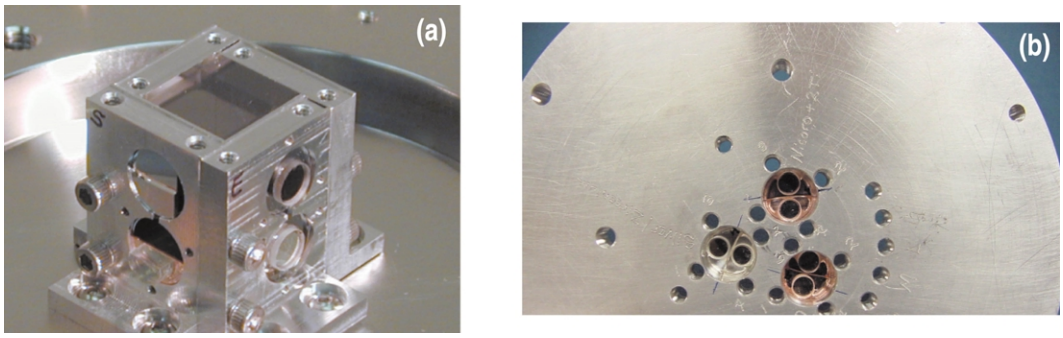

Fig. 3–107. (a) A typical EOS assembly that could be used on Z or Saturn. (b) An EOS assembly of the Star gun facility.

3.11. OPERATIONS

Operations Office Head: Wayne Miller

On-Site Target Fabrication at LLNL

Project Leader: Russell Wallace (LLNL)

Target Fabrication Technicians: Chris Bostick, Steven Gross, Craig Rivers (Schafer), and John Ruppe (GA)

Overview

The Operations Office supports the division in carrying out program activities, in supporting and monitoring the Division of IFT to help ensure customer satisfaction. The Operations Office also provides administrative support for on-site target fabrication technicians stationed at LLNL. (Technical direction is provided by the LLNL project leader.) The Operations Office is described in Section 4.3.7.

3.11.1. On-Site Support at LLNL (W. Miller; writing contributed by John Ruppe)

At LLNL, we support the target fabrication program by micro-machining and characterizing target components and, subsequently, assembling these components into a major portion of the completed targets that are used for LLNL experiments at UR/LLE's OMEGA facility. Targets and components of a myriad of shapes, sizes, and materials have been provided for this purpose over the past few years. In the following paragraphs, we discuss a representative sample of types currently in use.

The indirect-drive hohlraum target has been a workhorse of the LLNL ICF program dating back to the early days. Figure 3–108 shows an OMEGA-type target consisting of a GA produced split-case hohlraum within which, as is often required, a fuel capsule made by GA is suspended between two thin layers of plastic film. The hohlraum is mounted on a glass stalk at the nonorthogonal angle mandated by the OMEGA target chamber's geometry and in a specific orientation towards a circular pin-hole array.

Fig. 3–108. An OMEGA-type target with a capsule-containing hohlraum oriented towards a circular pinhole array.

Figure 3–109 shows stages and aspects of a hohlraum-type target where the central element is not a capsule, but an aerogel foam disk with cutouts machined into it (by LLNL). Figure 3–109(a) pictures the collection of parts that will comprise the target. (The foam disk is in the upper left hand corner, supported on a gold washer.) In Fig. 3–109(b), the target is at a stage in its assembly where the edge of the white foam disk can be seen sandwiched between two GA-produced

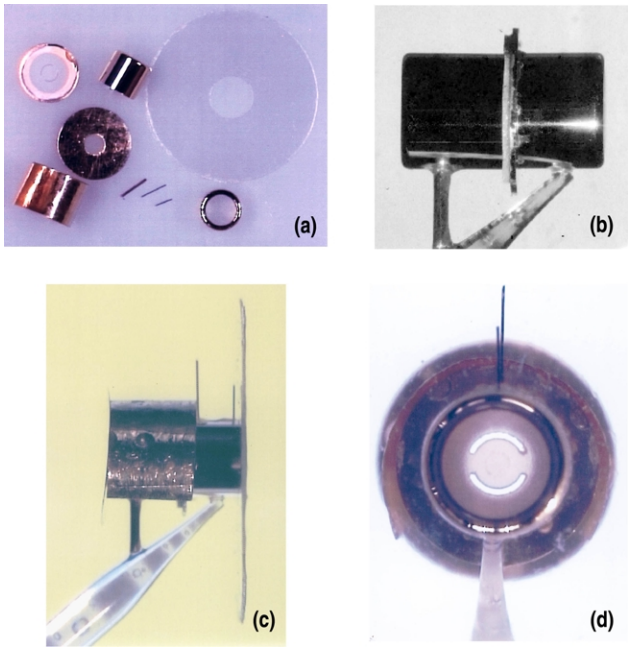

Fig. 3–109. Target parts, which include a washer-supported foam disk [top left corner of (a)], are first assembled into a sandwich comprised of GA half-hohlraums on both sides of the foam disk (b) and then turned into a completed target with the addition of shields and alignment fibers (c). Cutouts machined into the foam disc are most clearly viewed through one of the target's LEHs (d).

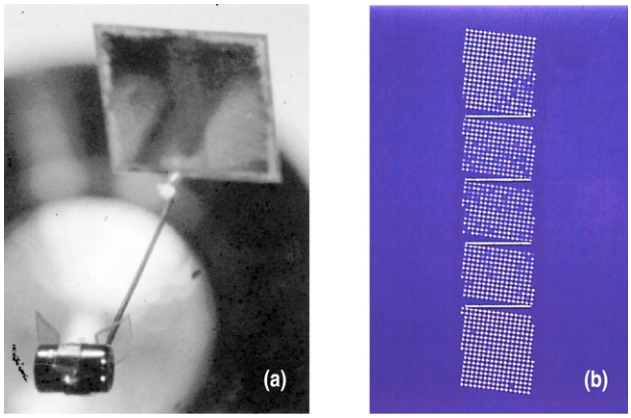

Fig. 3–110. In this variant of the target in Fig. 3–108, the pinhole array [the square piece shown foreshortened in top right corner of (a) and face-on in (b)] is attached such that a line projected at a certain angle from the center of the capsule inside the hohlraum through a diagnostic porthole in the hohlraum's side should pass through the centermost of the 1152 holes constituting the array.

half-hohlraum components, while Fig. 3–109(c) displays the completed target with its attendant shields and alignment fibers in place. Viewed through the target's LEH, the cutouts in the foam disk are most readily visible in Fig. 3–109(d). (The assembler's task was delicate in handling the foam disk, as it was unlikely to survive being dropped or otherwise mishandled.)

The target shown in Fig. 3–110, is a variant of the one pictured in Fig. 3–108, but here the 6.5×6.5 mm pinhole array seen foreshortened in the upper right corner of Fig. 3–110(a) virtually dwarfs the standard-sized GA-made capsule-enclosing split-case hohlraum at the lower left.

The array [shown face-on in Fig. 3–110(b)] is about 16 mm distant from the center of the capsule at the center of the hohlraum. Difficulty was introduced here by an experimental design requiring that a line drawn at a given angle from the center of the capsule through the center of a diagnostic port in the hohlraum's side should, with the array's substrate tilted at a given angle, come as close as possible to passing through the centermost 10 μm diameter pinhole in an array of about 1200. Unfortunately, objects 16 mm apart appear at opposite extreme outer limits of the field of view of our group's standard assembling microscopes, even at their lowest magnifications, where lens aberrations start to distort distances and angles and the coarse units of measurement that go with low magnification add further imprecision. It seemed a long shot that

these targets could be made to the requisite specifications, but the problem was abated by using a Powell scope, a device usually used for characterizing completed targets, as a second assembly stage. Briefly, this was done by first assembling the complete targets as reasonably close as could be done on our standard microscope setups. The completed target was then placed on the Powell scope. Using this instrument's ability to provide measured rotational movement around two axes in addition to x-y-z motion, several trigonometric calculations were used to determine the settings at which a line-of-sight could be projected from the scope through the hohlraum's center to the center of the pinhole array substrate positioned directly behind the hohlraum. The target was then positioned at these settings. If, as was almost always the case, the array's actual position deviated significantly from its ideal position, it could be physically nudged into the position where it was required by bending its support post manually or by micromanipulator.

Though hohlraums are probably the GA-produced components most commonly used as the centerpiece for LLNL OMEGA targets, other GA-made elements often find themselves in this role. In Fig. 3–111, a GA aluminum-rippled plastic witness plate mediates between the gold ring and beryllium washer-enclosed carbonized foam below it and the filter and backlighter stacked above it. In Fig. 3–112, a GA PVA-coated GDP capsule is the central element in the target, flanked by a backlighter and a pinhole slot. Appearances are deceiving here, since what looks like a fairly simple target is complicated. The assembly setup consists of the elements positioned at three different levels, mounted at different angles to their stalks, with the slot set at a certain angle within its substrate vis-à-vis the support stalk of the capsule and at a certain distance from the capsule's center, and the whole target placed into and rotated on a protractor wheel to set a specified angular distance between the horizontal axes of the slot substrate and of the backlighter.

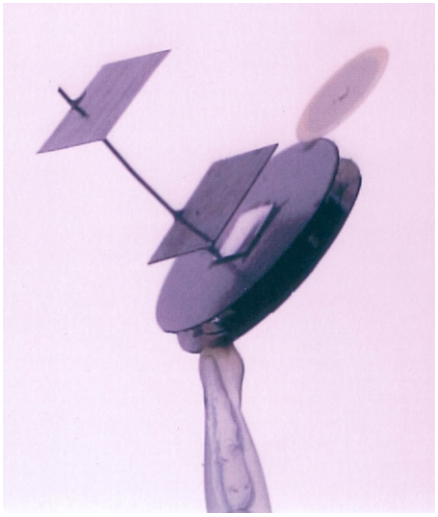

Fig. 3–111. In this target, the central element is the shiny GA aluminum-rippled plastic witness plate mounted on top of an encased circular foam and below a filter and a backlighter.

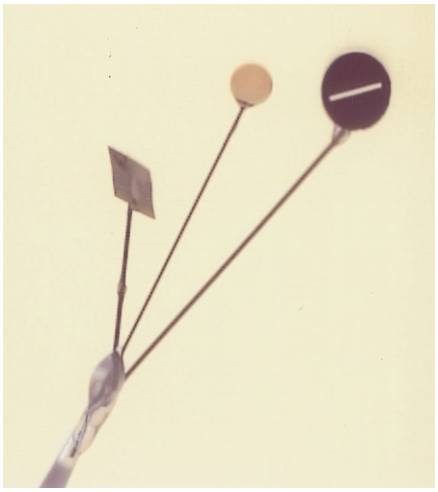

Fig. 3–112. The complexity of the interrelated angles and distances specified (e.g., slot at 54 deg to target support within substrate tilted 10.8 deg to vertical axis at line of sight distance of 4000 μm from slot center to center of capsule) provided a high level of difficulty in assembling this seemingly simple target consisting of a GA PVA-coated GDP capsule, a backlighter, and a pinhole slot.

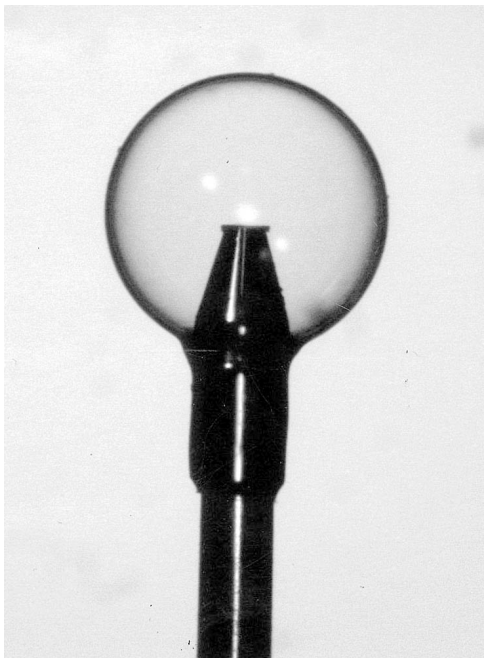

Fig. 3–113. Designed to provide a quicker, closer view of center-shell shot dynamics, this recent target features a hollow gold cone, with a 70 μm beryllium-capped hole at its tip, inserted directly into the fuel capsule as a viewing port.

Components of a newer entry in the target repertoire are shown in Fig. 3–113. Here the blunted and coned end of a bottle-shaped hollow gold cylinder has been inserted into a hole drilled into an approximately 900 μm diameter GA polymer fuel capsule. A 70 μm hole at the top of the 110 μm diameter neck end of the bottle serves as a viewing port inside the shell from which a quicker and closer look at shot dynamics at the center of the shell can be had than could be gotten from diagnostic devices looking exclusively from outside. Since the shell has to be permeation-filled with gas and thus needs to be leak-tight, the "bottle" is capped with a flat 120 μm square piece of beryllium foil and sealed with glue. (Any gaps between the cylinder and the shell at the drilled shell entrance hole are also sealed with glue.) Overall, our target fabrication support group at LLNL enjoys working on the wide variety of target types it now produces and is ever eager to expand and adapt its capabilities to meet whatever challenges the target designs of the future will present.

4. ORGANIZATION

4.1. INTRODUCTION

GA and Schafer are an experienced, highly skilled team of scientists, engineers, and technicians responsible for meeting the target support needs of the ICF Laboratories.

GA is one of the leading U.S. high technology companies, engaged in diversified research and development in energy, defense, and other advanced technologies. GA was established in 1955 to explore the peaceful uses of atomic energy. Today, GA is a privately held company with approximately 1500 employees. GA has the largest and most successful fusion program in private industry, including the DIII–D tokamak magnetic fusion experiment and the ICF Target Fabrication Laboratory. GA has provided over 60 TRIGA research reactors which are being operated in more than 15 countries around the world. GA is also the primary developer of gas-cooled nuclear power reactor technology in the U.S.

To best serve the needs of the ICF Program, GA teamed with the Livermore, California office of Schafer Corporation. Schafer provides analysis, research, development, test and evaluation of 21st century technology applications in the emerging markets of information management, computer networking, materials science, energy, environment, defense, and space. The firm has proven expertise in numerous science and engineering disciplines. Schafer's technical staff of 130 professionals at six principal offices constitutes a dedicated and highly trained team of experts.

The GA/Schafer Team is a very capable managerial and technical team that has proven abilities in the successful performance under our contracts for the past 10 years.

4.2. STRUCTURE

The GA/Schafer team is organized as the capabilities-based Division of Inertial Fusion Technology shown in Fig. 3–1. Organizations within GA that support the Division include QA, Contracts, Purchasing and Finance. The Division Director has overall responsibility for all Division and support activities. Center and Office heads report directly to the Division Director, and each Center Head has full line management responsibility for the employees and contractor personnel within his or her center as described in the sections following.

4.3. CENTERS

4.3.1. Program Management

The Program Manager, **Jill Dahlburg**, is director of the Division of Inertial Fusion Technology (IFT) and co-director of the Theory and Computing Center in the Fusion Group at General Atomics (GA) in San Diego, which she joined in February 2001. Dr. Dahlburg's IFT Division employs more than seventy full time technical and support personnel and ten students, including more than forty GA permanent employees. Ongoing areas of IFT Division activities include: target and component fabrication for inertial confinement fusion research; mass production techniques development for inertial fusion energy; cryogenics and target injection systems development and deployment; high intensity laser matter interaction research; efficient production of hydrogen; sources of iodine for high power gas lasers; development and micro-machined fabrication of optical components; and, research and development in a range of areas pertinent to ballistic delivery of miniaturized sensor systems.

Dr. Dahlburg, who received her Ph.D. in theoretical plasma physics from the College of William and Mary in May, 1985, is recognized as a technical authority on: high performance computing algorithms and techniques; fluid and gas dynamics; and, experimental data analysis, interpretation, and integration. Dr. Dahlburg joined the civil service research staff at the Naval Research Laboratory (NRL) in June 1985 as a computational physicist in the Laboratory for Computational Physics and Fluid Dynamics. As a member of the NRL Nike KrF Laser Program from its inception, and Head of the Laser Plasma Hydrodynamics Section for that Program, Dr. Dahlburg contributed to laser matter interaction research, with emphasis on the understanding of the Raleigh Taylor instability, implosion and coronal hydrodynamics, and laser beam imprinting. In particular, she spearheaded the development of RAD3D, the first three-dimensional multi-group radiation transport hydro-code appropriate for laser-plasma modeling. RAD3D has remained a premier simulation code in that field for more than a decade. In 2000, Dr. Dahlburg joined the Tactical Electronic Warfare Division of NRL, as Head of the Distributed Sensor Technology Office, where she was Co-PI on the ONR/MCWL-sponsored SECNAV Small UAV initiative, Dragon Eye, and PI for the NRL Micro Air Vehicle and Non-Conventional Aerodynamics Programs. Dr. Dahlburg's technical collaborations have included scientists in both the national and international physics and engineering communities. She has served on numerous review and other committees for the Department of Energy, the National Academy of Sciences/National Research Council, the National Science Foundation, and the American Physical Society (APS). Jill has chaired both the Maxwell Prize and Nominations Subcommittees for the APS/Division of Plasma Physics (DPP), is 2002 Vice-Chair Elect for the APS/DPP, and she served as Divisional Associate Editor (Plasma Physics) for The Physical Review Letters (1996-2000). Her professional honors include five NRL Alan Berman Research Publication Awards, and being named APS Centennial Speaker (1998-99) and APS/DPP Distinguished Lecturer (1999-00). Jill Dahlburg is a Fellow of the American Physical Society.

4.3.2. Center for Advanced and Cryogenic Technology

The Center for Advanced and Cryogenic Technology focuses on the design, assembly, and testing of cryogenic target systems for ICF, IFE, and Z-pinch machines. Working as a team with UR/LLE, LANL, NRL, and LLNL, we designed and built several cryogenic systems. A significant achievement for the center so far has been the design and testing of the OMEGA Cryogenic Target System with the significant participation of UR/LLE. This system fills, transports, and inserts cryogenic direct drive targets into the OMEGA target chamber in Rochester. Operational since late 2000, it is now used to fill cryogenic direct drive targets. We also completed fabrication of the Deuterium Test System, and supported LLNL in the installation of the system. This is the first apparatus available for conducting layering experiments on full-scale NIF indirect drive ignition targets, a crucial step in the ignition goal of Stockpile Stewardship. It will have the capability to fill targets by permeation to a pressure high enough that a full thickness fuel layer is generated upon cooling the target. We are an integral part of the design team for the NIF Cryogenic Target System, assigned to lead the development of the Target Cryostats subsystem and the Layering subsystem, and provide general design support as requested on other systems and subsystems. Also in support of NIF, we are working with LANL to develop and build the NIF Beryllium Capsule Deuterium-Tritium Fill System. This system is designed to fill hollow beryllium capsules with high-pressure DT gas by bonding two machined hemispherical shells together in a high temperature, high pressure, DT environment or laser-drilling holes through shells, filling them with DT, and sealing the micron sized holes.

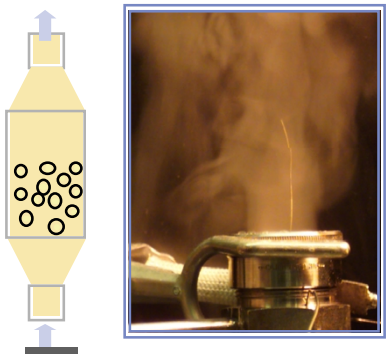

The Center for Advanced and Cryogenics Technology is also the center for developing innovations in target fabrication with the emphasis on mass production. This includes (under another DOE contract) developing techniques to substantially decrease the cost of an ICF target from approximately $2.5K per target today to 25¢ per target for future IFE plants.

The Center for Advanced and Cryogenics Technology supports the current ICF program in cryogenic engineering and is preparing for future programs by developing mass production techniques for target fabrication.

Gottfried Besenbruch (Ph.D. Inorganic Chemistry, Justus Liebig University) is Associate Director of the Division of Inertial Fusion Technology and head of the Center for Advanced and Cryogenics Technology. Dr. Besenbruch has 35 years of experience in research, the development of technologies, and the design and construction of process plants. In his first 20 years at GA, he worked in the nuclear field, first as a scientist and later as a program manager. The work centered on developing fuel for the High Temperature

Helium Gas-Cooled Reactor at GA. It included development of a UF_6 conversion process, sol-gel production of uranium and thorium microspheres, fluidized-bed coating of microspheres, preparation of fuel compacts by injection molding, advanced quality control techniques, and nuclear waste and off-gas treatment at bench-scale and pilot-scale levels. During construction of the Fort St. Vrain nuclear reactor, he spent three years at the site controlling close-out of action items and document turnover.

In addition to the nuclear effort, Dr. Besenbruch spent a significant time on providing technical and programmatic guidance for the scientific and engineering development of a number of non-nuclear processes including a thermochemical water-splitting process for hydrogen production.

Over the past years, he has guided the design and construction effort of the OMEGA Cryogenic Target System. He has also been in charge of designing and constructing cryogenic test systems for LLNL (Versatile Hohlraum Test Apparatus, D_2 Test system) and the CEA (System Study Fill Station).

Neil Alexander has a Ph.D. in Physics from Syracuse University. Dr. Alexander is responsible for development of ICF cryogenic target filling and transporting systems at General Atomics. Recent work has included design of high pressure, precise-control tritium systems, and design of cryostats for transporting and storing of filled cryogenic targets. He is Lead Scientist for NMR imaging of ICF fuels.


Neil Alexander


Rémy Gallix


John Sheliak

Rémy Gallix is a Senior Staff Engineer responsible for the design, analysis, and construction of cryogenic systems. He is a registered Professional Engineer (Mechanical) in California with a M.S. in Civil Engineering from the University of Louisville, KY. and a B.S. in Mechanical Engineering from the Ecole Nationale des Arts et Métiers in France. He has 32 years of international experience in the design, analysis, construction and testing of mechanical and structural systems for High Temperature Gas-Cooled Reactors, magnetic confinement fusion tokamaks, TRIGA nuclear research reactors, Direct Energy Conversion Fission Reactor research, and cryogenic target systems for NIF, the Z-P3 IFE project, and CEA.

John Sheliak has a B.S. from the University of Michigan in electrical engineering. His career in ICF spans from 1979: KMSF; LANL; and since 1992, with GA. He collaborates with the LANL team members on solid DT β-layering experiments, including optical system

and computer acquisition set-up, performing experiments, and data reduction and analysis. John Sheliak is author or co-author of numerous papers and presentations.

Tom Drake and **Bob Stemke** are a designer and senior technician, respectively, under the direction of Alexander. They are heavily involved in the design, assembly, and testing of the cryogenic systems.

Tom Drake

Bob Stemke

4.3.3. Center for Advanced Cryogenic Layering

The Center for Advanced Cryogenic Layering is responsible for developing layering techniques for cryogenic DT fuel inside the target capsules.

The NIF will require the development and fielding of complex cryogenic hohlraum target assemblies. The hohlraum target contains a spherical polymer capsule filled with frozen DT. The DT must be conformal to the interior of the capsule and be extremely smooth. The current baseline design calls for uniform DT layers approximately 100 µm thick on the interior of a 2 mm diameter capsule. The interior DT surface must be smoother than 0.5 µm rms. The development of suitable cryogenic targets is crucial to the success of NIF.

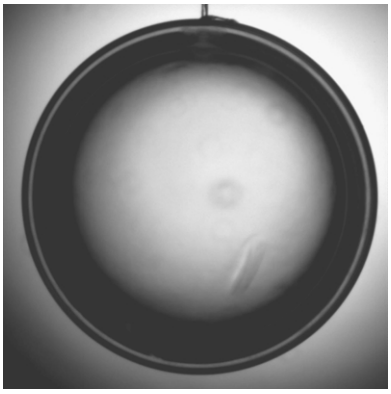

Don Bittner has a Ph.D. in Physics from the University of Michigan. Dr. Bittner has been developing techniques for redistributing cryogenic layers of isotopic hydrogen inside millimeter size transparent spherical capsules. He is a co-developer of the infrared layering technique. In this technique, hydrogen is illuminated with infrared radiation and the resulting absorbed energy is used to form uniform layers. He is currently working on infrared radiation injection techniques to form uniform layers inside hohlraums for NIF applications. Prior to joining Schafer in 1991, Dr. Bittner was a Research Scientist at KMS Fusion, Inc. There he studied the effects of ß decay heating on cryogenic deuterium-tritium (DT) liquid and solid layers in glass capsules using holographic interferometry. In conjunction with that work, he performed ray-trace computer modeling studies.

Don supervises John Burmann, Raymond “Bud” Fraze, and Jerry Stewart to study and develop techniques for layering solid DT and DD fuel for current and future ICF experiments and provide engineering design support for NIF cryogenic target hardware.

John Burmann has 17 years experience working as a technician in a R&D environment at LLNL. In 1987, Mr. Burmann received a certificate in “Vacuum Technology” from Chabot College in Livermore. Prior to joining Schafer, Mr. Burmann worked for eight years in the Atomic Vapor Laser Isotope Separation program at LLNL, assembling high power copper vapor laser heads for isotope separation experiments. He joined Schafer Corp. in 1993 and is the lead assembly technician in the cryogenic layering group in the ICF program at LLNL.

Mr. Burmann's responsibilities include assembly of the cryogenic experiments (which consist of NIF scale spherical capsules with ~ 30 μm diameter fill tubes). Mr. Burmann is also pursuing the assembly of fill tubes that are as small as 5 μm diameter into NIF scale capsules. Other duties include 3D CAD designing, machining, welding, vacuum leak detection, and polishing fiber-optic cables used for IR illumination experiments.

Jerry Stewart has an A.A. degree in Mechanical Design and Drafting, a Certificate of Completion in Vacuum Technology, and a B.A. degree in Business Administration. Before joining the Schafer Cryogenic Target Fabrication Group, Mr. Stewart was involved in the engineering, design and production of diode laser equipment, 200 and 300 millimeter size silicon wafer processing equipment, miniature laser development, the Shiva Laser Fusion Target Positioner, underground nuclear test components and canister assemblies, packaging of non-nuclear weapons components, remote manipulators and a variety of signal and ordnance developments and fabrication technologies. His current activities include designing cryogenic target delivery hardware for use on NIF.

Raymond (Bud) Fraze earned an A.A. degree in Mechanical Design. Mr. Fraze was involved in engineering and design of magnetic fusion experiments (TFTR/LLNL and Doublet III at LBL for General Atomics), spacecraft pyrotechnic systems at JPL, steam engine design for Lear Motors and solar experiments at SNL. Recently, as a mechanical engineer for EarthWatch Incorporated he was responsible for the clean room assembly and calibration of the EarlyBird satellite optical systems. He was launch manager for EarlyBird and QuickBird satellites launched from the Russian Federation. He is currently designing cryogenic target delivery hardware for use on NIF.

Jerry Stewart

Raymond Fraze

4.3.4. Center for Target Component Fabrication and Fabrication Development

The Center for Target Component Fabrication and Fabrication Development is responsible for producing and delivering (on time and within budget) millimeter and sub-millimeter components micromachined from a variety of materials for current ICF experiments. These parts can be made to tolerances with ±1 μm, and with surface finishes better than 100Å rms peak to valley. Some of the components also require plating of various metals by sputter coating, vacuum vapor deposition, ion plating, and electroplating. The components are required in many different designs, including flat plates, stepped plates, wedged plates, single wall hohlraums, and double wall hohlraums. Many components contain more than one material. We continually improve or develop new techniques as required for the ever changing designs of components needed for ICF.

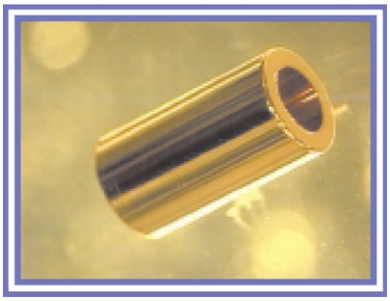

The Center for Target Component Fabrication and Fabrication Development is a key functional group within the U.S. ICF Program for the delivery of micromachined components used in current ICF experiments and for the development of new techniques required for making components for future ICF experiments.

James Kaae (Ph.D. Engineering, University of California, Los Angeles) is head of the Center for Target Component Fabrication and Fabrication Development. Dr. Kaae has experience in many areas of materials science including chemical vapor deposition of carbons and carbides, the structure of various forms of carbon, irradiation effects on carbon, properties and behavior of coated particle nuclear fuels, high-temperature fatigue of austenitic alloys, fabrication of composite materials, and fabrication of high-temperature radar absorbing materials. He was responsible for the transfer of the highly complex process for glow-discharge coating of ICF capsules from LLNL to GA. This capability has evolved to the point where all of the glow-discharge coating required for the ICF program is now carried out at GA. He also developed the micromachining capability at GA and is recognized as an expert in micromachining. He has directed the application of this technique to the production of gold hohlraums, witness plates, sine-wave plates and many other small components that are unique to ICF targets. He was responsible for the fabrication of many types of flat targets for the PBFA-II ion beam experiment. Dr. Kaae has over 70 publications and 5 patents.

Five people report to Dr. Kaae: Joe Smith, Clyde Shearer, David Woodhouse, Emilio Giraldez, and Jason Wall.

Joe N. Smith, Jr., has a Ph.D. in Surface Physics from the University of Leiden, Netherlands. Dr. Smith has thirty years experience in surface physics and the interactions of ions, electrons, atoms, and molecules with solid surfaces. This work has included studies of aerodynamic drag in rarified gas flows, e.g., orbiting satellites, surface chemical reactions, sputtering and ion neutralization, surface ionization, and other reactions that occur at the gas-solid interface. His work has included basic research, as well as the development of thermionic energy converters and specialized techniques for the study of plasma-wall interactions in the DIII–D tokamak device. Currently, Dr. Smith develops fabrication techniques for making ICF target components, specialized hohlraums, witness plates, foam shells and other components. Dr. Smith has approximately six dozen publications.

Emilio Giraldez (Ph.D. Material Science, Massachusetts Institute of Technology) has sixteen years experience in the area of materials science. His work has included development of functionally graded ceramic to metal seals, fabrication of high temperature superconducting devices, developing carbon-copper composites, and developing welding techniques for directionally solidified and single crystal superalloys. Currently, Dr. Giraldez works on fabrication techniques for making ICF target components. Dr. Giraldez has twelve publications, and one patent.

Clyde Shearer has an A.A. in Technical Engineering from San Diego City College. Previously, he worked at Solar International Harvester in the Research and Space Division helping to build the five thermo-electric generators that are on the moon, as well as the beryllium antennas that were used on the LEM lander. Joining GA in 1968, Mr. Shearer helped to build the first nuclear thermo-electric battery to be implanted in a human, and developed ion-plating coating techniques on the thermo-electric solar power program. He made the first 100 m of superconducting wire. In the ICF program, he built the first three GDP coaters at GA and qualified them for production, and is now working on micromachining and PVD coating. Mr. Shearer holds patents on thermo-electric alloy processing and in fabricating superconducting wire.

Clyde Shearer Emilio Giraldez Joe Smith Jim Kaae

David Woodhouse Jason Wall

David Woodhouse has taken Mechanical Engineering classes at the University of Illinois. Mr. Woodhouse has twenty years experience in the development and production of coated particle reactor fuel at General Atomics with emphasis on pyrolitic carbon and silicon carbide coatings, and was the supervisor of the fuel production group 1978-1986. Currently he micromachines ICF target components and has been involved in CVD coating and the production of glass and polymer microshells.

Jason Wall has a certificate in computer information science. He has worked at General Atomics in the ICF Target Fabrication Group for six years. During this time he has gained experience in micromachining ICF target components, assembly of ICF targets, electroplating, and physical vapor deposition.

4.3.5. Center for Polymer and Coatings and Foam Capsule Development

The Center for Polymer and Coatings and Foam Capsule Development is principally concerned with coating capsules and components for current ICF experiments with polymers and doped polymers such as Glow Discharge Polymer (GDP), a plasma polymer, and polyimide. As a second, but equally important, priority the center is heavily involved in the development of new and improved targets such as NIF quality targets, new capsule materials, foams for future targets, smart targets and hohlraums, and new and innovative processes. This year the center added the capability to make advanced foam capsules.

The Center for Polymer and Coatings and Foam Capsule Development plays a key role in the fabrication of current targets and is developing better and novel targets for future ICF experiments.

Abbas Nikroo (Ph.D. Condensed Matter Physics, University of California, Santa Barbara) is head of the Center for Polymer & Coatings Development. Before joining GA, Dr. Nikroo was a research associate at UC Santa Barbara, where he performed cryogenic laser pump-probe and Raman spectroscopies to study the fundamental vibrational and magnetic modes of various solid state systems. Since 1995, Dr. Nikroo has been responsible for directing the plasma coating operations at GA for development and fabrication of capsules and other targets for ICF experiments, and developing various techniques and processes. He developed techniques for incorporating various dopants in ICF targets and alternative methods for making large glass shells and permeation barriers. He has studied various techniques of shell agitation for various ICF related coatings and their effect on shell quality. Dr. Nikroo has fabricated thin wall polymer shells as cryogenic direct drive targets on OMEGA.

Two groups report to Dr. Nikroo, Plasma Polymer Coatings, and Polymer Capsules.

Plasma Polymer Coatings. Don Czechowicz, Erwin Castillo, Wes Baugh and Joe Pontelandolfo are involved in production activities for coating capsules with GDP and polyimide as well as determining various properties of ICF materials.

Don Czechowicz has a Ph.D. in Physical Chemistry from Penn State University. His expertise is in the behavior of materials in high-temperature environments, materials synthesis, solid-state materials characterization, chemical thermodynamics and kinetics, and materials engineering. He has several years experience in ICF target mandrel development and coating technology. Dr. Czechowicz is the author of approximately 20 technical reports and publications.

Wes Baugh has taken courses in electronics engineering and mathematics at San Diego City College. He designed and assembled a Chemical Vapor Deposition (CVD) apparatus for oriented tungsten cathode deposition and co-developed the Sol-Gel process to produce uranium and thorium microspheres. He is the co-inventor of the process for fabricating the lithium aluminate kernels used in the HTGR-New Production Reactor (NPR). His ICF experience includes production and coating of glass and polymer microshells, and the assembly, checkout, and testing of the OMEGA Cryogenic Target System. He developed cryogenic seals for fielding of targets at the National Ignition Facility. He holds patents in uranium and thorium microspheres and tritium recovery.

Don Czechowicz Erwin Castillo Joe Pontelandolfo

Erwin Castillo has taken classes at San Diego State University. He is experienced in operating the diamond turning machines used in the production of ICF target components and in operating the GDP coaters used to produce ICF target shells.

Joe Pontelandolfo has a B.S. in Mechanical Engineering from San Diego State University. He has experience in designing high-temperature presses for making nuclear fuel compacts and in designing high-temperature fluidized-bed CVD coaters for coating nuclear fuel particles. He developed processes for coating thin layers of gold and aluminum on Mylar films for PBFA-II targets and is currently designing, building and operating GDP coaters in the ICF Program.

Polymer Capsules. Barry McQuillan and Reny Paguio work on the development and production of PAMS shells and foams. They also coordinate their activities with LLNL's on-site employee Masaru Takagi.

Barry McQuillan has a Ph.D. in Solid State Chemistry from the University of California, Berkeley. He has experience in diverse inorganic and polymer systems: graphite chemistry, fluorine chemistry, fluoride glasses, xenon chemistry; general polymer synthesis and conducting polymers; ceramic oxide coatings, growth of ceramic oxide fibers, and sol-gel alkoxide synthesis. He is knowledgeable in the area of thermodynamic calculations and the reactivity of

materials and diffusion calculations. Within the ICF program, he has been intimately involved in the development of the microencapsulation process for PAMS shells, the synthesis of metal doped polymers, and foam materials. Dr. McQuillan has authored 17 publications and holds 3 patents.

Reny Paguio has a B.S. in Environmental Sciences with an emphasis in Chemistry from the University of California, Riverside. He has experience in photopolymer systems and polymer synthesis. In the ICF program he is currently working with microencapsulation of PAMS and is working on the development of RF, DVB, and Silica aerogel foam.

Masaru Takagi, an employee of LLNL on assignment in San Diego at GA, has a Ph.D. in Chemical Engineering from Osaka University. Dr. Takagi has done pioneering research in ICF capsule production by microencapsulation, especially by drop generator methods. He is a leader in developing processes appropriate for every variety of shell and foil made: solid, foam, foam/solid, solid/foam, and rippled. Dr. Takagi also developed a means for measuring tritium partial pressure and developed targets used to produce a Ge soft x-ray laser.

4.3.6. Center for Foam Target Development and Production

The Center for Foam Target Development and Production is responsible for the development and production of low density foam components used in many types of experiments: ICF, weapons physics, and EOS. There are two facilities required for this work, a routine production laboratory at the Schafer Livermore, CA facility and a research and development lab on-site at Sandia National Laboratories, NM. The production of foam-components can require micromachining the foam, micromachining a mold to produce the foam, embedding capsules or components at precise positions in a foam, and coating foam with metal. The Center has achieved many advancements in production techniques that allow fabrication of unique foam component designs.

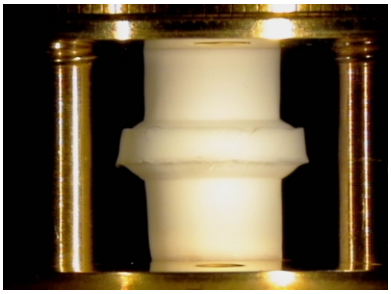

This work is carried out by a very able staff: Diana Schroen, Pat Collins, Scott Faulk, Chris Russell, John Varadarajan, Jon Streit, Dave Tanner, and Kelly Youngblood.

Diana Schroen has a B.S. in Polymer and Coatings from Eastern Michigan University. Ms. Schroen brings 26 years of experience in analytical and R&D chemistry, including 21 years in the ICF program. Since joining Schafer in 1991, she has produced polymer films, foams, and spheres for nuclear fusion research by casting and microencapsulation techniques. Most recently she has been producing low-density foams for experiments on Sandia's Z-pinch machine. These foams typically range in density from 3-to 50-mg/cm^3 and must meet tight dimensional tolerances. She previously produced a prototype NIF target (a multi-layer foam microencapsulated sphere) for LLNL and flat foam targets for NRL. Ms. Schroen has significant non-destructive characterization experience including techniques for surface finish, density, sphericity, and uniformity. She has over 20 publications.

Pat Collins has 34 years experience in the mechanical/technical field. Mr. Collins started his civilian technical experience in the Silicon Valley during the mid seventies with Memorex Corp. as an assembly technician and later as a technician supervisor for field service operations point of sale systems with National Semiconductor Corp. He joined Lawrence Livermore National Laboratory in 1981 as a mechanical technician and over the next fifteen years worked for Mirror Fusion and Laser Programs. Mr. Collins came to Schafer Laboratories in 1998 with a strong background in machining and fabrication and now operates the single point research lathe producing targets for SNL and NRL.

Scott Faulk has twenty years of experience in manufacturing and machining. Mr. Faulk joined Schafer in 1992 and is responsible for all machining activities. He developed many

innovative manufacture and fabrication techniques for the complex requests received from the various laboratories in the ICF community. Prior to joining Schafer in 1992, Mr. Faulk worked at LLNL in the AVLIS program on the development of dye lasers that ultimately became the world's most powerful visible laser.

Pat Collins

Scott Faulk

Jon Streit has a B.S. in Chemical Engineering from New Mexico State University. Mr. Streit joined Schafer in 2001 and brings with him over five years experience in monomer synthesis and polymer research. He is primarily involved with developing divinyl benzene foam shells for use in ICF applications. Mr. Streit also supports fabrication of foam components and characterization of parts for targets on Sandia's Z-pinch machine.

Chris Russell has an Associates degree in Metals Technology. He joined Schafer at the end of 2001, with four years experience as a production support administrator and with extensive AutoDesk CAD experience. Mr. Russell is responsible for obtaining components from suppliers, characterizing parts with a Veeco non-contact profilometer and a custom radiography system, and ensuring that Target Fabrication keeps pace with Sandia's shot schedules.

Jon Streit

Chris Russell

Dave Tanner is a senior target fabrication and assembly technician in the target laboratory at Sandia National Laboratories. As a Senior Experimental Technician working for K-Tech Corporation, Mr. Tanner gained 21 years experience operating both Saturn and Z drivers. He also is experienced in wire array target assembly having fielded the first wire array shots on Saturn and all of the standard designs now used by Z. He is skilled in multiple target characterization techniques and adds insight from his experience in operating the Z driver.

Kelly Youngblood has a B.S. in Chemistry from California State University, Chico. Prior to working for Schafer, Ms. Youngblood was an analytical chemist for an agricultural laboratory. She joined Schafer in 1997 where she develops production methods to expedite deliveries of foams. Ms. Youngblood also provides quality control characterization and documentation for the foams delivered to Sandia.


Dave Tanner


Kelly Youngblood

4.3.7. Center for Capsule Production

The Center for Capsule Production is principally concerned with fabricating and characterizing capsules and components for current ICF experiments. This includes fabrication of polymer and metallic capsules to state-of-the-art tolerances, complete capsule characterization, ensuring on-time delivery of all capsule orders, and seeking feedback from experimentalists to focus product improvement efforts. We anticipate that the future will include a production "Target Factory" and fully automated characterization techniques.

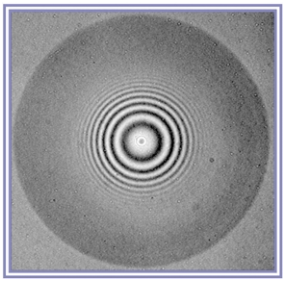

The Center for Inertial Fusion Capsule Production is the key functional group within the U.S. ICF Program for the fabrication and characterization of capsules used in current ICF experiments.

David Steinman (B.A. Mathematics, Oakland University) is head of the Center for Inertial Fusion Capsule Production. Before joining GA, Mr. Steinman began his involvement with ICF target fabrication at KMS Fusion in 1977. There, he developed concepts and proof-of-principle experiments for the mass production of ICF capsules and components. He later became the KMS Fusion Target Fabrication Group leader and was responsible for devising fabrication and characterization techniques for ICF targets and components including: capsules, hohlraums, thin film, and gas jet targets among others. At GA since 1992, he developed ICF target characterization techniques, conceived numerous innovative target fabrication processes, and brought them into production.

Mr. Steinman became a DOE-certified contractor Classification Officer for GA in 1992 and since then has held the post of Security Officer for the ICF project. He is also Head of GA HED Physics Targets Developments. He has over 20 publications and 1 patent.

Two groups report to Mr. Steinman, a Technical group and a Deliveries group.

Technical Group. Martin Hoppe supervises Sally Paguio, Ron Andrews, and Stephen Grant for chemical and physical analyses and the development or improvement of characterization and fabrication techniques.

Martin Hoppe has a Ph.D. in Chemistry from the University of Arizona. His expertise is in a wide variety of chemical characterization techniques including IC, XRF, SEM/EDXS, TEM, Auger, GC, AA, XRD, PES, TGA, IR, NMR and Mass Spectroscopy. He has played a

key role in developing and improving chemical and optical characterization methods for ICF targets and components. Dr. Hoppe developed a new method for making large glass shells for the ICF program starting from silicon-doped GDP.

Salvacion (Sally) Paguio has a B.S. in Chemistry from the University of San Agustin. Previously, Ms. Paguio developed methods for material synthesis of superconductor and defense-related materials and implemented analytical procedures in environmental chemistry and radiochemistry. She is currently involved in ICF capsule fabrication and development, responsible for solution preparations and characterization of targets.

Marty Hoppe Steve Grant

Salvacion Paguio

Stephen Grant spent 1.5 years in target assembly for Nova at LLNL. Mr. Grant is trained at target production including glass shell production and poly (vinyl alcohol) coating, and in the optical and physical characterization of deliverable targets. He is heavily involved in the maintenance of ICF facilities. His 11 years experience at General Atomics includes production of fission fuels as well as tritium, strontium, and cesium testing.

Ron Andrews' previous experience at General Atomics includes support of research and development of fission fuels. His work involved sol gel formation, coating, and heat treatment of uranium thorium fuel. Ron is currently involved in the development of PVA layer deposition by a spin coating technique. He is experienced in machining, welding and maintenance of laboratory equipment.

Deliveries Group. Annette Greenwood supervises Jane Gibson and Dale Hill for the "routine" processing and characterization of capsule and components deliveries.

Annette Greenwood has a B.S. in Chemistry from San Diego State University. Previously, Ms. Greenwood had a key role in the GA analytical chemistry laboratory, developing and implementing a wide range of instrumental, environmental, and radiochemical analyses. Currently, she is responsible for planning and coordinating production for ICF target deliveries. She has extensive involvement with the development of processes and procedures for the characterization of ICF targets and components.

Annette Greenwood Jane Gibson

Jane Gibson has a M.S. in Physical Sciences from Stanford University. She has 23 years experience at General Atomics on various fusion and fission programs including eight years in the Fusion Business Development group. She joined the Inertial Fusion Technology division in 1993 with on-site assignment at LANL. Currently, she is responsible for AFM Spheremapping and Wallmapping of capsules.

Dale Hill has a M.S. in Chemistry from Oregon State University. Mr. Hill is well experienced in the chemical analysis of diverse samples using a wide range of analytical instruments (gamma ray spectrometer, alpha spectrometer, proportional counter, LSC, XRF, ICP, AA, GC, UV-Vis). He has written application software for personal computer systems to perform multiple analytical tasks. Previously, Mr. Hill supervised the radiochemistry section of the Chemistry Laboratory at General Atomics.

4.3.8. Center for Advanced Planar Targets

The Center for Advanced Planar Targets develops and produces the planar targets required for a major portion of ICF research. Planar targets are ideal for exploring material properties, hydrodynamic instabilities, and laser-target material interactions. The Nike Laser at the NRL is designed only for experiments using planar targets. The laser's beam is very uniform and well characterized so experimenters can explore the effects of depositing a large amount of energy in a material without perturbations from anomalies in the laser beam. For experiments to have meaningful results, the quality of the targets must at least equal the uniformity of the beam and exceed the limits of the diagnostic equipment. Over the years, as diagnostic equipment and prediction codes have improved, the requirements for target surface finish, uniformity, flatness, and purity have increased. Additionally, the complexity of target designs has increased by the addition of material layers, dopants, intentional surface and mass perturbations, and foams. NRL has also developed a cryogenic capability requiring targets that are designed to work in the wall of a cryogenic Dewar.

Tom Walsh supervises Sue Carter, Ed Hsieh, Derrick Mathews, Brian Motta, and John Varadarajan for developing, fabricating, characterizing, and delivering planar targets to ICF customers.

Tom Walsh has an M.S. in Nuclear Engineering from the Air Force Institute of Technology. As a research scientist, Mr. Walsh developed new techniques for making flat film targets with greater precision and control. He brings to the project over 25 years of experience in research and development, technical program management, and team leadership. Prior to joining Schafer, he was a member of the Brilliant Pebbles (BP) Task Force where he served as the on-site liaison with the BP Concept Development Program at LLNL. He is also Head of Schafer HED Physics Targets Developments.

Ed Hsieh has a Ph.D. in Solid State Electronics from Oregon State University, and over 30 years of experience in thin film R&D, including 20 years in ICF programs. Since joining Schafer in 1998, Dr. Hsieh has established extensive vacuum technology infrastructure for thin film process developments. One of the more notable achievements was low stress tungsten film deposition on freestanding polymer film substrates. Prior to joining Schafer, he was a member of the technical staff at LLNL, specializing in thin film photovoltaic cells, thin film devices, and

ICF related coatings. He served on various DOE solar energy advisory panels. He was a target team leader responsible for weapon physics NOVA experiments. Dr. Hsieh has over 80 publications/presentations in the area of solid state devices, NOVA target fabrication, and NOVA target physics.

Sue Carter has been working on flat and patterned polystyrene film for NRL. She is responsible for the lifting, cutting down, and mounting the films onto the Nike frames. She spin-coats polyimide onto wafers and patterned quartz molds, lifts the films, and mounts them onto cryogenic target mounts. Currently, she is developing spin coating of silica aerogel onto a patterned mold.

Derrick Mathews is a technologist supporting NRL, LLE, and LLNL target production. He fabricates and characterizes EOS targets, flat and patterned polystyrene and Si-doped polystyrene films. Mr. Mathews also provides on-site support for LLNL, where he is responsible for complex micro assembly of ICF targets.

Brian Motta attended Los Positas College studying Mechanical Engineering and Vacuum Technology. Mr. Motta has an extensive background in ICF — with the Shiva, Nova and Novette laser systems at LLNL. He has 20 years of technical experience and excels at mechanical design, machining and welding and vacuum system design and operation.

John Varadarajan has a Ph.D. in Organic Chemistry from McMaster University. Dr. Varadarajan has over 18 years of experience in synthetic organic and organometallic chemistry with many publications and patents in these fields. He is new to the ICF team and will be working on the development of new polymers and foam targets for ICF applications.

Sue Carter

Derrick Mathews

Brian Motta

John Varadarajan

4.3.9. GA/Schafer Characterization Innovation and Development Office

The GA/Schafer Characterization Innovation and Development Office works with customers to understand their future target needs and identifies and develops characterization techniques required for target production.

Richard Stephens (Ph.D. Solid State Physics, Cornell University) is head of the Characterization Innovation and Development Office. Before joining GA, Dr. Stephens served 10 years as a staff scientist at Exxon Research and Engineering Co. (ER&E) where he concentrated on the connection between inhomogeneous and rough materials and their optical properties. He developed analytical techniques for simultaneously absorbing and scattering materials, using light and x-ray scattering to probe the chemical and structural evolution of thermally-cracked heavy oil. He also developed a pulsed dye laser based spectrometer which could measure the adsorption-induced changes in absorption spectra of sub-monolayers of surfactants.

After joining GA, he developed theoretical concepts for engineering the IR optical properties of durable paint coatings, performed analyses of superconducting magnetic energy storage devices, developed theoretical models and solid state physics for processing high Tc superconductor materials and performed experimental validation using focused laser heating to perform continuous processing, transforming the precursor (coated onto a wire) into aligned crystals.

Currently, in addition to developing analytical techniques, he is developing innovative inertial fusion target concepts, directing target material research programs for shells, and analyzing their optical and thermal properties. He is co-P.I. of an OFES funded experimental Fast Ignition concept exploration program, and was recently working with the Nova PW team on visualizing electron beam propagation in super-critical plasmas. Dr. Stephens organized a white paper at the 1999 Fusion Summer study analyzing the value of a Fast Ignition concept evaluation program.

Dr. Stephens has over 50 publications and 10 patents.

Michael McClellan, the Chief Scientist at Schafer, has a Ph.D. in Physical Chemistry from Massachusetts Institute of Technology. Dr. McClellan has over 20 years experience in precision optical systems design and manufacturing, advanced material development, and advanced technology integration. At Schafer Laboratories, Dr. McClellan is responsible for leading the precision machining effort including the development of ICF targets and advanced

space optics, and advancing the characterization capabilities at the submicron to Å level for components shape, finish, and material properties. Other ICF areas Dr. McClellan has participated in include the design and manufacture of a low temperature cryostat for hydrogen filling of shells, research and development of hollow low density foam shells, and designing and building a polymer film deposition film system.

4.3.10. Schafer Division of Inertial Fusion Technology

The Schafer Division of Inertial Fusion Technology is a major part of the Schafer Laboratories of Schafer Corporation located in Livermore, CA. The staff is organized to support the target fabrication needs of the ICF program, as the key industrial partner to General Atomics in the U.S. ICF Program for the fabrication and characterization of planar targets, the fabrication and delivery of foam targets, and the development of polymer foam chemistry systems and processing procedures. In addition, Schafer scientists and technicians are engaged in cryogenic fuel layering science for capsules used in ICF experiments and in engineering design of hardware required to implement the cryogenic fuel layering for NIF.

Keith Shillito (Ph.D. Ceramic Engineering, Rutgers) is director of the Schafer Division of Inertial Fusion Technology. Dr. Shillito is a materials scientist with 25 years experience with optical system materials and fabrication. He has been responsible for managing Schafer's activities in support of this contract. This includes the development of planar and foam target production capability at Schafer and its supporting micromachining and coating technologies. Dr. Shillito has had major responsibilities in the development of surveillance and High Energy Laser (HEL) substrate materials and processing of beryllium ceramic, and glass optics. He was the leading authority in developing a comprehensive contamination control technology program for large space-based optics for the Air Force's Rome Laboratory. He led a team that resolved production yield problems of PMN piezoelectric actuators for a major HEL mirror fabricator. He has served as an advisor in the planning and evaluation of nuclear survivability testing of Strategic Defense Initiative Organization (SDIO) Surveilance and HEL optics.

Dr. Shillito has published papers on materials and process development and holds a patent on laser mirror fabrication.

Four groups report to Dr. Shillito:

- Operations Office: Head — Keith Shillito
- Center for Advanced Cryogenic Layering: Head — Dr. Don Bittner
- Center for Foam Development and Production: Head— Diana Schroen
- Center for Advanced Planar Targets: Head — Tom Walsh

The three Centers are described in sections 4.3.3, 4.3.6, and 4.3.8, respectively.

Operations Office. The operations office, also headed by Dr. Shillito, ensures that the work performed is authorized and funded, monitors the cost and performance of each task, and prepares financial and other reports. The operations office provides administrative support

for on-site target fabrication technicians at LANL, LLNL and SNL — Ron Perea at LANL; and Chris Bostick, Steven Gross, and Craig Rivers at LLNL.

Ron Perea has an A.A. in Electrical Design from the University of Albuquerque. Mr. Perea has been assembling targets since 1998 for experiments at LANL for the Trident laser. Before joining the ICF program, he supported the production of test wafers, helped prepare the Plutonium Reclamation Facility to restart operations, and was an instrumentation and control engineer.

Craig Rivers is head of target component fabrication (Micro Machining) and gas target production and fill systems at LLNL. Mr. Rivers has 25 years experience in research and development, co authored papers, and holds a patent on a magnetic radio frequency (RF) seal for laser and computer enclosures. He contributed to the development of the gas cell target program with the design and fabrication of quality gas cell targets, including the gas mixing and fill systems. Since October of 1993, Mr. Rivers has coordinated over 2000 successful gas cell target shots at the Nova and OMEGA lasers. Prior to joining Schafer in 1991, he was in charge of laser fabrication and production for the Atomic Vapor Laser Isotope Separation program at LLNL.

Chris Bostick is currently working in the Laser Target Fabrication group at LLNL. She is responsible for the assembly of laser targets for various physicists at LLNL. She also works with the making of Formvar films that are used to encapsulate different types of spheres that are used in targets. Chris has 33 years of experience from the semiconductor wafer industry, working mostly in the research and development field.

Steven Gross has 10 years in the high vacuum industry as well as 15 years at LLNL in the laser program supporting the mechanical and vacuum side of the program. Since joining Schafer Labs in early 2001, Mr. Gross has been supporting the ICF program in the development and machining of molds for foam targets for the SNL's Z machine.


Ron Perea


Craig Rivers


Chris Bostick


Steven Gross

4.3.11. Operations Office

The Operations Office supports the division in carrying out program activities. This includes ensuring that the work performed is authorized by the task descriptions and funded, monitoring the cost and performance of each task, and preparing financial projections. The office schedules, assigns, and edits annual and monthly technical and financial reports. In addition, the operations office is responsible for the website of the Division of Inertial Fusion Technology. Off-site personnel are also managed by the operations office.

The Operations Office supports and monitors the division to help ensure customer satisfaction.

Wayne Miller (M.S. Chemistry, University of Michigan) is head of the Operations Office. He has 27 years experience in developing and fabricating targets for the ICF program and has been at General Atomics since 1992. Until recently he was responsible for the production and shipment of glass and plastic microshells for LLNL, LANL, UR/LLE, and SNL, meeting their stringent specifications and, frequently, short delivery schedules. In 1992 under his guidance, GA transferred technology and skills from the national laboratories and the previous contractor and set up the production of microshells for the ICF laboratories. Since then, he and his staff implemented and developed new technology to increase the range of microshell sizes more than 10-fold along with considerably more stringent specifications and a 10-fold increase in the number fabricated for the national program. Mr. Miller has been recognized by the ICF laboratories and DOE for the dedicated and responsive efforts of his group in meeting the glass and plastic microshell needs of the ICF experimental program. Mr. Miller has two patents.

One group reports to Mr. Miller, the Onsite Target Fabrication at LLNL.

Onsite Target Fabrication at LLNL. John Ruppe, Chris Bostick, Steve Gross, and Craig Rivers form our target fabrication team on-site at LLNL. They make target components and assemble and characterize targets for the LLNL ICF experiments.

John Ruppe has a M.S. from the University of Michigan. He was the senior target assembler at KMSF from 1979 through 1990 and has been on-site at LLNL for GA since 1991. He is a recognized expert in the arcane art of target assembly and characterization and author and co-author on several target fabrication papers and numerous target fabrication presentations.

Chris Bostick, **Steve Gross**, and **Craig Rivers** are employed by Schafer. Their short biographies are found in Section 4.3.10.

5. PUBLICATIONS

This is a full list of publications, invited talks, presentations and awards. Items with GA/Schafer efforts supported by the contract for Target Component Fabrication and Technology Development Support are marked with an asterisk.

5.1. LIST OF PUBLICATIONS

*Bailey, J.E., G.A. Chandler, G.R. Bennett, G. Cooper, J.S. Lash, S. Lazier, R. Lemke, T.J. Nash, D.S. Nielson, J. McGurn, T.C. Moore, C.L. Ruiz, D.G. Schroen, S.A. Slutz, J. Torres, R.A. Vesey, "X-ray Imaging Measurements of Capsule Implosions Driven by a Z-pinch Dynamic Hohlraum," Phys. Rev. Lett. **89**, 095004(4) (2003).

Barcus, B.J., N.B. Alexander, D.T. Goodin, L.C. Brown, G.E. Besenbruch, "Demonstration of Mass Production Layering of Inertial Fusion Energy Targets Using a Room Temperature Surrogate for DT," Bull. Am. Phys. Soc. **46**, 148 (2001).

Cowan, T.E., R. Stephens, P. Parks, M. Rosenbluth, Y. Omelchenko, J. Dahlburg, M.D. Perry, and E.M. Campbell, "Fast Ignition and Ultra-intense Laser Research at General Atomics," 2nd Int. Conf. on Inertial Fusion Science and Applications, September 9–14, 2001, Kyoto, Japan, to be published in Fusion Technology.

*Czechowicz, D.G., E.R. Castillo, and A. Nikroo, "Composition and Structural Studies of Strong Glow Discharge Polymer Coatings," 14th Target Fabrication Mtg., July 15–19, 2001 West Point, New York, Fusion Technology **41**, 188 (2002); General Atomics Report GA–A23753 (2002).

Goodin, D.T., A. Nobile, N. Alexander, R.W. Petzoldt, "Progress Towards Demonstrating IFE Target Fabrication and Injection," 2nd Int. Conf. on Inertial Fusion Science and Applications, September 9–14, 2001, Kyoto, Japan, p. 746; General Atomics Report GA–A23832 (2002).

Goodin, D.T., A. Nobile, N.B. Alexander, L.C. Brown, J.L. Maxwell, J. Pulsifer, A.M. Schwendt, M. S. Tillack, R.S. Willms, "A Credible Pathway for Heavy Ion Driven Target Fabrication and Injection," Proc. 14th Int. Symp. on Heavy Ion Inertial Fusion, May 26–32, 2002, Moscow, Russia, to be published in Laser and Particle Beams; General Atomics Report GA–A23969 (2002).

Goodin, D.T., G.E. Besenbruch, J.P. Dahlburg, K.R. Schultz, A. Nobile, and E.M. Campbell, "Reducing the Costs of Targets for Inertial Fusion Energy," 2nd Int. Conf. on Inertial Fusion Science and Applications, September 9–14, 2001, Kyoto, Japan, p. 827; General Atomics Report GA–A23833 (2002).

Goodin, D.T., C.R. Gibson, R.W. Petzoldt, N.P. Siegel, L. Thompson, A. Nobile, G.E. Besenbruch, and K.R. Schultz, "Developing the Basis for Target Injection and Tracking in Inertial Fusion Energy Power Plants," Fusion Engineering and Design **60**, 27 (2002); General Atomics Report GA–A23417 (2000)

*Hoppe, M.L., "Recent Developments in Making Glass Shells from Silicon Doped GDP Shells," 14th Target Fabrication Mtg., July 15–19, 2001 West Point, New York, Fusion Technology **41**, 234 (2002); General Atomics Report GA–A23746 (2002).

Key, M.H., F. Amiranoff, C.B. Andersen, D. Batani, S.D. Baton, T. Cowan, N. Fisch, R.R. Freeman, L. Gremillet, T. Hall, S.P. Hatchett, J. M. Hill, J. A. King, J. Koch, M. Koenig, B. Lasinski, B. Langdon, A. Mackinnon, E. Martinolli, P. Norreys, P. Parks, E. Perelli-Cippo, M. Rabec La Gloahec, M. Rosenbluth, C. Rousseaux, J.J. Santon, F. Scianitti, R. Snavely, and R.B. Stephens, "Studies of Energy Transport by Relativistic Electrons in the Context of Fast Ignition," 2nd Int. Conf. on Inertial Fusion Science and Applications, September 9–14, 2001, Kyoto, Japan.

Koch, J. A., M. H. Key, R. R. Freeman, S. P. Hatchett, R. W. Lee, D. Pennington, M. Tabak, and R.B. Stephens, "Experimental Measurements of Deep Directional Columnar Heating by Laser-generated Relativistic Electrons at Near-solid Density," Phys. Rev. E **65**, 1641 (2002).

*Kozioziemski, B.J., Randall L. McEachern, R.A. London, and D.N. Bittner, "Infrared Heating of Hydrogen Layers in Hohlraums," Fusion Science and Technology **41**, 296 (2002).

*McQuillan, B.W., and M. Takagi, "Removal of Mode 10 Surface Ripples in ICF PAMS Shells," 14th Target Fabrication Mtg., July 15–19, 2001 West Point, New York, Fusion Technology **41**, 209 (2002); General Atomics Report GA–A23747 (2002).

Meier, W.R., B.G. Logan, W.L. Waldron, G-L. Sabbi, D.A. Callahan-Miller, P.F. Peterson, D.T. Goodin, "Progress Toward Heavy Ion IFE," Proc. 6th Int. Symp. on Fusion Nucl. Technology, April 7–12, 2002, San Diego, California, to be published in Fusion Engineering and Design.

Meier, W.R., W. Hogan, M. Key, J. Latkowski, J. Perkins, S. Reyes, D. Goodin, R. Stephens, K.A. Tanaka, "Issues and Opportunities for IFE Based on Fast Ignition," 2nd Int. Conf. on Inertial Fusion Science and Applications, September 9–14, 2001, Kyoto, Japan, p. 689.

Najmabadi, F., Raffray, R., Tillack, M., Goodin, D., Haynes, D., Olson, C., and the ARIES Team, "Assessment of Chamber Concepts for Inertial Fusion Energy Fusion Power Plants - The ARIES-IFE Study," 2nd Int. Conf. on Inertial Fusion Science and Applications, September 9–14, 2001, Kyoto, Japan, p. 701.

*Nikroo, A., D.G. Czechowicz, E.R. Castillo, and J.M. Pontelandolfo, "Recent Progress in Fabrication of High-Strength Glow Discharge Polymer Shells by Optimization of Coating Parameters," 14th Target Fabrication Mtg., July 15–19, 2001 West Point, New York, Fusion Technology **41**, 214 (2002); General Atomics Report GA–A23758 (2002).

*Nikroo, A., J.M. Pontelandolfo, and E.R. Castillo, "Coating and Mandrel Effects on Fabrication of Glow Discharge Polymer NIF Scale Indirect Drive Capsules," 14th Target Fabrication Mtg., July 15–19, 2001 West Point, New York, Fusion Technology **41**, 220 (2002); General Atomics Report GA–A23757 (2002).

Obenschain, S.P., D.G. Colombant, M. Karasik, C.J. Pawley, V. Serlin, A.J. Schmitt, J.L. Weaver, J.H. Gardner, L. Phillips, Y. Aglitskiy, Y. Chan, J.P. Dahlburg, and M. Klapisch, "Effects of Thin High-Z Layers on the Hydrodynamics of Laser-Accelerated Plastic Targets," Phys. Plasmas **9**, 2234 (2002).

Olson, R.E., R.J. Leeper, S.C. Dropinski, L.P. Mix, G.A. Rochau, S.H. Glenzer, O.S. Jones, L.J. Suter, J.L. Kaae, C.H. Shearer, J.N. Smith, "Time and Spatially Resolved Measurements of X-ray Burnthrough and Re-emission in Au and Au:Dy:Nd Foils," submitted to 14th Top. Conf. on High Temperature Plasma Diagnostics, July 8, 2002, Madison, Wisconsin.

Pulsifer, J.E., M. Tillack, D.T. Goodin, and R.W. Petzoldt, "Thermal Control Techniques for Improved DT Layering of Indirect Drive IFE Targets," 2nd Int. Conf. on Inertial Fusion Science and Applications, September 9–14, 2001, Kyoto, Japan, p. 802.

Stephens, R.B., J.P. Dahlburg, and S. Hatchett, "Optimizing the Structure of Fast Ignition Targets," 2nd Int. Conf. on Inertial Fusion Science and Applications, September 9–14, 2001, Kyoto, Japan, to be published in Fusion Technology; General Atomics Report GA–A23803 (2002).

Stephens, R.B., S.W. Haan, and D.C. Wilson, "Characterization Specifications for Baseline Indirect Drive NIF Targets," Fusion Technology **41,** 226 (2002); General Atomics Report GA–A23749 (2002).

*Streit, J.E., D.G. Schroen, "Development of Divinylbenzene Shells for Use as Inertial Confinement Fusion Targets," submitted to Fusion Technology.

*Takagi, M., R. Cook, B. McQuillan, F. Elsner, R. Stephens, A. Nikroo, J. Gibson, S. Paguio, "Development of High Quality Poly (α-methylstyrene) Mandrels for NIF," 14th Target Fabrication Mtg., July 15–19, 2001 West Point, New York, Fusion Technology **41**, 278 (2002).

*Takagi, M., R. Cook, B. McQuillan, F. Elsner, R. Stephens, A. Nikroo, J. Gibson, and S. Paguio, "Development of High Quality Poly (α-methylstyrene) Mandrels for NIF," Fusion Technology **41,** 278 (2002).

Theobald, A.M., O. Legaie, P. Baclet and A. Nikroo, "Thick GDP Microshells for LIL and LMJ Targets," 14th Target Fabrication Mtg., July 15–19, 2001 West Point, New York, Fusion Technology **41**, 238 (2002).

5.2. LIST OF PRESENTATIONS

*Aglitskiy, Y. (Science Applications International Corporation), A. L. Velikovich, M. Karasik, V. Serlin, A.J. Schmitt, S. Obenschain, J.H. Gardner (Plasma Physics Division, Naval Research Laboratory), N. Metzler (Science Applications International Corporation), J. Varadarajan, T Walsh, and S. Faulk (Schafer Laboratories), "Hydrodynamic Experiments on Nike. Shooting Campaign of YY2001-2003," presented at the 32nd Anomalous Absorption Meeting, July 22–26, 2002, Turtle Bay, Hawaii.

Alexander, N.B., "Target Supply Systems for Z Pinch IFE," presented at the US/Japan Workshop on Target Fabrication, Injection, and Tracking, December 3–4, 2001, San Diego, California.

Alexander, N.B., L.C. Brown, G.E. Besenbruch, "Layering of IFE Targets Using a Fluidized Bed," presented at the 2nd IAEA Technical Meeting on Physics and Technology of Inertial Fusion Energy Targets and Chambers, June 17–19, 2002, San Diego, California.

Brown, L., "Fluidized Beds for IFE Target Fabrication," presented at the US/Japan Workshop on Target Fabrication, Injection, and Tracking, December 3–4, 2001, San Diego, California.

*Chandler, G.A., J.E. Bailey, G.R. Bennett, P.W. Lake, J.S. Lash, R.W. Lemke, J.J. MacFarlane, T.J. Nash, D.S. Nielson, C.L. Ruiz, D.G. Schroen, S.A. Slutz, R.A. Vesey, "Drive Temperature and Shock Trajectory Measurements in a Dynamic Hohlraum Source on the Z-accelerator," 43rd annual meeting, APS Division of Plasma Physics, Oct 29–Nov 2, 2001, Long Beach, California.

Cowan, T.E., H. Ruhl, Y. Sentoku, R. Stephens, M. Allen, I. Barton, M. Melendes, A. Newkirk, P. Parks, M. Rosenbluth, J. Dahlburg, E.M. Campbell, P. Audebert, J. Fuchs, J.-C. Gauthier, L. Gremillet, M. Roth, E. Bambrink, A. Blazevic, M. Geissel, T. Schlegel, M. Hegelich, S. Karsch, D. Habs, G. Pretzler, K. Witte, S.P. Hatchett, G.P. Le Sage, "Acceleration of Ultra-Low Emittance Proton and Ion Beams with High Intensity Lasers," APS-DPP, October 2002, Orlando, Florida (Invited).

Dahlburg, J.P., "Target Fabrication - Its Role in High Energy Density Plasma Phenomena," presented at the 2nd IAEA Technical Meeting on Physics and Technology of Inertial Fusion Energy Targets and Chambers, June 17–19, 2002, San Diego, California (Invited).

Freeman, R., C. Anderson, J.M. Hill, J. King, R. Snavely, S. Hatchett, M. Key, J. Koch, A. MacKinnon, R. Stephens, T. Cowan, "Understanding the Role of Fast Electrons in the Heating of Dense Matter: Experimental Techniques and Recent Results," presented at the Conference on Radiative Properties of Hot Dense Matter, October 2002.

Goodin, D.T., "GA Target Fabrication Tasks," presented at the HAPL Project Review, April 4–5, 2002, San Diego, California.

Goodin, D.T., "IFE Target Fabrication and Injection at General Atomics," presented at the US/Japan Workshop on Target Fabrication, Injection, and Tracking, December 3–4, 2001, San Diego, California.

Goodin, D.T., "Overview of GA Target Fabrication Effort," presented at the HAPL Project Review, November 13–14, 2001, Pleasanton, California.

Goodin, D.T., "Progress in IFE Target Fabrication," presented at the ARIES Meeting, January 2002, San Diego, California.

Goodin, D.T., "Status of IFE Target Fabrication," presented at the ARIES E-Meeting, October 21, 2001.

Goodin, D.T., "Update on Target Fabrication, Injection, and Tracking (Heavy Ion Targets)," presented at the ARIES Meeting, July 2002, San Diego, California.

Goodin, D.T., A. Nobile, J. Hoffer, A. Nikroo, G.E. Besenbruch, L.C. Brown, J.L. Maxwell, W. Meier, T. Norimatsu, J. Pulsifer, W. Rickman, W. Steckle, E. Stephens, M.S. Tillack, "Addressing the Issues of Target Fabrication and Injection for Inertial Fusion Energy," presented at the 22nd Symp. on Fusion Technology, September 9–13, 2002, Helsinki, Finland.

Goodin, D.T., A. Nobile, N.B. Alexander, L.C. Brown, J.L. Maxwell, J. Pulsifer, A.M. Schwendt, M. S. Tillack, R.S. Willms, "A Credible Pathway for Heavy Ion Driven Target Fabrication and Injection," presented at the 14th Int. Symp. on Heavy Ion Inertial Fusion, May 26–31, 2002, Moscow, Russia.

Greenwood, A., and E. Stephens, "High-Z Coatings for Targets," presented at the US/Japan Workshop on Target Fabrication, Injection, and Tracking, December 3–4, 2001, San Diego, California.

*Greenwood, A.L., A. Nikroo, C.H. Shearer Jr., and J.L. Kaae, "Thickness and Uniformity Measurements of Thin Sputtered Gold Layers on ICF Capsules," presented at the 2nd IAEA Tech. Meeting on Physics and Technology of Inertial Fusion Energy Targets and Chambers, June 17–19, 2002, San Diego, California.

*Hanson, D.L., R.A. Vesey, M.E. Cuneo, G.R. Bennett, J.L. Porter Jr., J.H. Hammer, G.A. Chandler, L.E. Ruggles, W.W. Simpson, H. Seamen, J. Torres, J. McGurn, T.L. Gilliland, P. Reynolds, D.E. Hebron, S.C. Dropinski, D.G. Schroen, "Measurement of Radiation Symmetry In Z-pinch Driven Hohlraums," 43rd Annual Meeting, APS Division of Plasma Physics, Oct 29-Nov 2, 2001, Long Beach, California.

Petzoldt, R.W., "Aerosol Limits for Target Tracking," presented at the ARIES Meeting, April 2002, Madison, Wisconsin.

Petzoldt, R.W., "Status of Target Injection and Tracking," presented at the HAPL Project Review, April 4–5, 2002, San Diego, California.

Petzoldt, R.W., "Status of Target Injector, In-Chamber Tracking, Electromagnetic Injector," presented at the HAPL Project Review, November 13–14, 2001, Pleasanton, California.

Petzoldt, R.W., "Target Injection for Inertial Fusion Energy," presented at the US/Japan Workshop on Target Fabrication, Injection, and Tracking, December 3–4, 2001, San Diego, California.

Petzoldt, R.W., "In-Chamber Target Tracking and Other Target Injection Considerations," presented at the ARIES IFE E-Meeting, October 21, 2001.

Petzoldt, R.W., "Target Injection in Sacrificial Wall/Aerosol-Filled Chambers," presented at the ARIES Meeting, January, 2002, San Diego, California.

Petzoldt, R.W., N.B. Alexander, G.E. Besenbruch, T. Drake, D.T. Goodin, M. Hollins, K. Jonestrask, and R. Stemke, "Experimental Target Injection and Tracking System," presented at the 2nd IAEA Technical Meeting on Physics and Technology of Inertial Fusion Energy Targets and Chambers, June 17–19, 2002, San Diego, California.

Rickman, W., and D. T. Goodin, "Cost Modeling for Fabrication of IFE Targets," presented at the 2nd IAEA Technical Meeting on Physics and Technology of Inertial Fusion Energy Targets and Chambers, June 17–19, 2002, San Diego, California.

Rickman, W.R., "Chemical Process Modeling for Target Fabrication Process Scaleup," presented at the US/Japan Workshop on Target Fabrication, Injection, and Tracking, December 3–4, 2001, San Diego, California.

*Rochau, G.A., J.E. Bailey, P.W. Lake, J.L. McKenney, J.J. MacFarlane, D.G. Schroen, "Absorption Spectroscopy of Al Tracers in Low-Density CH(2) Foam Heated By Z-pinch Radiation," High Temperature Plasma Diagnostics Conference, July 8–12, 2002, Madison, Wisconsin.

Ruhl, H., T.E. Cowan, R.B. Stephens, "Super-intense Quasi-neutral Proton Beams Interacting With Plasma: A Numerical Investigation," IAEA-Fusion Energy Conference, Lyon, France, October 2002.

Schroen, D.G., J.E. Streit, "Development of Prototype Samples of a Possible IFE Foam Capsule Target," 2nd IAEA Technical Meeting on Physics and Technology of Inertial Fusion Energy Target and Chambers, June 17–19, 2002, San Diego, California.

*****Schroen, D.G., P. Collins, M. Droege, S. Faulk, S. Gross, E. Hsieh, B. Motta, C.O. Russell, D.L. Tanner, J.E. Streit, K. Youngblood, "Overview of Foam Target Fabrication in Support of Sandia National Laboratories," 32nd Anomalous Absorption Conference July 21–26, 2002, Hawaii.

Stephens, E., "Coating Development," presented at the HAPL Project Review, April 4-5, 2002, San Diego, California.

Stephens, E.H., A. Nikroo, M. Dicken, R.W. Petzoldt, and D.T. Goodin, "Palladium and Palladium Gold Alloys as High Z Coating for IFE Targets," presented at the 2nd IAEA Technical Meeting on Physics and Technology of Inertial Fusion Energy Targets and Chambers, June 17-19, 2002, San Diego, California.

*Stephens, R., and H. Huang, "Characterization Development at General Atomics," CEA-Valduc October 2002.

Stephens, R., "Asymmetric Targets Suitable for Fast Ignition," Japanese IUS Fast Ignition Workshop, March 2002, Otsu, Japan (Invited).

Stephens, R., "Fast Ignition Target Experiments at OMEGA," Japan/US Fast Ignition Workshop, March 2002, Otsu, Japan.

Stephens, R., "X-ray Backlighting Diagnosis of Implosion Characteristics of Advanced Fast Ignition Targets," US/Japan Workshop on High Irradiance Lasers and Target Plasma Diagnostics, March 2002, San Diego, California.

Stephens, R.B., "Fast Ignition Target Fabrication Issues," Snowmass Summer Fusion Study, July 2002, Snowmass, Colorado.

Stephens, R.B., "Fast Ignition Targets for Fusion Energy," 6th Fast Ignition Workshop, November 2002, St. Pete Beach, Florida.

Stephens, R.B., "Implosion Hydro of Indirect Drive FI Targets," 6th Fast Ignition Workshop, November 2002, St. Pete Beach, Florida (Invited).

Stephens, R.B., "OFES Fast Ignition Concept Exploration Program Update," OFES Open house at Snowmass Summer Fusion Study, July 2002, Snowmass, Colorado.

Stephens, R.B., "OFES Fast Ignition IFE Development Program," Appendix to IFE report from the Snowmass Summer Fusion Study, July 2002, Snowmass, Colorado.

Stephens, R.B., S.P. Hatchett, R.E. Turner, K.A. Tanaka, R. Kodama, and J.M. Soures, "Compression Dynamics of a Fast Ignition Target," APS-DPP, October 2002, Orlando, Florida.

Stephens, R.B., S.P. Hatchett, R.E. Turner, K.A. Tanaka, R. Kodama, and J.M. Soures, "Test of an Indirect Drive Fast Ignition Target Concept," IAEA-Fusion Energy Conference, October 2002, Lyon, France.

Stephens, R.B., S.W. Haan, and D.C. Wilson, "Characterization Specifications for Baseline Indirect Drive NIF Targets," 14th Target Fabrication Mtg., July 15–19, 2001 West Point, New York, Fusion Technology **41**, 226 (2002); General Atomics Report GA–A23749 (2002).

Tanaka, K.A., R. Kodama, R. Turner, S. Hatchett, Y. Tohyama, T. Sato, T. Yabuuchi, K. Mima, Y. Sentoku, "Fast Ignition Status," APS-DPP, October 2002, Orlando, Florida (Invited).

Valmianski, E.I., R.W. Petzoldt, and N.B. Alexander, "Wake Shields for Protection of IFE Target During Injection," presented at the 2nd IAEA Technical Meeting on Physics and Technology of Inertial Fusion Energy Targets and Chambers, June 17–19, 2002, San Diego, California.

*Walsh, T., S. Carter, P. Collins, S. Faulk, S. Gross, E. Hsieh, D. Mathews, B. Motta, D. Schroen, J. Varadarajan, K. Youngblood (Schafer Laboratories), Y. Aglitskiy (Science Applications International Corporation), A. Mostovych, and A. L. Velikovich (Plasma Physics Division, Naval Research Laboratory), "Flat Target Fabrication in Support of Nike," presented at the 32nd Anomalous Absorption Meeting, July 22–26, 2002, Turtle Bay, Hawaii.

6. ACKNOWLEDGEMENT

This report of work was prepared for the U.S. Department of Energy under Contract No. DE-AC03-01SF22260.